University of Alberta

A Control Strategy for Forming Arbitrary Formations of Multiple Autonomous Helicopters

by

Guang Yang 

A thesis submitted to the Faculty of Graduate Studies and Research in partial fulfillment of the requirements for the degree of **Master of Science**.

Department of Mechanical Engineering

Edmonton, Alberta
Fall 2007

Your file Votre référence
ISBN: 978-0-494-33376-1
Our file Notre référence
ISBN: 978-0-494-33376-1

Abstract

The thesis presents a leader-follower control strategy for forming arbitrary formations of multiple autonomous helicopters. A six-degree-of-freedom dynamic model is considered for the helicopters. Sliding Mode Control is employed due to its robustness to the model uncertainties and perturbations. The first version of the controller produces four inputs, the main rotor thrust, the roll and pitch moments, and the tail rotor thrust. In the second version of the controller, the rotors' aerodynamic model and the main rotor's actuation mechanism model of the helicopter are incorporated in the controller design, in which the rotor's mechanism actuation commands are considered as the controller inputs. The controllers can successfully control an autonomous helicopter such that it follows another helicopter with any specified spatial distance. The controllers perform well even in the presence of unknown bounded external disturbance, and are robust to norm bounded dynamic model parameter uncertainties. Numerical examples and simulation results are given to illustrate the effectiveness and robustness of the designed controllers.

Acknowledgements

I would like to express my thanks to the people who have helped me during my M.Sc. study and made this thesis possible.

First of all, I would like to gratefully acknowledge my supervisor, Dr. Farbod Fahimi, who shows me an excellent model of a researcher who is always dedicated to seeking truth in the science and engineering world. Throughout my graduate studies, he provided inspiration, sound advice and guidance, and encouragement. His supervision will be a treasure in my life.

It also has been a great pleasure to work with my colleagues in the Advanced Control and Robotics Lab: Jun Zhao, Chris Van Kleeck, Mehdi Saffarian, Mojtaba Azadi, Siavash Rezazadeh, and Michael Dawson. They provided a stimulating environment where I could always learn and showed me a new perspective of thinking.

Most importantly, I would like to thank the unconditional support and love from my mother and my father, Mrs. Xiaoli Sun and Mr. Shengguo Yang. To them I dedicate this thesis.

TALBE OF CONTENTS

List of Tables

List of Figures

Table of Symbols

α	main rotor lift slope
α_T	tail rotor lift slope
B	tip loss factor
c, c_2, c_T	main/flybar/tail blade chord length
$D_{x,y,z}$	fuselage profile drag forces along body coordinate
f_B	external force applied along body coordinates
g	gravitational acceleration
$\mathbf{I}$	rotational inertia matrix of flybar
k_g	gyro gain for tail rotor
k_m	motor reaction torque gain
$K_1, ..., K_6$	proportional constants used for identification
l_r	distance between rotor axis and CG
l_T	distance between tail rotor axis and CG
$L_1, ..., L_9$	linkage lengths in rotor hub assembly
m	helicopter total mass
$M_{\phi,\theta,\psi}$	net moments on helicopter
n	number of main/flybar/tail blades
r	position along the main rotor blade
R	length of main rotor blade
R_T	length of tail rotor blade
R_1, R_2	distance between rotor axis and flybar tip, and rotor axis and flybar root
R_{IB}	rotational matrix between inertial and body frames
T	thrust generated by rotor
T_m	torque applied by motor
T_T	tail rotor translational lift force
v_i	induced air velocity through rotor disk
v_I	helicopter velocity with respect to inertial frame
$v_B, \dot{v}_B$	linear body velocity and acceleration
x_B, y_B, z_B	helicopter position in body frame
x_I, y_I, z_I	helicopter position in inertial frame
β	flybar flapping angle
β_{max}	maximum value of flybar flapping angle
δ_{cyc}	cyclic input displacement
δ_{fly}	cyclic input to flybar
$\delta_\theta, \delta_\phi$	roll and pitch command inputs
θ_o, θ_ψ	throttle/collective and yaw command inputs
θ_{fly}	angle of attack of flybar
θ_o	collective pitch angle of main rotor blades
θ_{cyc}	cyclic pitch angle of a main rotor blade
τ_B	external moment applied along body frame
$\phi.\theta, \psi$	angular position
ω_B	angular velocity
$\dot{\omega}_B$	angular acceleration
Ω, Ω_T	main and tail rotor angular velocity
η	main blade orientation angle
η_{max}	main blade orientation angle where $\beta_{max} isachieved$
$\mathbf{u}$	the control inputs without considering the rotors' actuation mechanism
$\mathbf{u}'$	the control inputs considering the rotors' actuation mechanism
ρ	air density

CHAPTER 1

INTRODUCTION

1.1 Background and Motivation

There is an increasing interest in autonomously controlling and stabilizing group formations of Unmanned Air Vehicles (UAVs) in the past decade. Autonomous formations of UAVs can be applied in situations and environments that are too hazardous for human interventions, or where minimal human supervision is desired. These tasks may be also too repetitive, or even impossible for human pilots. The military applications include border control, surveillance, synthetic aperture imaging with cluster of micro-satellites, and intelligence collection. On the other hand, civilian uses are forest fire monitoring and fighting, grid searching, inspection of pipelines, farm spraying, and search and rescue. For fire prevention, the UAVs can focus on one spot while maintain the formation. For the pipelines inspection, it does not need the layout information of the pipes. Instead, the UAVs track the pipelines with a certain distance above them. It can significantly improve the efficiency when it comes to the grid searching, farm spaying, and search and rescue. Other advantages of autonomous formation control are that it does not involve the design and building of full scale aircrafts to carry human operators, or the expensive training of the pilots.

Advances in computation capabilities, sensor technology, wireless communication, and differential GPS have led the development of advanced control technologies for coordinating and formatting multi-vehicle systems. As a result, it is possible to assemble small size, light, and efficient micro-processor, sensor, and wireless network devices to the small UAVs. The differential GPS system only has a degradation of just 0.22 m per 100 km [22], which is accurate enough for the formation control even considering the small sizes of the agents in the formation. Also, the research results in advanced controls and nonlinear dynamic modeling make it possible for the distributed control over wireless networks, and the modeling of highly nonlinear dynamics of light fixed-wing aircraft [24].

It is fundamental that in the formation flying, the UAVs are able to follow global trajectories and maintain the group formation at the same time. The group of UAVs can be considered as a mobile network system, which has the capabilities of agent-to-agent and

agent-to-ground communication, navigation, trajectory following, stabilization, and collision avoidance. The control system is capable of maintaining the dynamic system stable and giving high system performance and robustness to uncertainty and disturbance.

In this work, efforts are emphasized on the autonomous formations control of helicopters. The existing literature contains many methods in this area [4], [11], [3], [25], [33], [26], [6], and [8]. However, cooperative control of helicopters still faces many theoretical and technical challenges. The modeling of helicopter dynamics in the existing research results are usually governed by a set of simplified and linearized differential equations. This type of model sometimes is not accurate enough to represent the true dynamics of the helicopters. There is no study about the direct control of positions of the servo motors on the helicopters in the formation formatting. Furthermore, some parameters in the helicopter model inherits uncertainties. The unknown factors, such as wind disturbance, are also increasing the difficulty of achieving the control goal.

1.2 Scope and Objectives

This study emphasizes on a sliding control strategy for controlling a group of autonomous helicopters in arbitrary formations. The small scaled electric helicopter Ikarus ECO is employed for the convenience of system dynamics model. Formation control is to get a group of robots into and maintain a certain formation. Trajectory tracking is a platform based on which the formation control law is designed. Due to the uncertainties in the model dynamics and the wind disturbance, Sliding Mode Control is employed due to its advantage of dealing with the model uncertainties and perturbations. Global obstacle avoidance is achieved by defining the trajectory of the leader in the group, which makes sure the group as a whole does not collide. Local obstacle avoidance is not considered in this work.

First, a 6 DOF dynamic model of the helicopter is to be developed. Input-output equations are to be derived from the position analysis, velocity analysis, and acceleration analysis for the controller design. In this case, the controller produces four inputs, the main rotor thrust, the roll and pitch moments, and the tail rotor thrust. The motors' actuation mechanism of the helicopter is to be further investigated to be incorporated for a new controller design, which is more related to the real helicopter model. The parameter uncertainties in the dynamic model and wind disturbance are considered in the controller design. Also, it is necessary to present the numerical examples and simulation results to illustrate the effectiveness and robustness of the method.

Thus, the objective of this thesis is to first build a six DOF dynamic model and incorporate the rotors' aerodynamic models and the actuation mechanism model, then to design a control scheme that is robust in presence of the parameter uncertainties in the dynamic model and wind disturbance. The control scheme, which can be categorized as a follow-

leader approach for formation control, is to be developed so that the spatial distance and view angle of a helicopter with respect to a neighboring helicopter can be controlled and stabilized. The controller outputs have to be consistent with the real helicopter system.

1.3 Organization of Thesis

The thesis is organized as follows: Relevant literature survey is reviewed in Chapter 2. The dynamic model of a helicopter and the controller design are introduced and the simulation results are given in Chapter 3. In Chapter 4, the results of a new controller design when motors' actuation mechanism is considered are presented and the corresponding simulation results are shown. Chapter 5 is devoted to the hardware test for the helicopters servo motors. Finally, the summary and future recommendations are given in Chapter 6.

CHAPTER 2

LITERATURE REVIEW

2.1 Introduction

Recent developments in robotics have been applied to deploy groups of ground robots for the purposes such as surveillance and research. However, ground vehicles have the limitations because of the ground conditions and the obstacles that cannot be avoided. Unmanned Air Vehicle (UAV) systems can overcome these limitations to achieve their goals, to perform certain actions, or to collect data and information. UAVs have not only become an important part of military forces, but are considered for potential civilian applications, such as bridge inspection, disaster monitoring, border patrol, rescuing, environmental information collection. UAVs are also used for tasks that are too hazardous for manned aircrafts.

Coordination of multiple UAVs to perform such tasks remains a challenging area. Many interesting results have been reported in both the formation control and trajectory tracking control. Formation control is to get a group of robots into and maintain a certain formation. Trajectory tracking is a platform based on which the formation control law is designed. In this report, a review of the current Unmanned Air Vehicle systems is presented. Then, some results in formation control and trajectory tracking control for UAVs are studied. Sliding Mode Control (SMC) is employed in the controller design. Some brief introduction of SMC is also presented in this chapter. Finally, a comparison of our work with the previous results is discussed.

2.2 Unmanned Aerial Vehicles

Unmanned air vehicles are self-propelled air vehicles that are either remotely controlled or are capable of conducting autonomous operations [1]. The first generation UAVs started in the late 1970's. The information can be found in [30]. Generally speaking, there are three categories of UAVs: tactical, vertical takeoff and landing and endurance. Tactical UAV systems (RQ-7 Shadow 200, for example) have been used for the applications such as carrying day cameras or thermal imaging and infrared cameras, laser target designations,

and communication functions. Vertical takeoff and landing UAVs have two categories: helicopter types and transitional types. The transitional categories (the Bell Eagle Eyes) have the ability of vertical lift like a helicopter with the speed of a turboprop airplane. The endurance category (Global Hawk, produced by Northrop Grumman Corp) applies the UAVs that can work for the duration from 12 to 72 hours and altitudes above 20,000 feet [10].

The model that is to be used further in this project is a Maxi-Joker 2. It has a main rotor diameter of 1.8 m and can lift a weight of 2 kg. A rotorspeed of 1200-1300 rpm can be achieved. With a payload of 2 kg the all-up weight is about 8.0 kg. Equipped with a 10S3P-battery, a flight time up to 20 min can be reached, depending on the payload [20]. However, due to the unconducted system identification procedures, the simulation sets use the parameters of the Ikarus ECO electric helicopter.

2.3 Trajectory Tracking Control

Trajectory tracking control is served as a platform based on which the formation control law is designed. In many of mission scenarios UAV will be required to follow inertial reference trajectories accurately in 3D space, such as landing at an airport, terrain following and air combat maneuver. For common practice, the command given to an UAV may be flying from an initial location through a number of way points and performs some predefined maneuver when the final location is reached [31].

The approximate input-output linearization algorithm is applied in reference [17]. An output (positions and heading) controller is designed to track the path. The approximate input-output linearization designed in this work overcomes the limitation that the traditional input-output linearization is only valid for the minimum phase nonlinear system. The traditional method in non-minimum phase system will lead to high gain in the controller. In this work, the coupling between rolling (pitching) moments and the lateral (longitudinal) accelerations is neglected, which results in an approximated system with dynamic decoupling.

Mokhtari, M'Sirdi, Meghriche, and Belaidi [21] propose a control strategy including a linear Luenberger observer, an adaptive estimator, and a feedback linearization controller for a special kind of UAVs called quadrotor UAVs. First, a dynamic model of a quadrotor helicopter is developed. Then, three parts of the control method are derived respectively. The linear Luenberger observer is to reconstruct the non-available variables needed to make sure the robustness of the control law. The adaptive estimator is to estimate the effect of the external disturbances. As a result, this part reinforce the stability of the overall system. The feedback linearization control law allows good covergence of estimated values and satisfies tracking errors of desired trajectories with the existence of the disturbances.

This strategy also helps reduce the number of sensors to be used.

In [2], the authors propose a controller architecture that combines adaptive feedforward neural networks with feedback linearizaiton. The scheme is effective for both linear-in-the-parameters networks and the single-hidden-layer perceptron neural networks. In this work, the work has been done in the area of nonlinear, adaptive, and neural network flight controls has been briefly reviewed. It's noticed that artificial neural networks have the capability to approximate continuous nonlinear functions, which makes it as an ideal candidate for the adaptive control. Another advantage of the neural network over the traditional table lookup method is that it decrease the time for the calculation. However, it's also advised that it's difficult to incorporate the real helicopter model into the controller design in this method.

Wang and Gao [31] propose a control system design strategy for UAV trajectory tracking basing on the kinematics aircraft model. The control system includes three subsystems: command generation, transformation, and allocation. The robustness to the disturbance, such as wind and sensor noise, is enhanced by adopting a nonlinear disturbance observer. This method overcomes the disadvantages of the likely saturation, stability problems, and time-consuming problems from multi-loop hierarchical trajectory track control systems, and the poor generality from the approach that all loops are designed simultaneously.

In [23], three control approaches for a constrained nonlinear tracking for a small fixed-wing UAV have been examined. Instead of using twelve-state modeling, this work adapts a six-state model, such as heading, air speed, and altitude command inputs. Three different approaches based on the state dependent Riccati equation (SDRE), Sontag's formula, and a constrained control Lyapunov Function are compared graphically to show the disadvantages and advantages under different scenarios. Another contribution of this work is applying the well developed SDRE methodology and Sontag's formula to the UAV trajectory tracking problem.

In [19], the new image technologies and the advances in control have been combined together to achieve desired trajectory tracking control of UAVs. The authors develop a visual tracking control strategy for monitoring of structures and maintenance of bridges. The predefined trajectory is defined by a series of prerecorded images. The homographies are extracted using the current image, the corresponding desired image and a unique reference image. A parameter is then obtained by extracting the pose parameter from the homographies. An adaptive update law to estimate this unknown parameter is presented.

In [15], the output regulation is employed to a UAV trajectory tracking problem. The output regulation is also called servomechanism problem, where the reference trajectories and the disturbance are generated by an autonomous differential equation. It has the advantages of coping with uncertainties and dealing with a large class of complex system. It is more efficient than solving nonlinear differential equations of the servomechanism control

law.

In [3], multiple low-altitude and short-endurance UAVs are employed to monitor and track the forrest fires. The information about the progress of the fire is essential for the fire fighting and rescuing. Furthermore, the UAVs have more advantages than the ground vehicles and fire fighters. The method provides effective UAV path planning algorithm using infrared images that are collected onboard in real time. A EMBYR model is simulated for the propagation of a forest fire and then is integrated into the Simulink for the simulation. A new cooperative control mission concept is also addressed. The problems like coordination of UAV paths to cover the most critical areas, when and which UAV should be taken down for refueling, and how to measure the performance of the entire fleet of UAVs are considered as well.

In [11], the authors introduce and implement the safety critical avionics for the DragonFly UAVs. The server-client architecture of QNX Neutrino is used in the software architecture. The architecture is hierarchical and modular: it isolates user-defined applications from underlying low-level system that services for implementing inter-process communication, data-acquisition, and associated hardware management. Also, a new run-time scheduling algorithm to maximize the execution of tasks within a given deadline is employed. A compact avionics package that includes flight computer, data acquisition system, communications system, and GPS receiver, is built. Results of the avionic in car tests are also presented.

Formation control is to get a group of robots into and maintain a certain formation. Trajectory tracking is a platform based on which the formation control law is designed. The existing trajectory control methods do not apply for formation control problems. Formation control shemes must be studied separately.

2.4 Formation Control

Over the past few years, research on the coordination of multiple UAVs to get into and maintain a certain formation, such as rectangle or chain, has gained increasing interest. UAVs are capable to fly in a certain formation in and out of restricted areas that are considered too difficult or too dangerous for human pilots.

In [7], a controller for a two-aircraft formation is designed. It allows both trajectory tracking and formation geometry keeping. First, the distributed Horse-Shoe Vortex technique is used to achieve the aerodynamic coupling effects modeling. Then, a control strategy based on the behavior of migratory birds is proposed. Instead of the agents in the formation refer to each other, they are required to keep a specified distance from an imaginary point called Formation Geometry Center (FGC).

Formation control of two aircrafts using PID feedback is presented in [10]. The dynamics

of the two aircrafts are linearly modeled and coupled due to the kinematic effects. Simple aircraft models including Mach-, heading-, and altitude-hold autopilots in the inner loops are used. Furthermore, additional aerodynamic coupling effects are introduced due to the close formation. Finally, simulation results are presented for trajectory tracking and formation keeping.

In [8], a control scheme that is suitable for tight UAVs formation maneuvers at high Euler angles and moderately high angular rates flying is designed. A set of research UAVs is designed, built and instrumented. The identification of linear and nonlinear aircraft mathematical models from collected flight data is performed. The controller has the inner loop and the outer loop. The innerloop controller design is to increase the feedback gain as much as possible to achieve desirable disturbance attenuation along with desirable tracking capabilities. The outerloop controller consists of a 'vertical' block and a 'horizontal' block. The Robustness of the formation controller is assessed through a simulation study where the adverse effect on the closed-loop stability and tracking performance caused by the measurement noise and modeling error is evaluated. A two-aircraft testing result validates the design.

Work [27] studies the invertibility of input-output formation maps and the design of a robust nonlinear control system for a group of unmanned aerial vehicles. The inversion is achieved by introducing a simplified wind coordinate system. Then, a variable structure control law is obtained for the leader velocity, heading angle and flight path angle; variable structure control laws are also designed for the follower's trajectory tracking. These control laws asymptotically track each aircraft while the leader track the predefined path. Only the states and control input information from the preceding aircraft are needed for each follower. The main contribution of this work is investigating the inversion of certain input-output formation mapping.

In [18], the authors develop a fuzzy logic navigation method for close formation control of multiple UAVs. This method does not have to use the timely and accurate measurements. No communication link between two aircraft is needed to separate the follower from the leader while maintaining certain formation. The linguistic terms of the fuzzy logic controller output for trailing UAV are selected as the main parameters for optimization. The controller is able to estimate sufficient lateral and longitudinal distance under the system uncertainties and external bounded vortex disturbance.

Another interesting idea is presented in [28] where the authors design a feedback linearizing nonlinear adaptive control system for a group of UAVs in close formation flight. Backstepping design technique is employed for the adaptive control law. This work only considers each UAV as a point mass, instead of dealing with the 6 DOFs model of the aircrafts. This gives less accuracy, but simplifies the design of the formation flight control system. The longitudinal and lateral control systems are derived separately. It is noticed

that a decentralized control system is obtained from an overparameterization in the design process. Furthermore, the stability of the zero-error dynamics is examined, which leads to the stability of the closed-loop system.

In [33], the researchers build a hierarchical formation control system consisting two parts: the lower layer has the off-the-shelf autopilots capable of trajectory generation in waypoint mode or holding mode, and the higher layer has two nonlinear controllers that is integrated with an extremum-seeking algorithm, which can seek the maximum induced lift for the follower UAV. The higher layer does not need the information of the leader's velocity or acceleration.This control strategy is able to coordinate a group of UAVs to perform complex navigation tasks with limited communication overhead. Finally, the simulation results are presented to validate the performance of the controller design.

A different idea is pursued in [32], in which a formation controller that includes two modes, the safe mode and the danger mode, is developed. The safe mode is when there are no obstacles in the environment and the danger mode is when there is a possibility of collision or there are expected obstacles in the path. The formation is kept in the safe mode and broken in the danger mode. But the agents in the formation can rejoin each other when the path is clear again. The control strategy contains a two layered hierarchical structure in these two modes. A control structure with relative motion dynamics generates the path for the UAVs in the safe mode and a decentralized algorithm using a modified Grossberg Network for the danger mode.

In [9], the general model of the cooperation among UAVs is presented. Cooperation is fundamental for any collaborative group activity for UAVs formation. It focuses on the implicit sense of plan sharing where agents modify their plans considering other agents' plans and on how agents team up to form a collaborative pattern to achieve their goals. However, the work assumes that all agents are identical in every aspect. It is also assumed that the agents possess identical capabilities and limitation. These assumptions limit the scope of the work. Because the general model introduced here is not decentralized, use of different agents is not possible.

The work [12] describes the approach for performing vision-based UAVs formation control with the obstacles. There is no information communication between aircrafts. Instead, the passive 2-D vision information is employed to keep the formation. The controller estimates the range from 2-D vision information by using Extended Kalman Filters. Another alternative way is regulating the size of the image subtended by a leader aircraft on the image plane. The situation that the image size is not reliable is also considered. In this case, the bearing-only information is used. This is done by the design of a time-dependent formation geometry. Furthermore, the robustness to the unknown leader aircraft acceleration has been achieved by the Extended Kalman Filter with an adaptive neural network.

In the work of [5], a second/high order sliding mode formation controller consisting

three parts: tracking, placement, and anti-collision, is designed. The formation is obtained using triangular patterns following an original expansion process. The leader can track the predefined trajectory in the existence of the unknown bounded disturbances. The followers are to initiate and keep the formation. The placement part makes sure that no immediate lateral neighbors receives position commands in distance to the leader and the controller is to achieve satisfied placement. The anti-collision part makes sure the immediate lateral neighbors receive a set of safety distance from the neighbors. This strategy guarantees a robust, continuous, and smooth control that is suitable for the autopilots.

In [4], stabilizing and maneuvering a formation of UAVs have been studied. A generalized model predictive control algorithm is obtained that extends the existing theory that considers velocity control of kinematic robots. The model for each agent is nonlinear and constrained dynamics. The model predictive control is, in certain circumstance, the only way for control of systems that are with constrained dynamics. The distributed and synchronized model predictive control computes the effects of model errors between vehicles. The controller allows that agents are stabilized to a set of permissible equilibria, rather than a precise location for each vehicle in the formation.

Research efforts [6] are emphasized on the two-loop control approach to UAVs close-formation flight. A standard decentralized linear quadratic regulator (LQR)-based control structure is synthesized for each agent and for formation position error control using linearized equations of motion and a lifting line model of the aircraft wake. Another contribution of this work is that a formation management structure is defined, which is able to handle with situations like aircraft loss, transmitter failure, and receiver failure. The procedure is developed using a decentralized approach and relies on the Dijkstra algorithm.

Saber and Murray [25] propose a dynamic graph theoretic framework that enables modeling the flocking of agents in presence of multiple obstacles. First, the spatially induced graphs are used to define the nets and flocks, and framenets and energy of dynamics are presented. Then, flocking without any obstacles is discussed. The notion of α net is introduced and the flocking is achieved through dissipation of structural energy of a dynamic α-net. Finally, the approach to flocking with multiple obstacle avoidance for a dynamic α-net is summarized. However, the stability for this algorithm is not analyzed thoroughly.

In [34], emphasis is put on a hybrid structure to enable effective switching between formation keeping modes and formation reconfiguration modes. The group is able to start from the given initial configurations and reach the final configuration with the specified time by minimizing a given cost function. In addition, it has to consider the facts that there are certain inter- and intra- vehicles constraints. The problem is defined as Formation Reconfiguration Planning. The advantage of this approach is that on line formation reconfiguration can be more efficiently achieved and all the computationally intensive tasks involving optimizations are performed off-line. The assumption for this method is that all

information is accessible, which is very difficult in actual flight.

It is noticed that more effort on formation control has been emphasized on the generic fixed wing vehicles, the formation schemes are not truly 3-dimensional, dynamic model of the vehicles is simplified, and the robust controller design for formation control has not be considered. These shortcomings are to be addressed by considering helicopters specificly, by defining 2-D formation control schemes, by using full dynamic model of the helicopter, and by using robust sliding Mode Method. Furthermore, the method has to be decentralized. As a result, use of different agents in the group is possible.

In our work, a control algorithm for forming an arbitrary formation of multiple autonomous helicopters is studied. A leader-follower approach is presented to coordinate multiple helicopters to accomplish a common objective. One contribution of our work is that we consider a six DOFs dynamic model of the helicopter with the modeling of rotor's actuation mechanism in the controller design. Sliding mode control is successfully employed due to its advantage of dealing with uncertainties and disturbances. The helicopter controls its relative distance and orientation with respect to a neighbor helicopter (or called its 'leader'). The parameter uncertainties, model uncertainties, and perturbations are also considered in the controller design.

Chapter 3

Controller Design with Rotors' Forces and Moments as Inputs

In this chapter, a sliding mode controller, with rotors' thrusts and torques as outputs, is to be designed. The controller can be used to form arbitrary formations of multiple autonomous helicopters. A six-degree-of-freedom dynamic model needs first to be developed for the helicopters. A leader-follower scheme is chosen. In this scheme, a virtual helicopter is assumed as a group leader. The formation controller only needs to control the internal geometry of the formation, which is the 3D vectorial relative position of a helicopter with respect to a neighboring helicopter.

The chapter outline is as follows: First, the dynamic model of a helicopter is presented. Then, inputs and outputs of the controller are analyzed. Based on the kinematic analysis (position analysis, velocity analysis, and acceleration analysis), the input-output equations are derived. The sliding mode controller is designed. Finally, numerical examples and simulation results are given to show the effectiveness and robustness of the controller.

3.1 Dynamic Model of a Helicopter

This section describes the dynamic model of a helicopter shown in Fig. 3.1. The equations of motion for a helicopter are presented in a form that is useful for controller design. The following control inputs are assumed:

- T: The main rotor thrust
- T_T: The tail rotor thrust
- M_ϕ: The roll torque
- M_θ: The pitch torque

All the equations are written in the helicopter body frame, whose orientation is expressed by three Euler (ZYX) angles, rotation ψ about z-axis, θ about y-axis, and ϕ about x-axis.

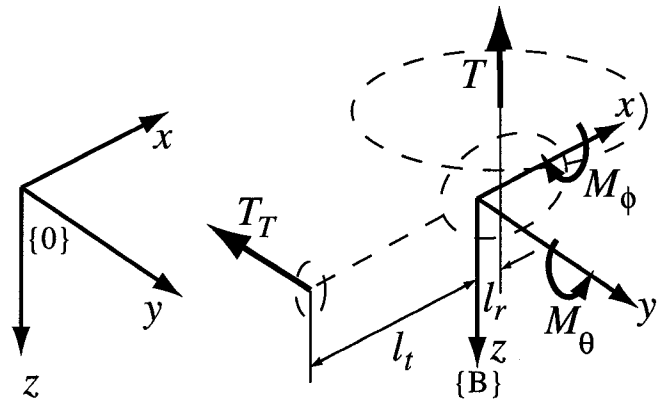

Figure 3.1: A 6 DOF dynamic model of a small helicopter with control inputs

z, y, and x are the body frame, with the origin at the helicopter's central of gravity. z is chosen to be downwards to comply with the aerospace engineering convention. ψ, θ, and ϕ are the yaw, pitch and roll angels, respectively. The following matrix represents this orientation:

$$\begin{aligned}\mathbf{R}_{IB} &= e^{(\hat{z}\times)\psi}e^{(\hat{y}\times)\theta}e^{(\hat{x}\times)\phi} \\ &= \begin{bmatrix}\cos\psi & -\sin\psi & 0\\ \sin\psi & \cos\psi & 0\\ 0 & 0 & 1\end{bmatrix}\begin{bmatrix}\cos\theta & 0 & \sin\theta\\ 0 & 1 & 0\\ -\sin\theta & 0 & \cos\theta\end{bmatrix}\begin{bmatrix}1 & 0 & 0\\ 0 & \cos\phi & -\sin\phi\\ 0 & \sin\phi & \cos\phi\end{bmatrix}\end{aligned} \tag{3.1}$$

Although this representation is singular at $\theta = \pm\frac{\pi}{2}$, the helicopter is not expected to operate in those orientations (pointing straight up or down). It is important to be able to write the inertial angular velocity of the helicopter frame described in the local frame in terms of the derivative of the Euler (ZYX) angles as:

$$\boldsymbol{\omega}_B = \begin{bmatrix}1 & 0 & -\sin\theta\\ 0 & \cos\phi & \cos\theta\sin\phi\\ 0 & -\sin\phi & \cos\theta\sin\phi\end{bmatrix}\begin{bmatrix}\dot{\phi}\\ \dot{\theta}\\ \dot{\psi}\end{bmatrix} \tag{3.2}$$

If $[x_I, y_I, z_I]$ donates the inertial coordinates of the helicopter's center of mass, three translational equations of motion are:

$$m\begin{bmatrix}\ddot{x}_I\\ \ddot{y}_I\\ \ddot{z}_I\end{bmatrix} = \mathbf{R}_{IB}\begin{bmatrix}f_{Bx}\\ f_{By}\\ f_{Bz}\end{bmatrix} \tag{3.3}$$

where $\mathbf{f}_B = [f_{Bx}, f_{By}, f_{Bz}]^T$ is the resultant force vector expressed in the body coordinates. The three rotational equations of motion in body coordinate are:

$$\mathbf{I}\dot{\boldsymbol{\omega}}_B + \boldsymbol{\omega}_B \times \mathbf{I}\boldsymbol{\omega}_B = \boldsymbol{\tau}_B \tag{3.4}$$

where $\mathbf{I}$ is the moment of inertia with regard to the body frame B.

$$\mathbf{I} = \begin{bmatrix} I_{xx} & 0 & -I_{xz} \\ 0 & I_{yy} & 0 \\ -I_{xz} & 0 & I_{zz} \end{bmatrix} \tag{3.5}$$

and $\tau_B = [\tau_{Bx}, \tau_{By}, \tau_{Bz}]^T$ is the resultant torque vector in body frame. Assume the state variable vector as:

$$\mathbf{q} = \begin{bmatrix} x_I & y_I & z_I & \dot{x}_I & \dot{y}_I & \dot{z}_I & \phi & \theta & \psi & \omega_{Bx} & \omega_{By} & \omega_{Bz} \end{bmatrix} \tag{3.6}$$

The first order equations of motion are derived as follows. The kinematic translational equations of motion are:

$$\begin{bmatrix} \dot{x}_I \\ \dot{y}_I \\ \dot{z}_I \end{bmatrix} = \begin{bmatrix} u_I \\ v_I \\ w_I \end{bmatrix} \tag{3.7}$$

The inertial frame force balance can be derived from Eq. (3.3):

$$m \begin{bmatrix} \dot{u}_I \\ \dot{v}_I \\ \dot{w}_I \end{bmatrix} = \mathbf{R}_{IB} \begin{bmatrix} f_{Bx} \\ f_{By} \\ f_{Bz} \end{bmatrix} \tag{3.8}$$

According to Eq. (3.2), the kinematic relation for Euler angles and angular velocity is as follows:

$$\begin{bmatrix} \dot{\phi} \\ \dot{\theta} \\ \dot{\psi} \end{bmatrix} = \begin{bmatrix} 1 & \sin\phi\tan\theta & \cos\phi\tan\theta \\ 0 & \cos\phi & -\sin\phi \\ 0 & \sin\phi\sec\theta & \cos\phi\sec\theta \end{bmatrix} \begin{bmatrix} \omega_{Bx} \\ \omega_{By} \\ \omega_{Bz} \end{bmatrix} \tag{3.9}$$

$$\begin{bmatrix} \dot{\omega}_{Bx} \\ \dot{\omega}_{By} \\ \dot{\omega}_{Bz} \end{bmatrix} = \mathbf{I}^{-1}\{ \begin{bmatrix} \tau_{Bx} \\ \tau_{By} \\ \tau_{Bz} \end{bmatrix} - \boldsymbol{\omega}_B \times \mathbf{I}\boldsymbol{\omega}_B \} \tag{3.10}$$

The forces acting on the helicopter are:

$$\mathbf{f}_B = \begin{bmatrix} -D_x \\ -D_y - T_T \\ -D_z - T \end{bmatrix} + \mathbf{R}_{IB}^T \begin{bmatrix} 0 \\ 0 \\ mg \end{bmatrix} \tag{3.11}$$

$$\boldsymbol{\tau}_B = \begin{bmatrix} M_\phi \\ M_\theta + Tl_r \\ M_\psi + \tau_m \end{bmatrix} \tag{3.12}$$

where D_x, D_y, and D_z are the drag forces. M_ϕ, M_θ, and M_ψ are the roll, pitch, and yaw moments generated by the rotors, respectively. τ_m is the motor torque. If the center of gravity is towards the front with respect to the rotor axis, l_r is positive. τ_m is a function of T: $\tau_m = -k_m T$. A negative τ_m indicates that the rotor is rotating about the positive $\hat{z}$ direction so that the reaction torque on the helicopter is about the negative $\hat{z}$ axis. Substituting Eq. (3.11) into Eq. (3.8) results in:

$$\begin{bmatrix} \dot{u}_I \\ \dot{v}_I \\ \dot{w}_I \end{bmatrix} = \frac{1}{m}\mathbf{R}_{IB} \begin{bmatrix} 0 \\ -T_T \\ -T \end{bmatrix} + \frac{1}{m}\mathbf{R}_{IB} \begin{bmatrix} -D_x \\ -D_y \\ -D_z \end{bmatrix} + \begin{bmatrix} 0 \\ 0 \\ g \end{bmatrix} \tag{3.13}$$

Substituting Eq. (3.12) into Eq. (3.10) and assuming $I_{xz} = 0$:

$$\begin{bmatrix} \dot{\omega}_{Bx} \\ \dot{\omega}_{By} \\ \dot{\omega}_{Bz} \end{bmatrix} = \begin{bmatrix} M_\phi / I_{xx} \\ (M_\theta + Tl_r)/I_{yy} \\ (T_T l_t - k_m T)/I_{zz} \end{bmatrix} - \mathbf{I}^{-1}\{\boldsymbol{\omega}_B \times \mathbf{I}\boldsymbol{\omega}_B\} \tag{3.14}$$

3.2 Proposed Formation Control Scheme

Formation control is to coordinate the behavior of multiple robots, aircraft, spacecraft, underwater vessels, and surface vehicles. The most fundamental goal of all these applications is to coordinate multiple agents to accomplish a common objective. In this work, the bulk motion of the whole group of helicopters can be determined by common trajectory planning. A virtual helicopter is assumed as a group leader, who adapts the bulk motion of the group as its desired trajectory. Any helicopter in the group follows either the virtual leader or their neighboring helicopter. As a result, the formation control is now equal to the control of the internal geometry of the formation, which is defined based on the relative position of neighboring helicopters. A control scheme, called $l - \alpha$ (Fig. 3.2), is developed in this work that controls the 3D vectorial relative position of a helicopter with respect to a neighboring helicopter.

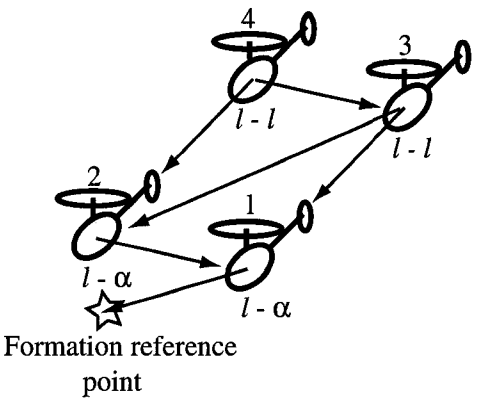

Figure 3.2: General formation control configuration

First, a reasonable formation scheme for $l - \alpha$ should be defined. Things to note are:

1. The helicopters are separated by a vectorial distance $\mathbf{l}_{12} + \mathbf{z}_{12}$ between the centre of the mass of the leader and an arbitrary control point, p, on follower helicopter. The arbitrary point has a fixed distance d with the centre of mass along the negative z direction of the body frame $\{2\}$.

2. If the control point is chosen from some point in the local frame of the follower (for example, the CG of the follower helicopter) instead of p, roll and pitch motions of the follower will not affect the controller outputs. Then the controller will be blind to the roll and pitch disturbances, which will be disastrous.

3. The control point is chosen somewhere on the local frame z-axis. This choice makes the yaw dynamics of the helicopter decoupled from the other degree-of-freedom.

4. The control point must be on the negative local z-axis. This makes more sense physically. If the leader goes forward the follower has to go forward. To go forward the follower has to gain a negative pitch. This helps the control point catch up with the leader faster. The same argument can be made for the roll angle and lateral motion.

The $\mathbf{l}_{12}$ vector is chosen to be in the leader's $x - y$ plane and the $\mathbf{z}_1$ vector to be always perpendicular to the $\mathbf{l}_{12}$ vector (or leader's $x-y$ plane). These ensure that the 3D formation will be kept as a solid structure, and simplify the derivation of the input-output relations.

3.2.1 Input-Output Analysis

The formation parameters that define the formation internal geometry are $l_{12}, \alpha_{12}, z_{12}$, and ψ_2. These are also the controller outputs. The control inputs are T, T_T, M_ϕ, and M_θ. The input-output equations are needed for the sliding mode controller design.

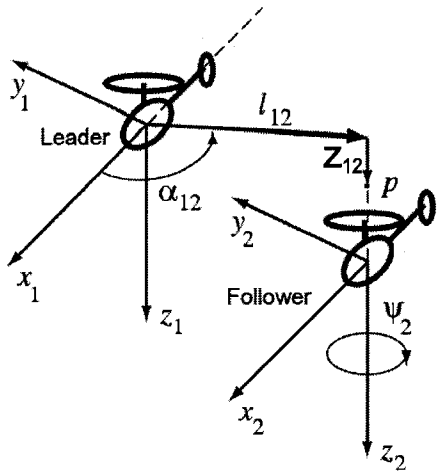

Figure 3.3: $l - \alpha$ control configuration

3.2.2 Kinematic Analysis

Position Analysis. It is necessary to do the kinematic analysis in order to find the errors and input/output equations. They are very important in order to find the control law of the $l - \alpha$ scheme. Furthermore, $l_{12}, \alpha_{12}, z_{12}$ are solved in the position analysis.

The moving body frames of both the leader and the follower helicopters are considered (Fig. 3.3). Two points, point p_1, attached to frame $\{1\}$, and point p_2, attached to frame $\{2\}$ are assumed. In frame $\{1\}$, the position vector of the control point p expressed in the local frame of the leader is as follows:

$$\mathbf{P}_{p/1}^{(1)} = l_{12}\cos\alpha_{12}\hat{\mathbf{i}}_1 + l_{12}\sin\alpha_{12}\hat{\mathbf{j}}_1 + z_{12}\hat{\mathbf{k}}_1 \tag{3.15}$$

In frame $\{2\}$, the position vector of the control point p relative to the origin of the local frame of the follower is defined as follows:

$$\mathbf{P}_{p/2}^{(2)} = -d\hat{\mathbf{k}}_2 \tag{3.16}$$

The position vectors of the leader and follower expressed in the inertial frame are described separately as follows:

$$\begin{aligned} \mathbf{P}_1^{(0)} &= x_1\hat{\mathbf{i}}_1 + y_1\hat{\mathbf{j}}_1 + z_1\hat{\mathbf{k}}_1 \\ \mathbf{P}_2^{(0)} &= x_2\hat{\mathbf{i}}_1 + y_2\hat{\mathbf{j}}_1 + z_2\hat{\mathbf{k}}_1 \end{aligned} \tag{3.17}$$

All the vectors will be expressed in frame $\{1\}$ for simplicity of formulations. The transfor-

mation matrix that transforms frame $\{1\}$ into the inertial frame $\{0\}$ is:

$$\mathbf{R}_{01} = \begin{bmatrix} c\psi_1\, c\theta_1 & -s\psi_1\, c\phi_1 + c\psi_1\, s\theta_1\, s\phi_1 & s\psi_1\, s\phi_1 + c\psi_1\, s\theta_1\, c\phi_1 \\ s\psi_1\, c\theta_1 & c\psi_1\, c\phi_1 + s\psi_1\, s\theta_1\, s\phi_1 & -c\psi_1\, s\phi_1 + s\psi_1\, s\theta_1\, c\phi_1 \\ -s\theta_1 & c\theta_1\, s\phi_1 & c\theta_1\, c\phi_1 \end{bmatrix} \tag{3.18}$$

where $s = \sin$ and $c = \cos$; ψ_1, θ_1, and ϕ_1 are the yaw, pitch, and roll rotational degrees of freedom of helicopter 1. These Euler angles define the orientation of the body frame with respect to the inertial frame. Similarly, $\mathbf{R}_{02}$ will consist of ψ_2, θ_2, and ϕ_2. Then, the inertial position of the origin of frames 1 and 2 can be written as:

$$\begin{aligned} \mathbf{P}_1^{(1)} &= \mathbf{R}_{01}^T \mathbf{P}_1^{(0)} \\ \mathbf{P}_2^{(1)} &= \mathbf{R}_{01}^T \mathbf{P}_2^{(0)} \end{aligned} \tag{3.19}$$

From the configuration $(l - \alpha)$ shown in the figure:

$$\mathbf{P}_1^{(1)} + \mathbf{P}_{p/1}^{(1)} = \mathbf{P}_2^{(1)} + \mathbf{P}_{p/2}^{(1)} \tag{3.20}$$

Since the position of the leader, $\mathbf{P}_1^{(1)}$, and the position of the follower, $\mathbf{P}_2^{(2)}$, are assumed to be known from on-board sensors, all terms in Eq. (3.20) are at hand except $\mathbf{P}_{p/2}^{(1)}$:

$$\mathbf{P}_{p/2}^{(1)} = \mathbf{R}_{01}^T \mathbf{P}_{p/1}^{(0)} \tag{3.21}$$

$$\mathbf{P}_{p/2}^{(2)} = \mathbf{R}_{02}^T \mathbf{P}_{p/2}^{(0)} \tag{3.22}$$

or

$$\mathbf{P}_{p/2}^{(0)} = \mathbf{R}_{02} \mathbf{P}_{p/2}^{(2)} \tag{3.23}$$

Combining Eq. (3.22) and Eq. (3.23) results in:

$$\mathbf{P}_{p/2}^{(1)} = \mathbf{R}_{01}^T \mathbf{R}_{02} \mathbf{P}_{p/2}^{(2)} \tag{3.24}$$

Therefore, Eq. (3.20) becomes:

$$\mathbf{P}_{p/1}^{(1)} = \mathbf{R}_{01}^T (\mathbf{P}_2^{(0)} - \mathbf{P}_1^{(0)}) + \mathbf{R}_{01}^T \mathbf{R}_{02} \mathbf{P}_{p/2}^{(2)} \tag{3.25}$$

where $\mathbf{P}_{p/2}^{(2)} = [0, 0, -d]^T$.

As long as position and orientation of $\{1\}$ and $\{2\}$, i.e. $[x_1, y_1, z_1, \psi_1, \theta_1, \phi_1]$ and $[x_2, y_2, z_2, \psi_2, \theta_2, \phi_2]$, are known from the on-board sensors, the components of $\mathbf{P}_{p/1}^{(1)} = [P_{p/1x}, P_{P/1y}, P_{p/1z}]^T$ can

be calculated. From Eq. (3.15), the following can be obtained:

$$l_{12} = \sqrt{P_{p/1x}^2 + P_{p/1y}^2} \tag{3.26}$$

$$\alpha_{12} = \arctan\left(\frac{P_{p/1y}}{P_{p/1x}}\right) \tag{3.27}$$

$$z_{12} = P_{p/1z} \tag{3.28}$$

Note that these three formation parameters will be the controller output. ψ_2, the yaw angle of the helicopter, will be the fourth output. Defining the desired values for l_{12}, α_{12}, z_{12} and ψ_2 is straightforward, since they come from the geometry of the desired formation.

Velocity analysis. Velocity analysis is undertaken in this section. Through the velocity analysis, the expressions of $\dot{l}_{12}$, $\dot{\alpha}_{12}$, and $\dot{z}_{12}$ can be derived, which is going to be used in the controller design.

Consider the control point p attached to the follower helicopter, the velocity of point p can be related to the velocity of the leader as follows:

$$\dot{\mathbf{P}}_p^{(1)} = \mathbf{V}_1^{(1)} + (\dot{\mathbf{l}}_{12} + \dot{\mathbf{z}}_{12}) + \boldsymbol{\omega}_1^{(1)} \times (\mathbf{l}_{12} + \mathbf{z}_{12}) \tag{3.29}$$

On the other hand, the velocity of point p in terms of the velocity of the follower's center of mass can be written as:

$$\dot{\mathbf{P}}_p^{(2)} = \mathbf{V}_2^{(2)} + \boldsymbol{\omega}_2^{(2)} \times \mathbf{d}_2^{(2)} \tag{3.30}$$

First $\dot{\mathbf{P}}_p^{(2)}$ must be written in frame 1. We have:

$$\dot{\mathbf{P}}_p^{(2)} = \mathbf{R}_{02}^T \dot{\mathbf{P}}_p^{(0)} \tag{3.31}$$

$$\dot{\mathbf{P}}_p^{(1)} = \mathbf{R}_{01}^T \dot{\mathbf{P}}_p^{(0)} \tag{3.32}$$

Combining Eq. (3.31) and Eq. (3.32) leads to:

$$\dot{\mathbf{P}}_p^{(1)} = \mathbf{R}_{01}^T \mathbf{R}_{02} \dot{\mathbf{P}}_p^{(2)} \tag{3.33}$$

Also,

$$\mathbf{V}_1^{(1)} = \mathbf{R}_{01}^T \mathbf{V}_1^{(0)} \tag{3.34}$$

and

$$\mathbf{V}_2^{(2)} = \mathbf{R}_{02}^T \mathbf{V}_2^{(0)} \tag{3.35}$$

Now, combining Eq. (3.34) and Eq. (3.29) results in:

$$\dot{\mathbf{P}}_p^{(1)} = \mathbf{R}_{01}^T \mathbf{V}_1^{(0)} + (\dot{\mathbf{l}}_{12} + \dot{\mathbf{z}}_{12}) + \boldsymbol{\omega}_1^{(1)} \times (\mathbf{l}_{12} + \mathbf{z}_{12}) \tag{3.36}$$

And combining Eq. (3.30), Eq. (3.33) and Eq. (3.35) gives:

$$\dot{\mathbf{P}}_p^{(1)} = \mathbf{R}_{01}^T \mathbf{R}_{02} (\mathbf{R}_{02}^T \mathbf{V}_2^{(0)} + \boldsymbol{\omega}_2^{(2)} \times \mathbf{d}_2^{(2)}) \tag{3.37}$$

Now, we can combine Eq. (3.36) and Eq. (3.37) to solve for $\dot{\mathbf{l}}_{12}$ and $\dot{\mathbf{z}}_{12}$:

$$(\dot{\mathbf{l}}_{12} + \dot{\mathbf{z}}_{12}) = \mathbf{R}_{01}^T (\mathbf{V}_2^{(0)} - \mathbf{V}_1^{(0)}) + \mathbf{R}_{01}^T \mathbf{R}_{02} (\boldsymbol{\omega}_2^{(2)} \times \mathbf{d}_2^{(2)}) - \boldsymbol{\omega}_1^{(1)} \times (\mathbf{l}_{12} + \mathbf{z}_{12}) \tag{3.38}$$

All the terms on the righthand side of Eq. (3.38) is known, so the unknown terms in the lefthand side of Eq. (3.38), $\dot{l}_{12}$ $\dot{\alpha}_{12}$ and $\dot{z}_{12}$ can be calculated. The RHS is assumed as $\dot{\mathbf{P}}_{p/1}^{(1)}$ or $\mathbf{V}_{p/1}^{(1)}$.

$$\begin{bmatrix} \dot{l}_{12}\cos\alpha_{12} - l_{12}\dot{\alpha}_{12}\sin\alpha_{12} \\ \dot{l}_{12}\sin\alpha_{12} + l_{12}\dot{\alpha}_{12}\cos\alpha_{12} \\ \dot{z}_{12} \end{bmatrix} = \begin{bmatrix} V_{p/1x} \\ V_{p/1y} \\ V_{p/1z} \end{bmatrix} \tag{3.39}$$

from which we can find:

$$\begin{aligned} \dot{l}_{12} &= V_{p/1x}\cos\alpha_{12} + V_{p/1y}\sin\alpha_{12} \\ \dot{\alpha}_{12} &= (V_{p/1y}\cos\alpha_{12} - V_{p/1x}\sin\alpha_{12})/l_{12} \\ \dot{z}_{12} &= V_{p/1z} \end{aligned} \tag{3.40}$$

Acceleration analysis. The derivation of the input-output description for the control system needs the information about the acceleration of $\ddot{\mathbf{l}}_{12}$ and $\ddot{\mathbf{z}}_{12}$. They are obtained by relating the absolute acceleration of the control point p attached to the follower and the absolute acceleration of the centre of mass of helicopter 2. Consider two coincident points, $p1$ and $p2$, at the instantaneous location of the control point p. It's assumed that point p_1 is attached to frame 1 and point p_2 is attached to frame 2. $\mathbf{a}_p^{(1)}$ and $\mathbf{a}_p^{(2)}$ are the acceleration of the point p expressed in frame 1 and 2.

The acceleration of point p can be related to the acceleration of the leader as follows:

$$\begin{aligned} \mathbf{a}_p^{(1)} &= \mathbf{a}_1^{(1)} + (\ddot{\mathbf{l}}_{12} + \ddot{\mathbf{z}}_{12}) + 2\boldsymbol{\omega}_1^{(1)} \times (\dot{\mathbf{l}}_{12} + \dot{\mathbf{z}}_{12}) \\ &+ \dot{\boldsymbol{\omega}}_1^{(1)} \times (\mathbf{l}_{12} + \mathbf{z}_{12}) + \boldsymbol{\omega}_1^{(1)} \times (\boldsymbol{\omega}_1^{(1)} \times (\mathbf{l}_{12} + \mathbf{z}_{12})) \end{aligned} \tag{3.41}$$

On the other hand, the acceleration of point p in terms of the acceleration of the follower's

center of mass can be written as:

$$\mathbf{a}_p^{(2)} = \mathbf{a}_2^{(2)} + \dot{\boldsymbol{\omega}}_2^{(2)} \times \mathbf{d}_2^{(2)} + \boldsymbol{\omega}_2^{(2)} \times (\boldsymbol{\omega}_2^{(2)} \times \mathbf{d}_2^{(2)}) \tag{3.42}$$

Equating Eq. (3.41) and Eq. (3.42) yields:

$$\mathbf{a}_p^{(1)} = \mathbf{R}_{01}^T \mathbf{a}_p^{(0)} \tag{3.43}$$

$$\mathbf{a}_p^{(2)} = \mathbf{R}_{02}^T \mathbf{a}_p^{(0)} \tag{3.44}$$

Equating Eq. (3.43) and Eq. (3.44) gives:

$$\mathbf{a}_p^{(1)} = \mathbf{R}_{01}^T \mathbf{R}_{02} \mathbf{a}_p^{(2)} \tag{3.45}$$

Also:

$$\mathbf{a}_1^{(1)} = \mathbf{R}_{01}^T \mathbf{a}_1^{(0)} \tag{3.46}$$

$$\mathbf{a}_2^{(2)} = \mathbf{R}_{02}^T \mathbf{a}_2^{(0)} \tag{3.47}$$

Now, combining Eq. (3.41) and Eq. (3.46) results in:

$$\begin{aligned} \mathbf{a}_p^{(1)} &= \mathbf{R}_{01}^T \mathbf{a}_1^{(0)} + (\ddot{\mathbf{l}}_{12} + \ddot{\mathbf{z}}_{12}) + 2\boldsymbol{\omega}_1^{(1)} \times (\dot{\mathbf{l}}_{12} + \dot{\mathbf{z}}_{12}) \\ &+ \dot{\boldsymbol{\omega}}_1^{(1)} \times (\mathbf{l}_{12} + \mathbf{z}_{12}) + \boldsymbol{\omega}_1^{(1)} \times (\boldsymbol{\omega}_1^{(1)} \times (\mathbf{l}_{12} + \mathbf{z}_{12})) \end{aligned} \tag{3.48}$$

Combining Eq. (3.42), Eq. (3.45) and Eq. (3.47) leads to:

$$\mathbf{a}_p^{(1)} = \mathbf{R}_{01}^T \mathbf{R}_{02} (\mathbf{R}_{02}^T \mathbf{a}_2^{(0)} + \dot{\boldsymbol{\omega}}_2^{(2)} \times \mathbf{d}_2^{(2)} + \boldsymbol{\omega}_2^{(2)} \times (\boldsymbol{\omega}_2^{(2)} \times \mathbf{d}_2^{(2)})) \tag{3.49}$$

Solving Eq. (3.48) and Eq. (3.49) for the vector $\ddot{\mathbf{l}}_{12} + \ddot{\mathbf{z}}_{12}$ gives:

$$\begin{aligned} \ddot{\mathbf{l}}_{12} + \ddot{\mathbf{z}}_{12} = \; & \mathbf{R}_{01}^T \mathbf{a}_2^{(0)} + \mathbf{R}_{01}^T \mathbf{R}_{02} (\dot{\boldsymbol{\omega}}_2^{(2)} \times \mathbf{d}_2^{(2)} + \boldsymbol{\omega}_2^{(2)} \times (\boldsymbol{\omega}_2^{(2)} \times \mathbf{d}_2^{(2)})) \\ & - \mathbf{R}_{01}^T \mathbf{a}_1^{(0)} - 2\boldsymbol{\omega}_1^{(1)} \times (\dot{\mathbf{l}}_{12} + \dot{\mathbf{z}}_{12}) - \dot{\boldsymbol{\omega}}_1^{(1)} \times (\mathbf{l}_{12} + \mathbf{z}_{12}) \\ & - \boldsymbol{\omega}_1^{(1)} \times \boldsymbol{\omega}_1^{(1)} \times (\mathbf{l}_{12} + \mathbf{z}_{12}) \end{aligned} \tag{3.50}$$

Eq. (3.50) must be solved for $\ddot{l}_{12}$, $\ddot{\alpha}_{12}$, and $\ddot{z}_{12}$. To simplify the solution procedure, the righthand side of the Eq. (3.50) is written in the following form:

$$\ddot{\mathbf{l}}_{12} + \ddot{\mathbf{z}}_{12} = \begin{bmatrix} \cos\alpha 12 & -l_{12}\sin\alpha_{12} & 0 \\ \sin\alpha 12 & l_{12}\cos\alpha_{12} & 0 \\ 0 & 0 & 1 \end{bmatrix} \begin{bmatrix} \ddot{l}_{12} \\ \ddot{\alpha}_{12} \\ \ddot{z}_{12} \end{bmatrix} + \begin{bmatrix} -2\dot{l}_{12}\dot{\alpha}_{12}\sin\alpha_{12} - l_{12}\dot{\alpha}_{12}\cos\alpha_{12} \\ 2\dot{l}_{12}\dot{\alpha}_{12}\cos\alpha_{12} + l_{12}\dot{\alpha}_{12}\sin\alpha_{12} \\ 0 \end{bmatrix} \tag{3.51}$$

or equivalently:

$$\ddot{\mathbf{l}}_{12} + \ddot{\mathbf{z}}_{12} = \mathbf{A}_1\ddot{\mathbf{z}}_1 + \mathbf{B}_1 \tag{3.52}$$

3.2.3 Input-output Equations

To find a controller law that determines the inputs $[T, M_\phi, M_\theta, T_T]^T$ based on the errors in the outputs, the input-output description of the control system is required. Eq. (3.50) contains the output derivatives. It also contains the acceleration of the follower 2. Note that the dynamic equations, Eq. (3.13) and Eq. (3.14), also relate $\dot{\boldsymbol{\omega}}_2$ and $\dot{\mathbf{a}}_0$ to the inputs. If the accelerations of the follower in Eq. (3.50) are substituted for from Eq. (3.13) and Eq. (3.14), the input-output relations are obtained. The details are as follow: Rearranging Eq. (3.13) results in:

$$\mathbf{a}_2^{(0)} = \begin{bmatrix} \dot{u}_I \\ \dot{v}_I \\ \dot{w}_I \end{bmatrix} = \frac{1}{m}\mathbf{R}_{02}\mathbf{b}_0 \begin{bmatrix} T \\ M_\theta \\ M_\theta \\ T_T \end{bmatrix} + \frac{1}{m}\mathbf{R}_{02} \begin{bmatrix} -D_x \\ -D_y \\ -D_z \end{bmatrix} + \begin{bmatrix} 0 \\ 0 \\ g \end{bmatrix} \tag{3.53}$$

where

$$\mathbf{b}_0 = \begin{bmatrix} 0 & 0 & 0 & 0 \\ 0 & 0 & 0 & -1 \\ -1 & 0 & 0 & 0 \end{bmatrix} \tag{3.54}$$

$$\mathbf{a}_2^{(0)} = \mathbf{C}_1\mathbf{u} + \mathbf{D}_1 \tag{3.55}$$

where

$$\mathbf{C}_1 = \frac{1}{m}\mathbf{R}_{02}\mathbf{b}_0 \tag{3.56}$$

and

$$\mathbf{D}_1 = \frac{1}{m}\mathbf{R}_{02} \begin{bmatrix} -D_x \\ -D_y \\ -D_z \end{bmatrix} + \begin{bmatrix} 0 \\ 0 \\ g \end{bmatrix} \tag{3.57}$$

In Eq. (3.14), it is assumed that I_{xz} is negligible. Now, Eq. (3.14) can be rearranged. It is repeated here for convenience.

$$\dot{\boldsymbol{\omega}}_2^{(2)} = \begin{bmatrix} M_\phi/I_{xx} \\ (M_\theta + Tl_r)/I_{yy} \\ (T_T l_r - K_m T)/I_{zz} \end{bmatrix} - \mathbf{I}^{-1}(\boldsymbol{\omega}_2^{(2)} \times \mathbf{I}\boldsymbol{\omega}_2^{(2)}) \tag{3.58}$$

In Eq. (3.50), $\dot{\omega}_2^{(2)} \times \mathbf{d}_2^{(2)}$ appears ($\mathbf{d}_2^{(2)} = [0, 0, -d_2]^T$). This term can be calculated as:

$$\dot{\omega}_2^{(2)} \times \mathbf{d}_2^{(2)} = \begin{bmatrix} -d_2(M_\theta + Tl_r)/I_{yy} \\ d_2 M_\phi / I_{xx} \\ 0 \end{bmatrix} - \mathbf{I}^{-1}(\omega_2^{(2)} \times \mathbf{I}\omega_2^{(2)}) \times \mathbf{d}_2^{(2)} \tag{3.59}$$

$$\dot{\omega}_2^{(2)} \times \mathbf{d}_2^{(2)} = \mathbf{C}_2\mathbf{u} + \mathbf{D}_2 \tag{3.60}$$

where

$$\begin{aligned} \mathbf{C}_2 &= \begin{bmatrix} -d_2 l_r & 0 & -d_2/I_{yy} & 0 \\ 0 & d_2/I_{xx} & 0 & 0 \\ 0 & 0 & 0 & 0 \end{bmatrix} \\ \mathbf{D}_2 &= -[\mathbf{I}^{-1}(\omega_2^{(2)} \times \mathbf{I}\omega_2^{(2)})] \times \mathbf{d}_2^{(2)} \end{aligned} \tag{3.61}$$

Eq. (3.50) is combined with Eq. (3.57) and Eq. (3.60), which gives:

$$\begin{aligned} \mathbf{A}_1\ddot{\mathbf{Z}}_1 + \mathbf{B}_1 &= \mathbf{R}_{01}^T\mathbf{C}_1\mathbf{u} + \mathbf{R}_{01}^T\mathbf{R}_{02}\mathbf{C}_2\mathbf{u} + \mathbf{R}_{01}^T\mathbf{R}_{02}\mathbf{D}_2 \\ &+ \mathbf{R}_{01}^T\mathbf{R}_{02}(\omega_2^{(2)} \times (\omega_2^{(2)} \times \mathbf{d}_2^{(2)})) + \mathbf{R}_{01}^T\mathbf{D}_1 \\ &- \mathbf{R}_{01}^T\mathbf{a}_1^{(0)} - 2\omega_1^{(1)} \times (\dot{\mathbf{l}}_{12} + \dot{\mathbf{z}}_{12}) \\ &- \dot{\omega}_1^{(1)} \times (\mathbf{l}_{12} + \mathbf{z}_{12}) - \omega_1^{(1)} \times (\omega_1^{(1)} \times (\mathbf{l}_{12} + \mathbf{z}_{12})) \end{aligned} \tag{3.62}$$

$$\ddot{\mathbf{Z}}_1 = \mathbf{A}_1^{-1}(\mathbf{R}_{01}^T\mathbf{C}_1 + \mathbf{R}_{01}^T\mathbf{R}_{02}\mathbf{C}_2)\mathbf{u} + \mathbf{f}_1 + \mathbf{g}_1 \tag{3.63}$$

or

$$\ddot{\mathbf{z}}_1 = \mathbf{f}_1 + \mathbf{b}_1\mathbf{u} \tag{3.64}$$

where

$$\begin{aligned} \mathbf{f}_1 &= \mathbf{A}_1^{-1}[\mathbf{R}_{01}^T\mathbf{R}_{02}(\omega_2^{(2)} \times (\omega_2^{(2)} \times \mathbf{d}_2^{(2)}))] - \mathbf{R}_{01}^T\mathbf{a}_1^{(0)} \\ &- 2\omega_1^{(1)} \times (\dot{\mathbf{l}}_{12} + \mathbf{z}_{12}) - \dot{\omega}_1^{(1)} \times (\mathbf{l}_{12} + \mathbf{z}_{12}) \\ &- \omega_1^{(1)} \times (\omega_1^{(1)} \times (\mathbf{l}_{12} + \mathbf{z}_{12})) - \mathbf{B}_1 + \mathbf{R}_{01}^T\mathbf{R}_{02}\mathbf{D}_2 + \mathbf{A}_1^{-1}(\mathbf{R}_{01}^T\mathbf{D}_1) \\ \mathbf{b}_1 &= \mathbf{A}_1^{-1}(\mathbf{R}_{01}^T\mathbf{C}_1 + \mathbf{R}_{01}^T\mathbf{R}_{02}\mathbf{C}_2) \end{aligned} \tag{3.65}$$

Eq. (3.65) contains only three components of the output ($\mathbf{l}_{12}, \alpha_{12}$, and $\mathbf{z}_{12}$). The last component ψ_2 should be added using the kinematics described in Eq. (3.9). The third

component of Eq. (3.9) is given again:

$$\dot{\psi} = (\sin\phi\sec\theta)\omega_{By} + (\cos\phi\sec\theta)\omega_{Bz} \tag{3.66}$$

The time derivative of the above equation is:

$$\begin{aligned} \ddot{\psi} &= (\dot{\phi}\cos\phi\sec\theta + \dot{\theta}\sin\theta\sec\theta\tan\theta)\omega_{2y}^{(2)} \\ &+ (-\dot{\phi}\sin\phi\sec\theta + \dot{\theta}\cos\theta\sec\theta\tan\theta)\omega_{2z}^{(2)} \\ &+ \sin\theta\sec\theta(M_\theta + Tl_r)/I_{yy} + \cos\theta\sec\theta(T_T l_r - k_m T)/I_{zz}) \\ &+ (\sin\phi\sec\theta)a_2 + (\cos\phi\sec\theta)a_3 \end{aligned} \tag{3.67}$$

Note that the subscript 2 is dropped from Eq. (3.67) for simplicity. Eq. (3.67) can be written in the standard form:

$$\ddot{\psi}_2 = f_2 + \mathbf{b}_2\mathbf{u} \tag{3.68}$$

where

$$\mathbf{u} = \begin{bmatrix} T \\ M_\phi \\ M_\theta \\ T_T \end{bmatrix} \tag{3.69}$$

$$\begin{aligned} f_2 &= (\dot{\phi}\cos\phi\sec\theta + \dot{\theta}\sin\theta\sec\theta\tan\theta)\omega_{2y}^{(2)} \\ &+ (-\dot{\phi}\sin\phi\sec\theta + \dot{\theta}\cos\theta\sec\theta\tan\theta)\omega_{2z}^{(2)} \\ &+ (\sin\phi\sec\theta)a_2 + (\cos\phi\sec\theta)a_3 \end{aligned} \tag{3.70}$$

$$\mathbf{b}_2 = \begin{bmatrix} \frac{\sin\theta\sec\theta l_r}{I_{yy}} & -\frac{\cos\theta\sec\theta k_m}{I_{zz}} & 0 & \frac{\sin\phi\sec theta}{I_{yy}} & \frac{\cos\theta\sec\theta}{I_{zz}} \end{bmatrix} \tag{3.71}$$

Equation (3.68) and Eq. (3.64) must be combined to have the full input-output equations.

$$\begin{bmatrix} \ddot{l}_{12} \\ \ddot{\alpha}_{12} \\ \ddot{z}_{12} \\ \ddot{\psi}_2 \end{bmatrix} = \begin{bmatrix} \mathbf{f}_1 \\ \\ f_2 \end{bmatrix} + \begin{bmatrix} \mathbf{b}_1 \\ \\ b_2 \end{bmatrix} \begin{bmatrix} T \\ M_\phi \\ M_\theta \\ T_T \end{bmatrix} \tag{3.72}$$

or

$$\ddot{\mathbf{z}} = \mathbf{f} + \mathbf{b}\mathbf{u} \tag{3.73}$$

3.2.4 Sliding Mode Controller Design

In the previous section, the input-output equations were found through kinematic analysis. A feedback control law for controlling inputs $[T, M_\phi, M_\theta, T_T]^T$ is to be determined to control helicopter 2 such that the desired distance l_{12}^d, view angle α_{12}^d, and height offset z_{12}^d, all of which are defined in frame 1, are maintained. Meanwhile, the yaw angle of helicopter 2, ψ_2^d, follows a desired trajectory.

The sliding mode control method is employed in the controller design process. Sliding mode control method is a model based control strategy. Assume some parameter uncertainty exist.

The input-output equation with the nominal parameters is written:

$$\ddot{\mathbf{z}} = \hat{\mathbf{f}} + \hat{\mathbf{b}}\mathbf{u} \tag{3.74}$$

It is first assumed that the actual input-output model with uncertain parameters and disturbance as:

$$\ddot{\mathbf{z}} = \mathbf{f} + \mathbf{b}\mathbf{u} + \mathbf{w} \tag{3.75}$$

Four first order surfaces are defined as:

$$\mathbf{s} = \begin{bmatrix} s_1 \\ s_2 \\ s_3 \\ s_4 \end{bmatrix} = \begin{bmatrix} (\dot{l}_{12} - \dot{l}_{12}^d) + \lambda_1(l_{12} - l_{12}^d) \\ (\dot{\alpha}_{12} - \dot{\alpha}_{12}^d) + \lambda_2(\alpha_{12} - \alpha_{12}^d) \\ (\dot{z}_{12} - \dot{z}_{12}^d) + \lambda_3(z_{12} - z_{12}^d) \\ (\dot{\psi}_2 - \dot{\psi}_2^d) + \lambda_4(\psi_{12} - \psi_2^d) \end{bmatrix} \tag{3.76}$$

For simplicity in notations, the following is defined:

$$\mathbf{s} = \dot{\mathbf{z}} - \mathbf{s}_r \tag{3.77}$$

where

$$\mathbf{s}_r = \dot{\mathbf{z}}^d - \boldsymbol{\lambda}(\mathbf{z} - \mathbf{z}^d) \tag{3.78}$$

and $\lambda = \text{diag}(\lambda_1\ \lambda_2\ \lambda_3\ \lambda_4)$, $\lambda_i > 0$. The following control law stabilizes the outputs:

$$\mathbf{u} = \hat{\mathbf{b}}^{-1}(-\hat{\mathbf{f}} + \dot{\mathbf{s}}_r - \mathbf{k} \cdot \text{sat}(\frac{\mathbf{s}}{\boldsymbol{\Delta}})) \tag{3.79}$$

where

$$\text{sat}(x) = \begin{cases} x, & |x| \le 1 \\ 1, & |x| \ge 1 \end{cases} \tag{3.80}$$

where $\mathbf{k} = \text{diag}[k_1, k_2, k_3, k_4]^T$ and $\mathbf{s}/\boldsymbol{\Delta} = [s_1/\delta_1, s_2/\delta_2, s_3/\delta_3, s_4/\delta_4]^T$. δ_1 to δ_4 are the boundary layers of the surfaces, and k_1 to k_4 are the controller's nonlinearity gains.

The boundary layers prevent the chatter of the trajectory about the surface at the cost of slower surface approach. If $\mathbf{k}$ is large enough, the controller will work despite parameter uncertainty. The following bounds are assumed for the parameter uncertainties and disturbances in order to determine the controller nonlinearity gains:

$$|\mathbf{f} - \hat{\mathbf{f}}| \leq \mathbf{F} \tag{3.81}$$

$$|\mathbf{w}| \leq \mathbf{W} \tag{3.82}$$

$$\mathbf{b} = (\mathbf{I} + \boldsymbol{\zeta})\hat{\mathbf{b}} \tag{3.83}$$

$$|\boldsymbol{\delta}_{ij}| \leq \boldsymbol{\Delta}_{ij} \quad i, j = 1..4 \tag{3.84}$$

Based on these bounds, the nonlinearity gains can be determined such that the reaching conditions

$$s_i \cdot \dot{s}_i \leq -\eta_i |s_i| \qquad \eta_i \geq 0 \qquad i = 1..4 \tag{3.85}$$

are satisfied, where $\eta_i > 0$ determines the reaching speed. This is done by substituting the first order derivative of components of Eq. (3.72) in Eq. (3.85) and using Eq. (3.75) and Eq. (3.79) in the results. After some algebraic manipulation, rearranging in terms of k_1 to k_4, and applying inequalities (3.81) to (3.84), the following condition can be obtained [29]:

$$(1 - \Delta_{ii})k_i + \sum_{j \neq i}^{4} \Delta_{ij} k_j = F_i + W_i + \eta_i + \sum_{j=i}^{4} \Delta_{ij} |-\hat{f}_j + \dot{s}_{rj}| \tag{3.86}$$

When k_i's satisfy Eq. (3.86), it is guaranteed that the outputs reach the surfaces despite the existence of parameter uncertainties and disturbances defined Equations. (3.81) to (3.84). After the outputs are on their corresponding surfaces, s_1 to s_4 are zero. Therefore, the outputs slide on the surface to their desired values as in observed from Eq. (3.76).

3.3 Simulations

Numerical simulations show the effectiveness of the controller design. In the simulations, λ_i are selected to be 1. λ_i can be any positive number. The value of 1 for all λ_i proves to give a fast converge of the simulations. The boundary layers $\delta_{1,3}$=1.0 m/s, $\delta_{2,4} = \frac{\pi}{4}$rad/s are used. These boundary layers minimize the chatter about the surface. The numerical values of the nominal dynamic parameters of the helicopters are corresponding to the Ikarus ECO small electric helicopter, which has been determined by experimental parameter identification

[16]:

$$\begin{aligned} \hat{m} = 1.36 \text{ kg} \qquad & \hat{I}_{xx} = 0.137 \text{ kgm}^2 \\ \hat{I}_{yy} = 0.221 \text{ kgm}^2 \qquad & \hat{I}_{zz} = 0.0323 \text{ kgm}^2 \\ \hat{l}_r = 0.1 \text{ m} \qquad \hat{l}_t = 0.635 \text{ m} \qquad & d = 1.0 \text{ m} \end{aligned} \tag{3.87}$$

3.3.1 Taking Off

The first simulation set is to simulate the motion of the follower when the leader helicopter is taking off. The initial positions for the leader and follower are $(0, 0, 0)$ m and $(0, 15, 0)$ m, respectively. The leader has no motion in either x-axis or y-axis direction. It only has an upward speed of -1m/s (the positive direction is defined downwards) in the z direction. The follower receives a command to follow the leader in the way that the lateral distance is $l_{12}^d = 10$ m, the view angle is $\alpha_{12}^d = \pi/2$ rad, the vertical distance is $z_{12}^d = -1$ m, and a yaw angle is $\psi_2^d = 0$ rad. Figures. 3.4 to 3.5 show the states of the follower. As seen in Fig. 3.4(a), the x component of the helicopter is constant. The y component is initially 15 m, however, it approaches the the desired value of 10 m. The z component is increasing with the leader's. For the velocities, the x component is zero; the y and z components have some fluctuations at the beginning, but go to zero at around 10 seconds and 5 seconds, respectively. The roll component of the Euler angles ϕ undertakes some fluctuations, then converges to zero. Both the pitch θ and yaw ψ components are zero. For the angular velocities, the y component and the z components are around 0 rad/s; the x component has some fluctuations at the beginning, but moves around 0.03 rad/s afterwards. Figures. 3.6(a) to 3.6(b) show the formation parameters and control forces. It can been seen that l_{12} begins at 15 m, but approaches the desired value of 10 m as specified in the simulation; α_{12} is $\pi/2$ rad; z_{12} goes to -1 m as desired after around 10 seconds; and ψ_2 is constantly 0. The control forces are: 14.4 N for the main rotor thrust, 0 Nm for the tail rotor thrust, -1.43 Nm for the roll torque, and 0.4 N for the pitch torque when the helicopter converges a stable state. As can be seen in the simulation results that the effectiveness of the new controller has been verified. From the 3D drawing of the two helicopters' trajectories (Figures. 3.7), it is noticed that the follower does follow the leader's taking off perfectly. The controller displays good time response while the control inputs are not too large and physically achievable.

3.3.2 Sinusoidal Wave Movement

This part is to simulate the motion of the follower when the leader is moving on a sinusoidal path in the $x - y$ plane. For the leader helicopter, the initial position is $(0, 0, 0)$ m. The leader has a constant velocity in the x-axis direction, while its velocity in the y-axis direction is $1 \times \sin(t + \pi/2)$ m/s. The leader has no motion in the z-axis direction. The follower

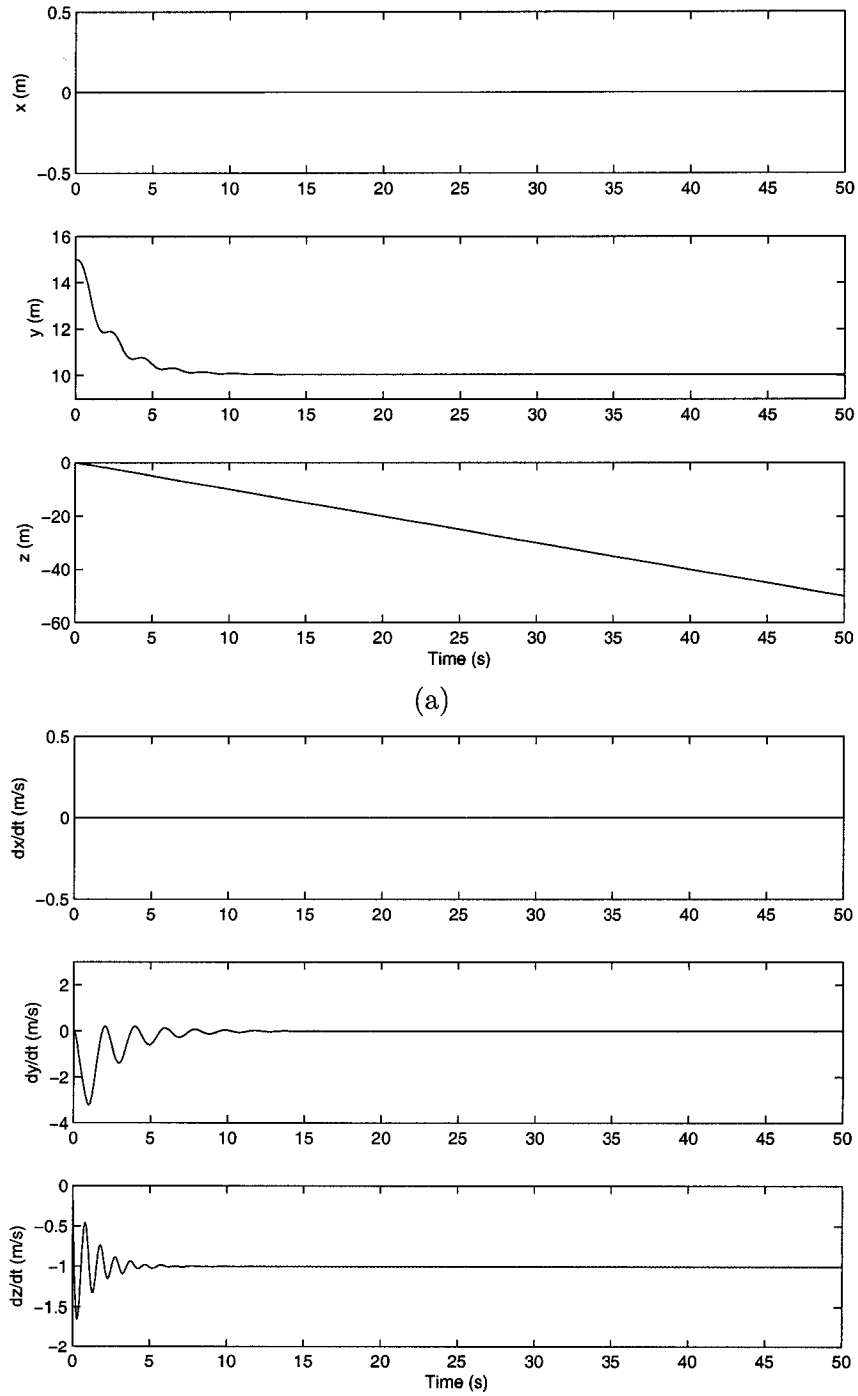

Figure 3.4: The states of the follower when the leader is taking off. (a) Position, and (b) Velocities.

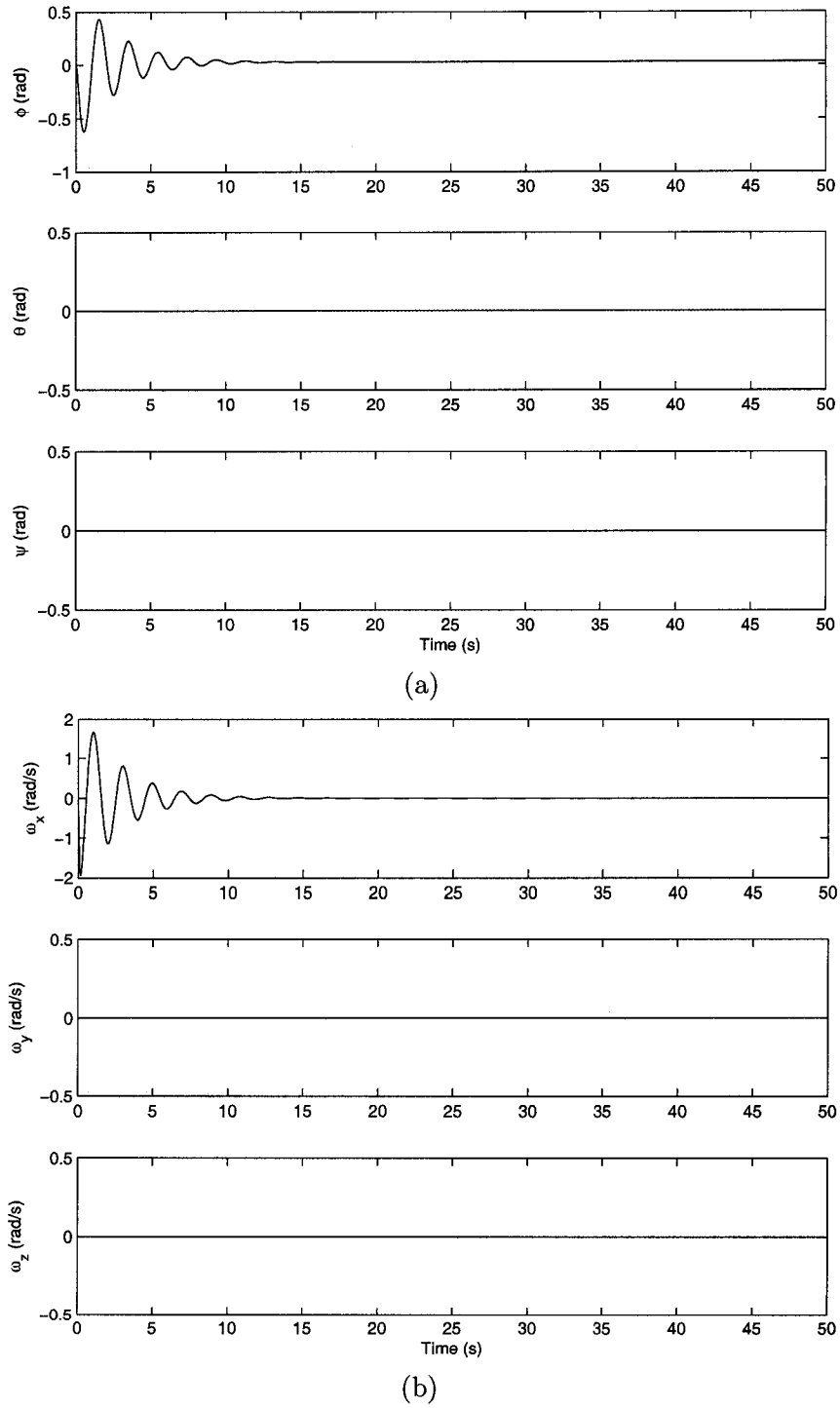

Figure 3.5: The states of the follower when the leader is taking off. (a) Euler angles, and (b) Angular velocities.

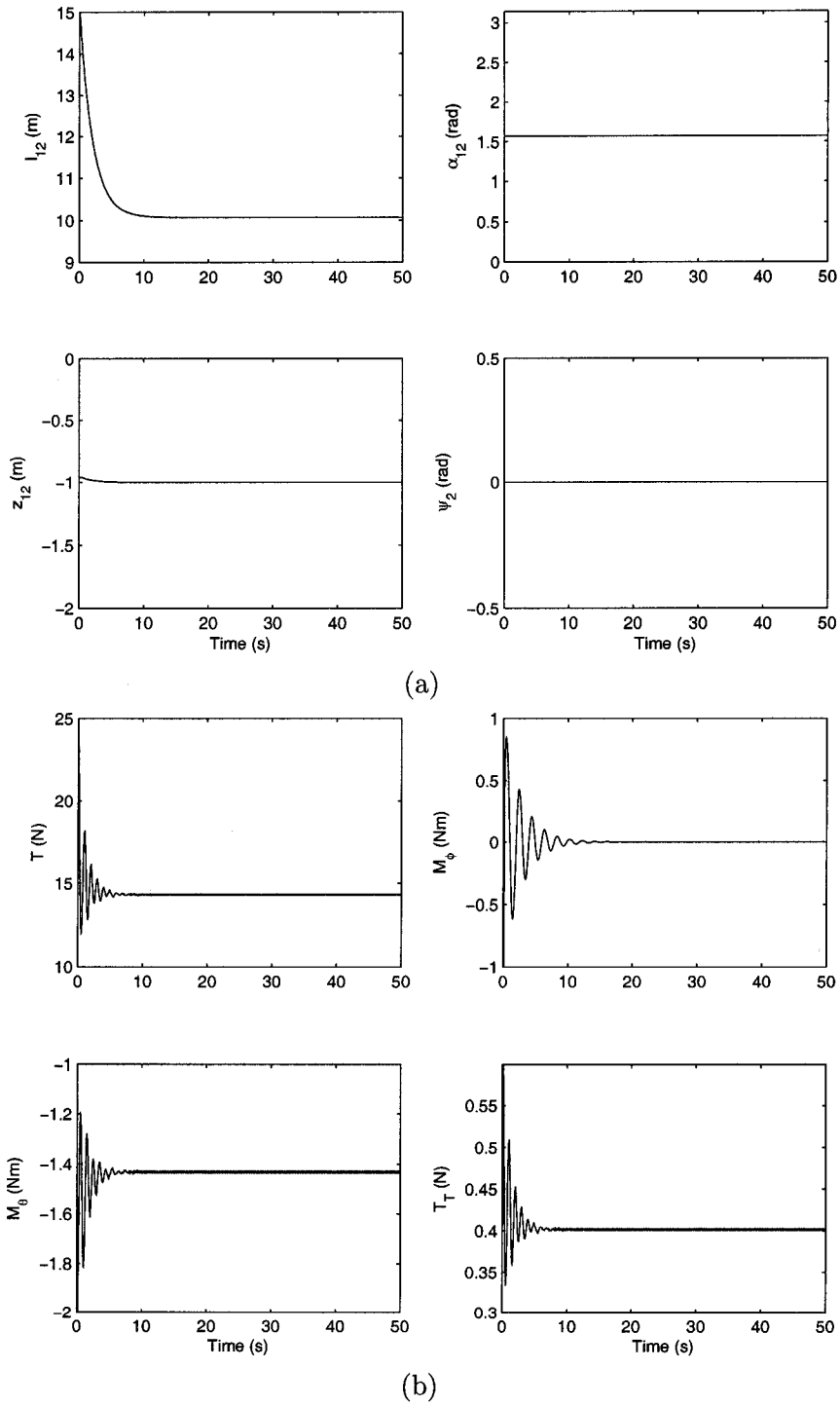

Figure 3.6: (a) Formation parameters, (b) Control forces of the controller when the leader is taking off.

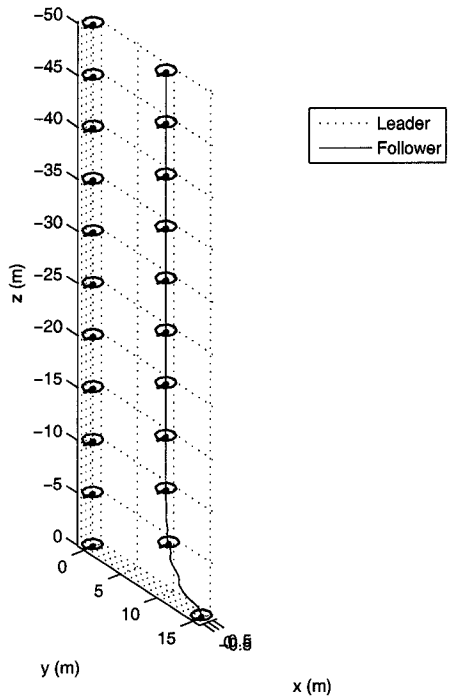

Figure 3.7: Trajectories of both helicopters when the leader is taking off.

starts at $(0, 15, 0)$ m and receives a command to follow the leader in the way that the lateral distance is $l_{12}^d = 10$ m, the view angle is $\alpha_{12}^d = \pi/2$ rad, a vertical distance is $z_{12}^d = -1$ m, and a yaw angle is $\psi_2^d = 0$ rad. Figures. 3.8 to 3.9 show the states of the follower. As seen in Fig. 3.8(a), the x component of the helicopter is increasing with the leader's. The y component is following the leader's sinusoidal lateral motion. The z component has a small fluctuation around 0 m. For the velocities, the x component initially has some fluctuation, however, it approaches to 1 m/s within 10 seconds; the y component is a sinusoidal wave; and z component has some fluctuations at the beginning, but goes to zero faster than the x component. The roll component of the Euler angles ϕ undertakes a sinusoidal change. the pitch component of the Euler angles θ has some fluctuations at the beginning, but goes to around -0.075 rad at around 10 seconds. The yaw components of the Euler angles ψ is zero. For the angular velocities, the y component and the z components have some fluctuations at the beginning, but moving around 0 rad/s afterwards; the x component has sinusoidal lateral motion. Figures. 3.10(a) and 3.10(b) show the formation parameters and control forces. It can been seen that l_{12} begins at 15 m, but approaches the desired 10 m as specified at the beginning; α_{12} is $\pi/2$ rad; z_{12} goes to -1 m as desired after around 10 seconds; and ψ_2 is constantly 0. The control forces are: 13.4 N for the main rotor thrust, around 13 Nm for the tail rotor thrust, -1.34 Nm for the roll torque, and 0.37 N for the pitch torque when the helicopter converts a stable state. From the 3D plot of the two helicopters'

trajectories (Figures. 3.11), it is noticed that the follower does follow the leader's sinusoidal motion perfectly. Furthermore, the controller displays good time response.

3.3.3 Circular Movement

This simulation set is to simulate the motion of the follower when the leader is moving on a circular path in the $x-y$ plane. In this case, the initial position of the leader is $(10, 0, -4)$ m. The leader moves in a counterclockwise circle with radius of 10 m in the $x-y$ plane at the height of 4 m and the linear velocity is 1 m/s. Both helicopters' yaw angles start at $\pi/2$ and the yaw angle rate of leader is 0.1 rad/s, which means the helicopters do not face the same direction as defined in the initial condition while moving on a circle. They rotate such that their local x-axis is always tangent to the circle of motion. The initial position of the follower is $(8, 0, 0)$ m. The follower receives a command to follow the leader in the way that the lateral distance is $l_{12}^d = 10$ m, the view angle is $\alpha_{12}^d = \pi/2$ rad, a vertical distance is $z_{12}^d = -1$ m, and the yaw angle rate is 0.1 rad/s. Figures 3.12 and 3.13 show the states of the follower. As seen in Fig. 3.12(a), the x component of the helicopter and the y component present sinusoidal shapes as desired because of the circular path. The z component reaches -4 m, e.g. the same height as the leader. For the velocities, the x component and the y component initially have some fluctuations, however, they approach to sinusoidal movements in 5 seconds; z component goes to zero. The roll component of the Euler angles ϕ undertakes a sinusoidal change. The pitch component of the Euler angles θ has some fluctuations at the beginning, but moving around 0 rad afterwards. The yaw component of the Euler angles ψ is around 1.16 rad. For the angular velocities, the x component and the y component have some fluctuations at the beginning, but moving around 0 rad/s afterwards; z component is around 0.1 rad/s. Figures. 3.14(a) and 3.14(b) show the formation parameters and control forces. It can been seen that l_{12} begins at 2 m, and approaches the desired 7.5 m as specified in the simulation; α_{12} is $\pi/2$ rad; z_{12} goes to -1 m as desired; and ψ_2 is around 1.15 rad. The control forces are: 13.32 N for the main rotor thrust, and 0.3754 N for the tail rotor thrust; 0 Nm for the roll torque, and -1.33 Nm after some initial fluctuations for the pitch torque when the helicopter converts a stable state. From the 3D plot of the two helicopters' trajectories (Figures. 3.15), it is noticed that the follower does follow the leader's circular path perfectly. Furthermore, the controller displays good time response.

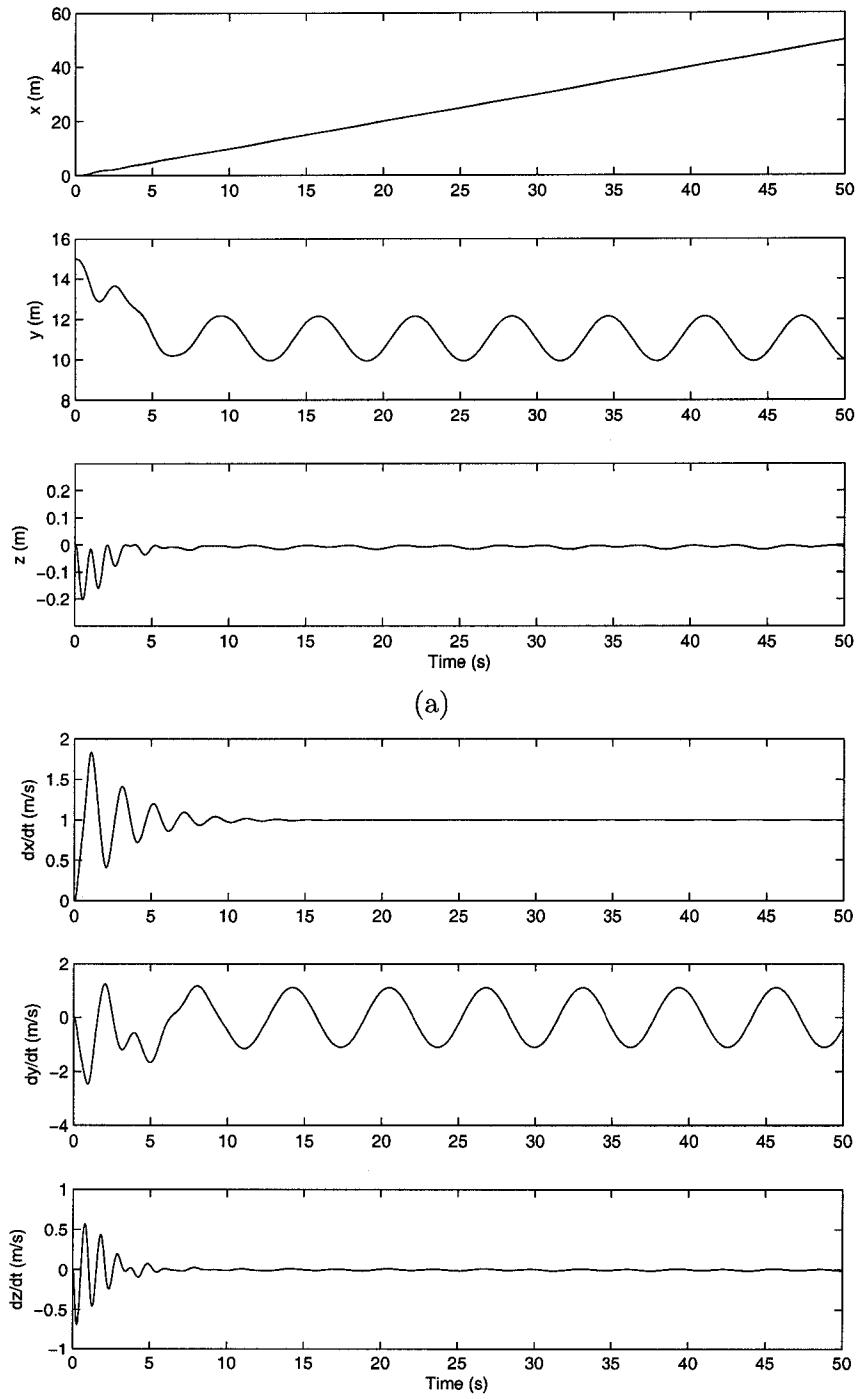

Figure 3.8: The states of the follower when the leader is moving on a sinusoidal path. (a) Position, and (b) Velocities

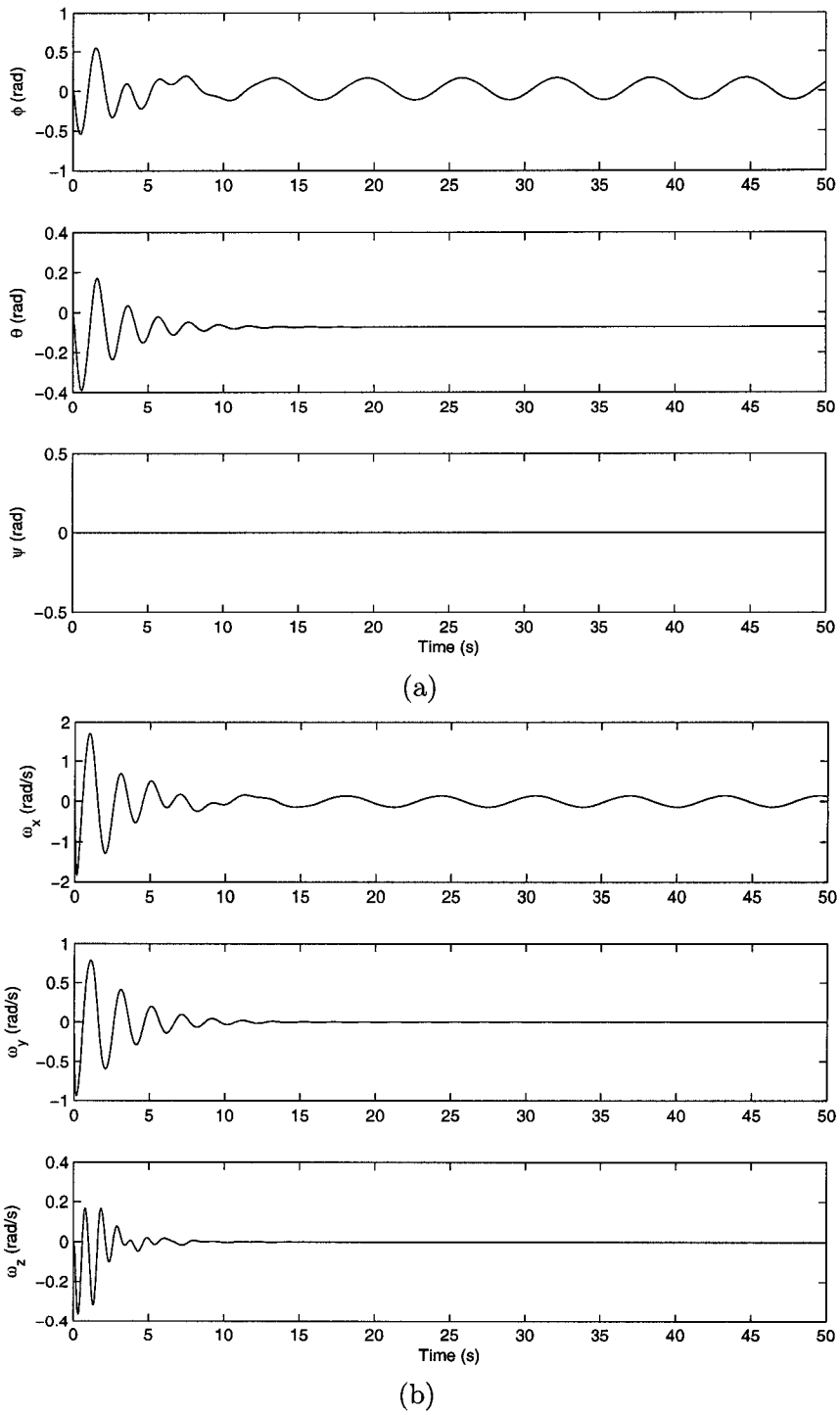

Figure 3.9: The states of the follower when the leader is moving on a sinusoidal path. (a) Euler angles, and (b) Angular velocities

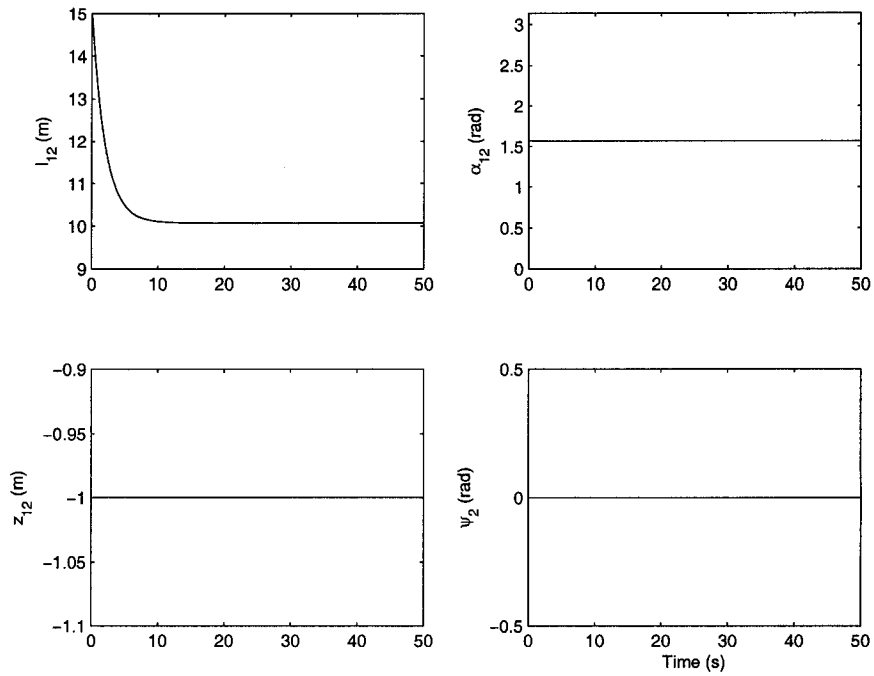

(a)

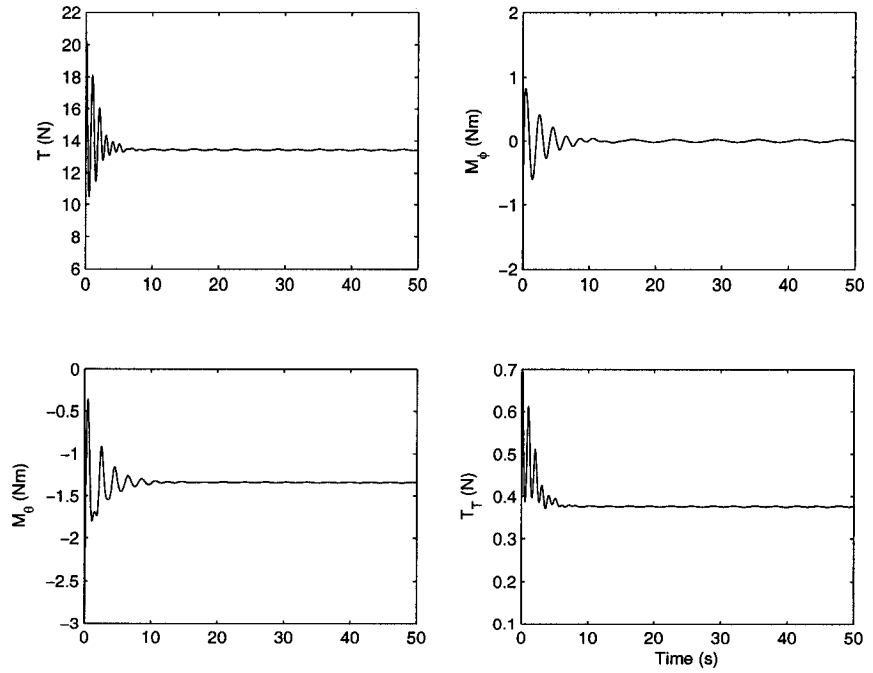

(b)

Figure 3.10: (a) Formation parameters, (b) Control forces of the controller when the leader is moving on a sinusoidal path

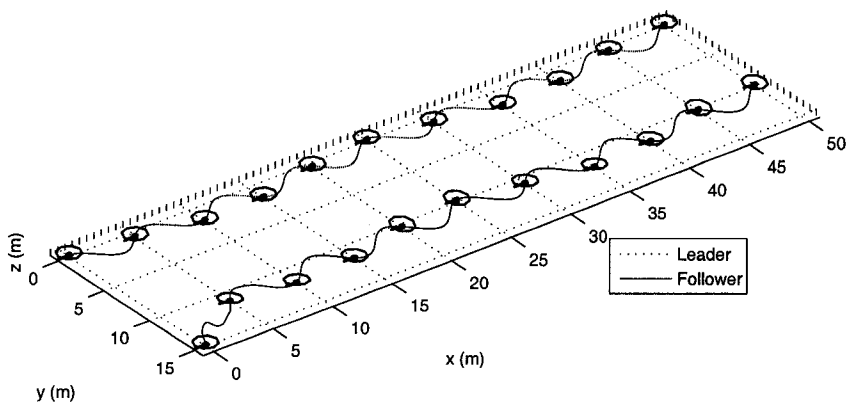

Figure 3.11: Trajectories of both helicopters when the leader is moving on a sinusoidal path

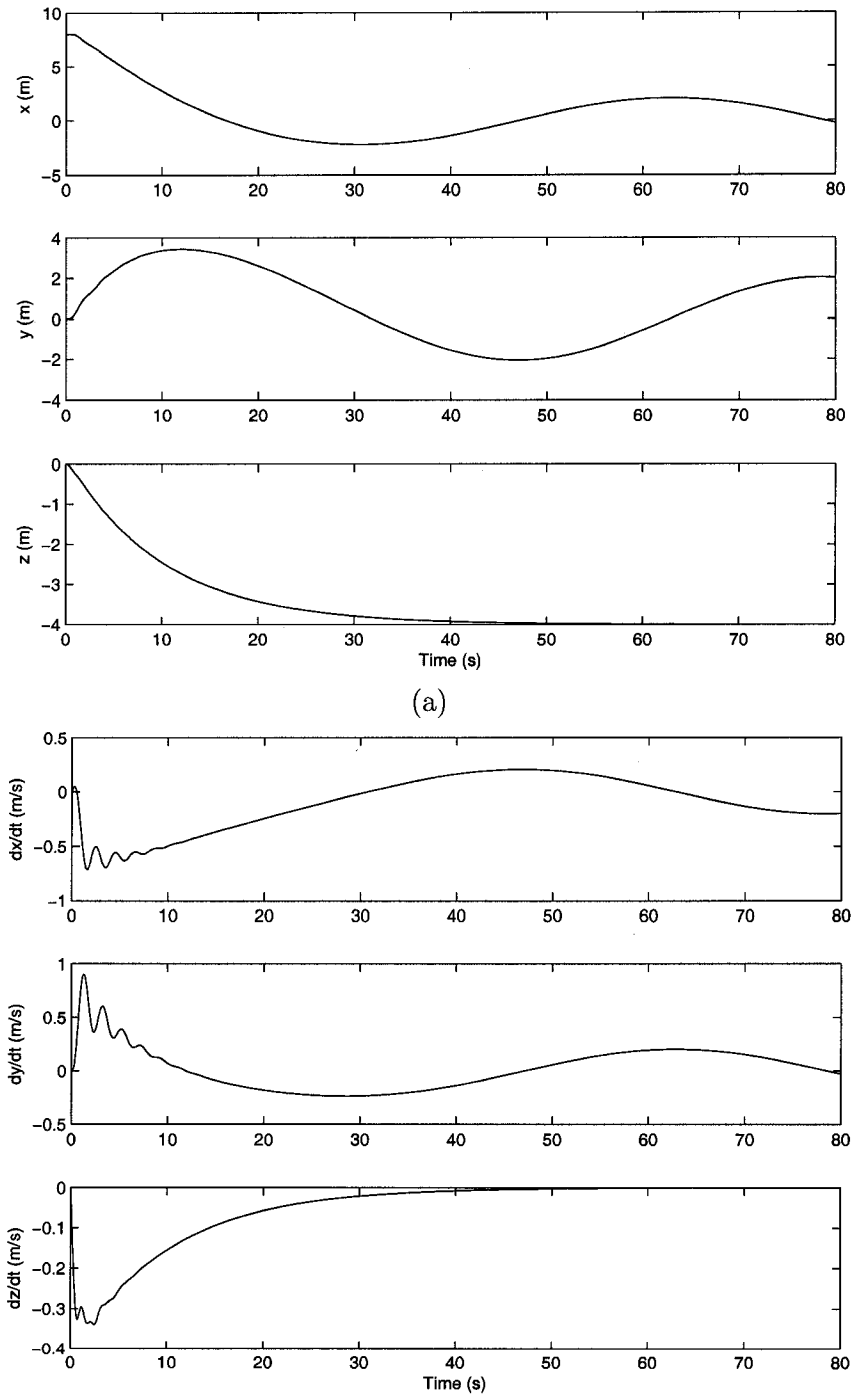

Figure 3.12: The states of the follower when the leader is moving on a circular path. (a) Position, and (b) Velocities

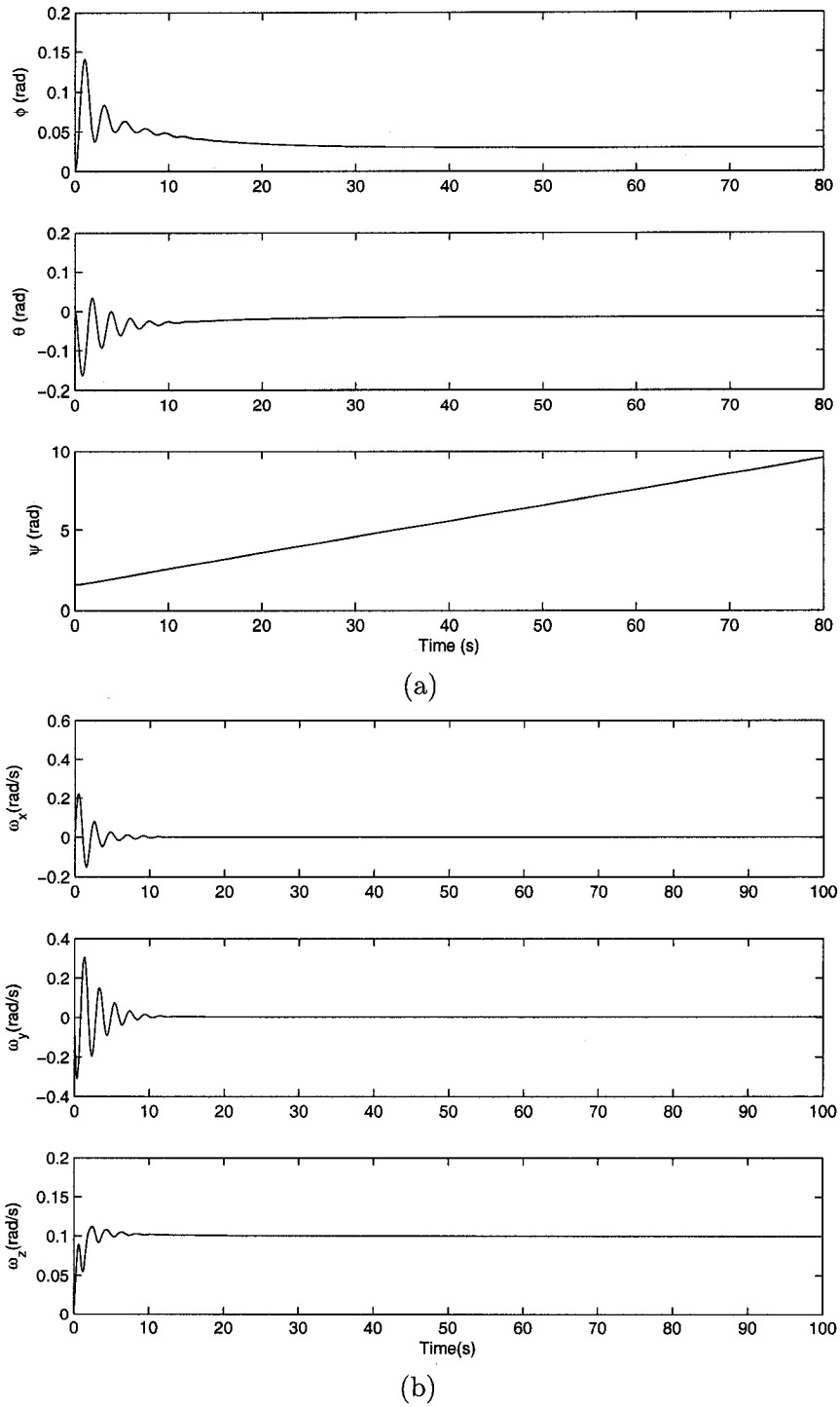

Figure 3.13: The states of the follower when the leader is moving on a circular path. (a) Euler angles, and (b) Angular velocities

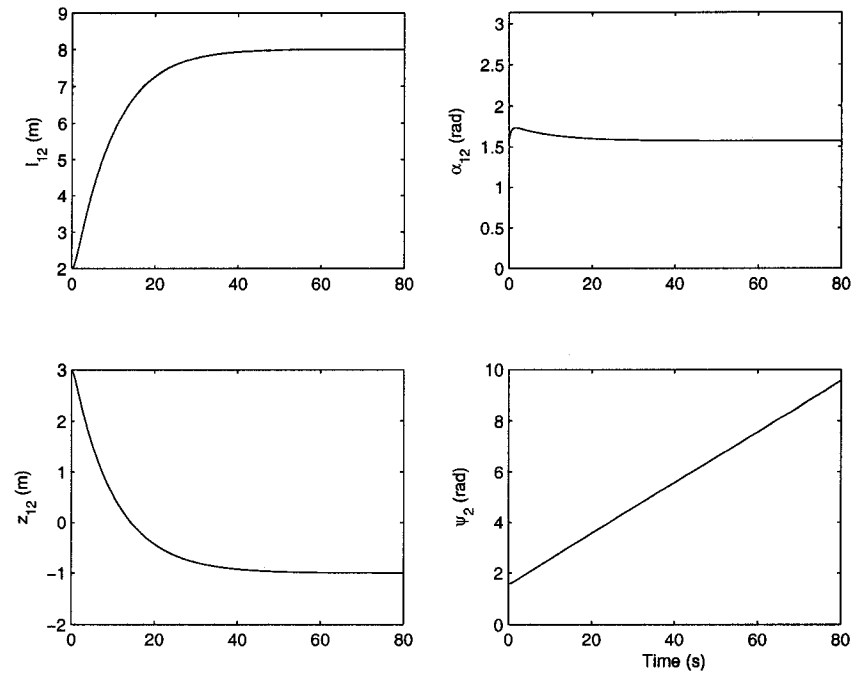

(a)

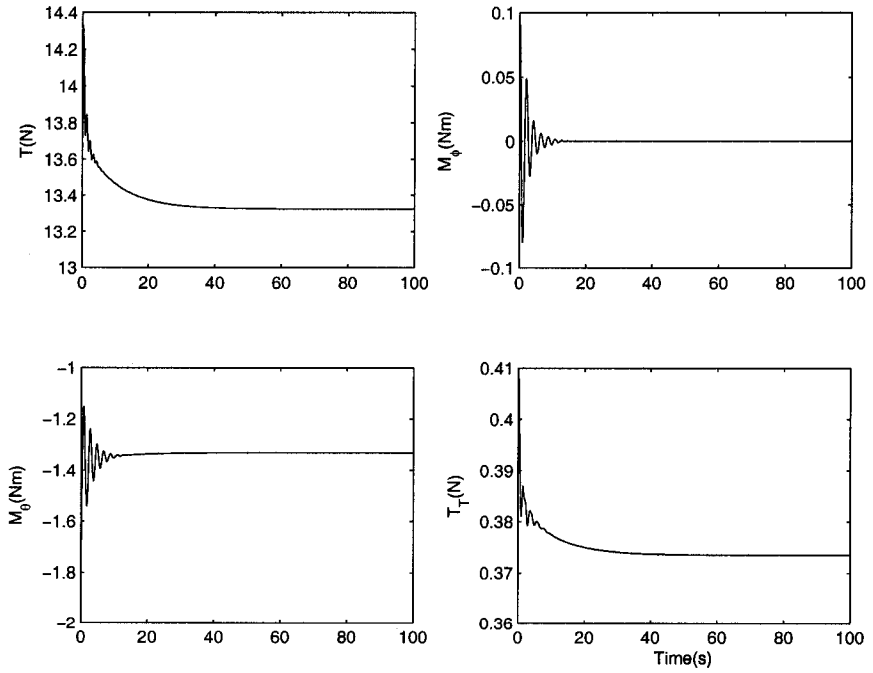

(b)

Figure 3.14: (a) Formation parameters, (b) Control forces of the controller when the leader is moving on a circular path

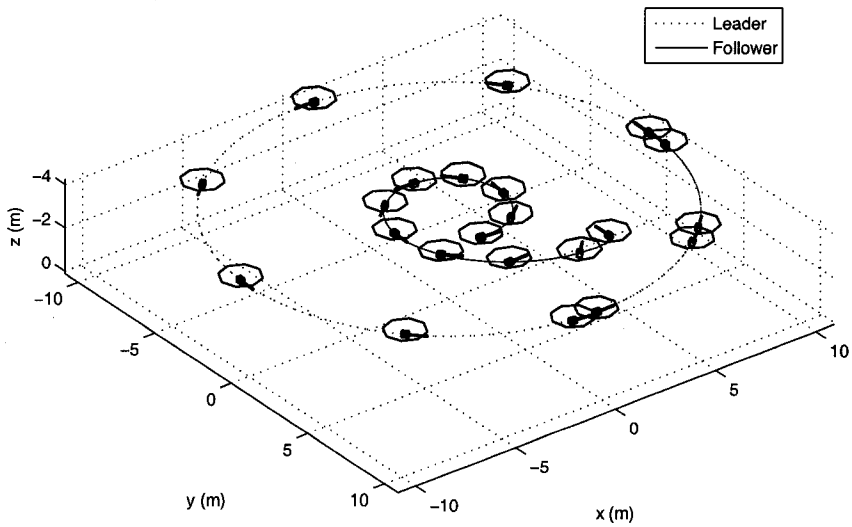

Figure 3.15: Trajectories of both helicopters when the leader moves on a circular path

Chapter 4

Controller Design with Rotor's Actuation Commands as Inputs

In previous chapter, a sliding mode controller with forces and moments (T, T_T, M_ϕ, and M_θ) as outputs was developed. However, in a real helicopter system, the actuation is the positions of the servo motors that drive the rotors' control mechanism. The changes of these positions create the collective and cyclic pitches of the main and the tail rotors, via changing the position of the swashplate. Then, the collective and cyclic pitches of the rotor blades generate the actuation forces and moments. As a result, capability to calculate the appropriate servo motors' positions as the control inputs must be achieved to design an applicable controller.

Since the flapping of the flybar improves the stability of the helicopter and affects the actuation, it is important to include its model with the rotor's actuation model and to consider the flybar effect in the controller design. In this chapter, the swashplate's cyclic roll and pitch actuation commands and the pitch angles of the main and the tail blades are assumed as the outputs of the controller.

4.1 Rotor's Actuation mechanism Model

Flybar is an aerodynamic damping device that is a fundamental stability augmentation for the modern helicopters. Due to the complex nature of flying a small scale helicopter via remote control, assisting the pilot in stabilizing the aircraft is desirable [14]. This section is to model the flybar with the main rotor blade and the fuselage movement. An assumption through the derivation is that the rotor system does not apply reaction forces back to the actuators (including the flybar). This is a reasonable assumption since the airfoil of main blades is symmetric and the blades are hinged along the center of lift. Ideally, the moment required to rotate the blade at this point should be very small [16].

The structure of the model helicopter's rotor-flybar assembly is shown in Fig. 4.1 [16]. The blade pitch can be changed directly from the cyclic servo actuator by the movement

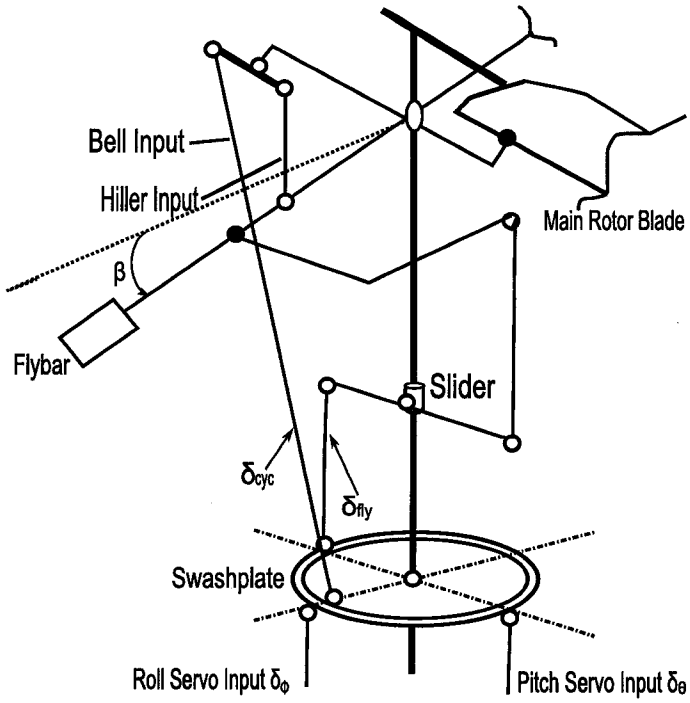

Figure 4.1: The structure of the mode helicopter's rotor-flybar assembly.

of the Bell input (as shown in Fig. 4.1). The response with respect to this arm is fast, but lacks stability. At the same time, the pitch of the flybar can be changed through the Hiller input (as shown in Fig. 4.1). This leads to the flapping of the flybar, which further leads to the change of the main blade pitch. The pilot's cyclic control input δ_θ and δ_ϕ are the displacements of the lower swashplate as per Fig. 4.1. There is direct relationship between the cyclic input applied to the main blades δ_{cyc} (which is a function of δ_θ and δ_ϕ) and the cyclic angle of the rotor blades θ_{cyc}. A similar relationship exists between the cyclic input applied to the flybar δ_{fly} and the flapping angle of the flybar β [16]. The orientation of the main blade with respect to the x axis of the helicopter body frame is given by ξ.

The following control inputs are assumed:

- θ_o: The collective pitch of the rotor blades, which can be actuated by application of equal δ_ϕ and δ_θ
- δ_ϕ and δ_θ: the pitch and roll commands that vary the the rotor blades' cyclic pitch θ_{cyc} around every cycle of rotation, therefore create the pitch and roll moments
- θ_ψ: The collective pitch of the tail rotor blades

In the mechanism, the inputs are $[\theta_o, \delta_\phi, \delta_\theta, \theta_\psi]^T$ and the output are $[T, M_\phi, M_\theta, T_T]^T$. Internal variables include the rotor orientation ξ and the flybar flapping angle β. n and

B are the number of the blades and the constant loss factor, respectively. The loss factor takes into account the fact that a finite length airfoil would lose some of the lift generated due to the wing tip vortex effect [13]. It has the equal effect that the length of blade is reduced by a factor of B, which is around 0.97.

The following equation holds [16]:

$$T = \frac{n}{2} ac\rho\pi R^3\Omega^2(\frac{B^3}{3}\theta_0 - \frac{B^2}{2}\lambda) \tag{4.1}$$

where a is the blades' correction factor for velocity, c is the widths of the main blades, ρ is density of the air, R is the radius of the main blades, Ω is the angular velocity of the main blades, λ is the inflow ratio, which can be written as follow [16]:

$$\lambda = \frac{v_i - v_{q3}^b}{R\Omega} \tag{4.2}$$

where v_{q3}^b is the component of the helicopter velocity in the z direction of the helicopter's body coordinate, v_i is the velocity of the air through the rotor blade. v_i is to be determined empirically and is between 0.6 to 0.9 times v_{q3}^b. Here, for simplicity, λ is considered as 0.

For the tail rotor, relationship between the pilot input and the force output can be expressed [16]:

$$T_T = \frac{n}{2} ac_T\rho\pi({R_{T1}}^3 - {R_{T2}}^3){\Omega_T}^2\frac{B^3}{3}\theta_\psi \tag{4.3}$$

where c_T, $R_{T1} - R_{T2}$, Ω_T are the width, the length and the angular velocity of the tail rotor, respectively.

The relationships between the roll moment M_ϕ and the roll cyclic pitch command δ_ϕ, and between the pitch moment M_θ and the pitch cyclic pitch command δ_θ) are as follow [16]:

$$M_\phi = \frac{n\rho\Omega^2 acR^4B^4}{16L_1(L_2+L_3)}(\alpha_3(\frac{L_3L_8}{L_9}\delta_\phi - L_2L_4\beta) - \alpha_4L_1L_2 + L_3)\frac{\omega_{Bx}}{\Omega} \tag{4.4}$$

$$M_\theta = \frac{n\rho\Omega^2 acR^4B^4}{16L_1(L_2+L_3)}(\alpha_3(\frac{L_3L_8}{L_9}\delta_\theta - L_2L_4\beta) - \alpha_4L_1L_2 + L_3)\frac{\omega_{By}}{\Omega} \tag{4.5}$$

where ω_{Bx} and ω_{By} are the inertial angular velocities of the helicopter in the x and y directions expressed in the body frame, and $L_1, L_2, L_3, L_4, L_5, L_6, L_7, L_8$, and L_9 are the corresponding lengths of the linkages in the rotor's actuation mechanics (Fig. 4.2).

For simulation purpose, the flapping angle β (the angle between the plane of the main rotor and the plane of the flybar) is approximated as a sinusoidal function [16]. This assumption can be made because the time that one rotor revolution takes is small enough, and β_{max} and ξ_{max} can be assumed constant during that time.

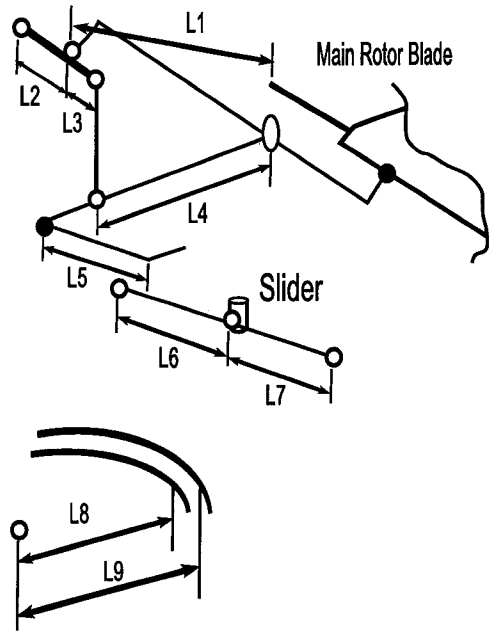

Figure 4.2: Length of the linkage in the model helicopter's rotor-flybar assembly structure

$$\beta = \beta_{max} \cos(\xi - \xi_{max}) \tag{4.6}$$

Fig. 4.3 shows β_{max} and ξ_{max} in the main rotor plane and flybar plane. β_{max} and ξ_{max} are obtained as follow:

$$\cos(\beta_{max}) = \mathbf{k}' \cdot \mathbf{k} \tag{4.7}$$

where $\mathbf{k}' = [0\ 0\ 1]^T$, which is perpendicular to the flybar plane; and the expression of $\mathbf{k}$ is given in Eq. (4.8), which is perpendicular to the main rotor plane. It is equal to project $\mathbf{k}'$

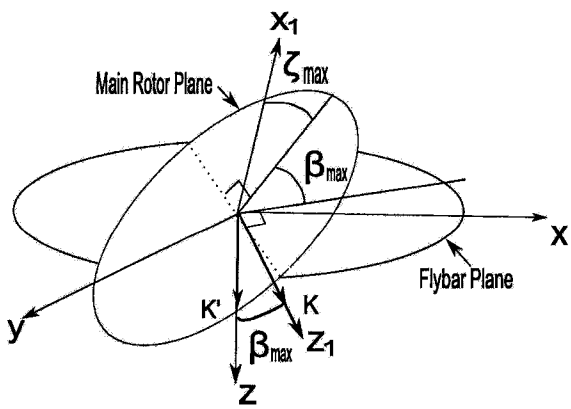

Figure 4.3: β_{max} and ξ_{max} in the main rotor plane and flybar plane

in the main rotor's frame.

$$\mathbf{k} = \begin{bmatrix} k_{r1} \\ k_{r2} \\ k_{r3} \end{bmatrix} = e^{(\hat{y}\times)\theta} e^{(\hat{x}\times)\phi} \begin{bmatrix} 0 \\ 0 \\ 1 \end{bmatrix} \tag{4.8}$$

$$\xi_{max} = \arctan(\frac{k_{r2}}{k_{r1}}) \tag{4.9}$$

For simplification, all the derivation can be expressed in the matrix form:

$$\begin{bmatrix} T \\ M_\phi \\ M_\theta \\ T_T \end{bmatrix} = \begin{bmatrix} A_{11} & 0 & 0 & 0 \\ 0 & A_{22} & 0 & 0 \\ 0 & 0 & A_{33} & 0 \\ 0 & 0 & 0 & A_{44} \end{bmatrix} \begin{bmatrix} \theta_o \\ \delta_\phi \\ \delta_\theta \\ \theta_\psi \end{bmatrix} + \begin{bmatrix} 0 \\ B_2 \\ B_3 \\ 0 \end{bmatrix} \tag{4.10}$$

Or

$$\begin{bmatrix} T \\ M_\phi \\ M_\theta \\ T_T \end{bmatrix} = \mathbf{A}_{sp} \begin{bmatrix} \theta_o \\ \delta_\phi \\ \delta_\theta \\ \theta_\psi \end{bmatrix} + \mathbf{B}_{sp} \tag{4.11}$$

$$\mathbf{u} = \mathbf{A}_{sp}\mathbf{u}' + \mathbf{B}_{sp} \tag{4.12}$$

where

$$\begin{aligned} A_{11} &= \tfrac{n}{2} ac\rho\pi R^3\Omega^2 \tfrac{B^3}{3} \\ A_{22} &= \tfrac{n\rho\Omega^2 acR^4B^4}{16L_1(L_2+L_3)} \alpha_3 \tfrac{L_3L_8}{L_9} \\ A_{33} &= \tfrac{n\rho\Omega^2 acR^4B^4}{16L_1(L_2+L_3)} \alpha_3 \tfrac{L_3L_8}{L_9} \\ A_{44} &= \tfrac{n}{2} ac_T\rho\pi({R_{T1}}^3 - {R_{T2}}^3){\Omega_T}^2 \tfrac{B^3}{3} \\ B_2 &= -\tfrac{n\rho\Omega^2 acR^4B^4}{16L_1(L_2+L_3} (\alpha_3 L_2L_4\beta_{max}\cos\xi_{max} + \alpha_4 L_1(L_2+L_3)) \tfrac{\omega_{Bx}}{\Omega} \\ B_3 &= -\tfrac{n\rho\Omega^2 acR^4B^4}{16L_1(L_2+L_3} (\alpha_3 L_2L_4\beta_{max}\sin\xi_{max} + \alpha_4 L_1(L_2+L_3)) \tfrac{\omega_{By}}{\Omega} \end{aligned} \tag{4.13}$$

Note that the matrices $\mathbf{A}_{sp}$ and $\mathbf{B}_{sp}$ include uncertain parameters, which will be accounted for by the controller when $\mathbf{u}'$ is used as the control inputs, instead of $\mathbf{u}$.

4.2 Input-output Equations

The modeling of the helicopter, the $l-\alpha$ scheme, the velocity analysis and the acceleration analysis are the same after the rotor actuation mechanism is considered into the controller

design. The following parts are mainly investigating the new form of the input-out equations, and the new sliding mode controller.

To find a controller law that determines the inputs $[\theta_o, \delta_\phi, \delta_\theta, \theta_\psi]^T$, the input-output and relationship is required. Eq. (3.50) contains the output derivatives. It also contains the acceleration of the follower 2. As explained in the previous section, Eq. (3.13) and Eq. (3.14), also relate $\dot{\boldsymbol{\omega}}_2$ and $\dot{\mathbf{a}}$ to the inputs. If the accelerations of the follower in Eq. (3.50) is substituted for from Eq. (3.13) and Eq. (3.14) and then consider Eq. (4.12), the input-output relations are obtained. The details are as follow:

Substituting Eq. (3.75) into Eq. (3.55) results in:

$$\mathbf{a}_2^{(2)} = \mathbf{C}_1\mathbf{u} + \mathbf{D}_1 \tag{4.14}$$

$$\mathbf{a}_2^{(2)} = \mathbf{C}_1(\mathbf{A}_{sp}\mathbf{u}' + \mathbf{B}_{sp}) + \mathbf{D}_1 = \mathbf{C}_1\mathbf{A}_{sp}\mathbf{u}' + \mathbf{C}_1\mathbf{B}_{sp} + \mathbf{D}_1 \tag{4.15}$$

or

$$\mathbf{a}_2^{(2)} = \mathbf{C}_1'\mathbf{u}' + \mathbf{D}_1' \tag{4.16}$$

where

$$\mathbf{C}_1' = \mathbf{C}_1\mathbf{A}_{sp} \tag{4.17}$$

and

$$\mathbf{D}_1' = \mathbf{C}_1\mathbf{B}_{sp} + \mathbf{D}_1 \tag{4.18}$$

Substituting Eq. (4.12) into Eq. (3.59) gives:

$$\dot{\boldsymbol{\omega}}_2^{(2)} \times \mathbf{d}_2^{(2)} = \begin{bmatrix} -d_2((A_{33}\delta_\theta - B_3) + (A_{11}\theta_o - B_1)l_r)/I_{yy} \\ d_2(A_{22}\delta_\phi - B_2)/I_{xx} \\ 0 \end{bmatrix} - \mathbf{I}^{-1}(\boldsymbol{\omega}_2^{(2)} \times \mathbf{I}\boldsymbol{\omega}_2^{(2)}) \times \mathbf{d}_2^{(2)} \tag{4.19}$$

Substituting Eq. (3.75) into Eq. (3.60) gives:

$$\dot{\boldsymbol{\omega}}_2^{(2)} \times \mathbf{d}_2^{(2)} = \mathbf{C}_2(\mathbf{A}_{sp}\mathbf{u}' + \mathbf{B}_{sp}) + \mathbf{D}_2 = \mathbf{C}_2\mathbf{A}_{sp}\mathbf{u}' + \mathbf{C}_2\mathbf{B}_{sp} + \mathbf{D}_2 \tag{4.20}$$

or

$$\dot{\boldsymbol{\omega}}_2^{(2)} \times \mathbf{d}_2^{(2)} = \mathbf{C}_2'\mathbf{u}' + \mathbf{D}_2' \tag{4.21}$$

where

$$\mathbf{C}_2' = \mathbf{C}_2\mathbf{A}_{sp} \tag{4.22}$$

and

$$\mathbf{D}_2' = \mathbf{C}_2\mathbf{B}_{sp} + \mathbf{D}_2 \tag{4.23}$$

Eq. (3.50) is combined with Eq. (4.21) and Eq. (4.16) gives:

$$\begin{aligned}\mathbf{A}_1\ddot{\mathbf{z}}_1 + \mathbf{B}_1 &= \mathbf{R}_{01}^T\mathbf{C}_1'\mathbf{u} + \mathbf{R}_{01}^T\mathbf{R}_{02}\mathbf{C}_2'\mathbf{u} + \mathbf{R}_{01}^T\mathbf{R}_{02}\mathbf{D}_2' \\ &+ \mathbf{R}_{01}^T\mathbf{R}_{02}(\boldsymbol{\omega}_2^{(2)} \times (\boldsymbol{\omega}_2^{(2)} \times \mathbf{d}_2^{(2)})) + \mathbf{R}_{01}^T\mathbf{D}_1' \\ &- \mathbf{R}_{01}^T\mathbf{a}_1^{(0)} - 2\boldsymbol{\omega}_1^{(1)} \times (\dot{\mathbf{l}}_{12} + \dot{\mathbf{z}}_{12}) \\ &- \dot{\boldsymbol{\omega}}_1^{(1)} \times (\mathbf{l}_{12} + \mathbf{z}_{12}) - \boldsymbol{\omega}_1^{(1)} \times (\boldsymbol{\omega}_1^{(1)} \times (\mathbf{l}_{12} + \mathbf{z}_{12}))\end{aligned} \tag{4.24}$$

$$\ddot{\mathbf{z}}_1 = \mathbf{A}_1^{-1}(\mathbf{R}_{01}^T\mathbf{C}_1' + \mathbf{R}_{01}^T\mathbf{R}_{02}\mathbf{C}_2')\mathbf{u}' + \mathbf{f}_1' \tag{4.25}$$

or

$$\ddot{\mathbf{z}}_1 = \mathbf{f}_1' + \mathbf{b}_1'\mathbf{u}' \tag{4.26}$$

where

$$\begin{aligned}\mathbf{f}_1' &= \mathbf{A}_1^{-1}[\mathbf{R}_{01}^T\mathbf{R}_{02}(\boldsymbol{\omega}_2^{(2)} \times (\boldsymbol{\omega}_2^{(2)} \times \mathbf{d}_2^{(2)}))] - \mathbf{R}_{01}^T\mathbf{a}_1^{(0)} \\ &- 2\boldsymbol{\omega}_1^{(1)} \times (\dot{\mathbf{l}}_{12} + \mathbf{z}_{12}) + \mathbf{R}_{01}^T\mathbf{W}_1 - \dot{\boldsymbol{\omega}}_1^{(1)} \times (\mathbf{l}_{12} + \mathbf{z}_{12}) \\ &- \boldsymbol{\omega}_1^{(1)} \times (\boldsymbol{\omega}_1^{(1)} \times (\mathbf{l}_{12} + \mathbf{z}_{12})) - \mathbf{B}_1 + \mathbf{R}_{01}^T\mathbf{R}_{02}\mathbf{D}_2' + \mathbf{A}_1^{-1}(\mathbf{R}_{01}^T\mathbf{D}_1)' \\ \mathbf{b}_1' &= \mathbf{A}_1^{-1}(\mathbf{R}_{01}^T\mathbf{C}_1' + \mathbf{R}_{01}^T\mathbf{R}_{02}\mathbf{C}_2')\end{aligned} \tag{4.27}$$

Rearranging Eq. (3.67) and Eq. (4.12) leads to:

$$\begin{aligned}\ddot{\psi} &= (\dot{\phi}\cos\phi\sec\theta + \dot{\theta}\sin\theta\sec\theta\tan\theta)\omega_{2y}^{(2)} \\ &+ (-\dot{\phi}\sin\phi\sec\theta + \dot{\theta}\cos\theta\sec\theta\tan\theta)\omega_{2z}^{(2)} \\ &+ \sin\theta\sec\theta(A_{33}\delta_\theta - B_3 + (A_{11}\theta_o - B_1)l_r)/I_{yy} \\ &+ \cos\theta\sec\theta((A_{44}\theta_\psi)l_r - K_m(A_{11}\theta_o - B_1))/I_{zz}) \\ &+ (\sin\phi\sec\theta)a_2 + (\cos\phi\sec\theta)a_3\end{aligned} \tag{4.28}$$

Note that the subscript 2 is dropped from Eq. (4.28) for simplicity. Eq. (4.28) can be written in the standard form:

$$\ddot{\psi}_2 = f_2' + \mathbf{b}_2'\mathbf{u}' \tag{4.29}$$

where

$$\mathbf{u}' = \begin{bmatrix} \theta_o \\ \delta_\phi \\ \delta_\theta \\ \theta_\psi \end{bmatrix} \tag{4.30}$$

$$\begin{aligned} f_2' &= (\dot{\phi}\cos\phi\sec\theta + \dot{\theta}\sin\theta\sec\theta\tan\theta)\omega_{2y}^{(2)} \\ &+ (-\dot{\phi}\sin\phi\sec\theta + \dot{\theta}\cos\theta\sec\theta\tan\theta)\omega_{2z}^{(2)} \\ &+ (\sin\phi\sec\theta)a_2 + (\cos\phi\sec\theta)a_3 \\ &+ \sin\theta\sec\theta(-B_3 - B_1 l_r)/I_{zz} + \cos\theta\sec\theta k_m B_1/I_{zz} \end{aligned} \tag{4.31}$$

$$\mathbf{b}_2' = \left[\begin{array}{cccc} \frac{\sin\theta\sec\theta l_r A_{11}}{I_{yy}} & -\frac{\cos\theta\sec\theta k_m A_{11}}{I_{zz}} & 0 & \frac{\sin\phi\sec\theta A_{33}}{I_{yy}} \end{array} \quad \frac{\cos\theta\sec\theta}{I_{44}} \right] \tag{4.32}$$

Eq. (4.29) and Eq. (4.26) must be combined to have the full input-output equations.

$$\begin{bmatrix} \\ \ddot{\mathbf{z}}_1 \\ \\ \ddot{\psi} \end{bmatrix} = \begin{bmatrix} \ddot{l}_{12} \\ \ddot{\alpha}_{12} \\ \ddot{z}_{12} \\ \ddot{\psi} \end{bmatrix} = \begin{bmatrix} \\ \mathbf{f}_1' \\ \\ f_2' \end{bmatrix} + \begin{bmatrix} \\ \mathbf{b}_1' \\ \\ b_2' \end{bmatrix} \mathbf{u}' \tag{4.33}$$

or

$$\ddot{\mathbf{z}} = \mathbf{f}' + \mathbf{b}'\mathbf{u}' \tag{4.34}$$

4.3 Sliding Mode Controller Design

A new feedback control law for controlling inputs $[\theta_o, \delta_\phi, \delta_\theta, \theta_\psi]^T$ is determined to control helicopter 2 such that the desired distance l_{12}^d, view angle α_{12}^d, and height offset z_{12}^d, all of which are defined in frame 1, are maintained. Meanwhile, the yaw angle of helicopter 2, ψ_2^d, follows the yaw of helicopter 1. The sliding mode control method is again employed in the controller design process. It is noticed that the design procedure is the same as before, except the new input-output equation for the nominal parameters is considered:

$$\ddot{\mathbf{z}} = \hat{\mathbf{f}}' + \hat{\mathbf{b}}'\mathbf{u}' \tag{4.35}$$

4.4 Calculation of the Control Gains

The $l - \alpha$ controller's nonlinearity gains are determined according to Eq. (3.86). η_i's in Eq. (3.85) are selected to be 1.0 for a fast convergence of the approaching phase. Other assumptions are the maximum velocities for the helicopter along x, y, and z axis directions are 2 m/s and the maximum angle velocities along x, y, and z axis directions are $\frac{\pi}{4}$ rad/s. The following analysis is employed.

ζ is derived according to Eq. (3.84). For the parameters I_{xx}, I_{yy}, I_{zz}, K_1, K_2, K_4, K_5, and K_6 (only K_4 and K_6 appear in the Fly-Bar dynamics), they are identified with average values with standard deviation [16]. A program is written where a loop is applied.

Table 4.1: List of parameters identified using the system identification method (adapted from [16])

Parameters	Average values with standard deviation
I_{xx}	0.137 ± 0.0228 kg·m^2
I_{yy}	0.221 ± 0.0478 kg·m^2
I_{zz}	0.0323 ± 0.00234 kg·m^2
K_1	0.886 ± 0.00954 N·s·kg^{-1}·m^{-1}
K_2	1.12 ± 0.250 N·kg^{-1}·m^{-1}
K_4	976.676 ± 161.748 N·kg^{-1}·deg^{-1}
K_5	27.7 ± 1.20 N·s·kg^{-1}·deg^{-1}
K_6	5760 ± 302 N·kg^{-1}·deg^{-1}

32 combinations of the five uncertainties are investigated to find the maximum $\mathbf{b}$, and then ζ.

$\mathbf{F}$ is obtained using Eq. (3.81). It is noticed that besides the uncertainties appear in the expression of $\mathbf{f}$, different initial velocity conditions also result in different $\mathbf{f}$. Using the assumptions about different velocities and angular velocities above, a 0.1 increment for the velocities ranging from 0 to 2 m/s and $\pi/80$ increment for the angular velocities ranging from 0 to $\frac{\pi}{4}$ rad/s are selected in a loop to find the maximum $\mathbf{f}$ additional to the uncertainties consideration.

For the $|-\hat{\mathbf{f}}_j + \dot{\mathbf{s}}_{rj}|$ part in Eq. (3.86), it is also assumed that:

$$\begin{aligned} l_{12} - l_{12}^d &\leq 10 \text{ m} \\ \alpha_{12} - \alpha_{12}^d &\leq \pi \text{ rad} \\ z_{12} - z_{12}^d &\leq 10 \text{ m} \\ \psi_{12} - \psi_{12}^d &\leq \pi \text{ rad} \end{aligned} \tag{4.36}$$

The first equation in Eq. (3.76) can be rewritten as:

$$s_1 = \dot{e}_1 + \lambda_1 e_1 \tag{4.37}$$

where

$$\begin{aligned} e_1 &= l_{12} - l_{12}^d \\ \dot{e}_1 &= \dot{l}_{12} - \dot{l}_{12}^d \end{aligned} \tag{4.38}$$

When sliding surface is zero, one can get

$$\dot{e}_1 + \lambda_1 e_1 = 0 \tag{4.39}$$

The maximum value for $\dot{l}_{12} = 10$ m is obtained when $e_1 = 10$ and $\dot{l}_{12}^d = 0$ are both satisfied. In the similar way, the maximum values for $\dot{\alpha}_{12} = \pi$, $\dot{z}_{12} = 10$ m, and $\dot{\psi}_2 = \pi$ are determined.

For the disturbance W, as an example, the wind is applied only in the y axis direction. Also, it is assumed that the wind is applied to a flat planar area of 0.15 m$\times$ 0.15 m in the x axis and 0.2 m$\times$ 0.15 m in the y axis. The following formulation is used:

$$f_w = (\frac{1}{2}\rho v^2)A \tag{4.40}$$

where f_w is the force from the wind, ρ is the density of the air, v is the velocity in the corresponding axis.

The numerical values for the variables mentioned above are as follows:

$$\zeta = \begin{bmatrix} 0.2648 & 0 & 0 & 0 \\ 0 & 0.1664 & 0 & 0 \\ 0 & 0 & 0.2163 & 0 \\ 0 & 0 & 0 & 0.0724 \end{bmatrix} \tag{4.41}$$

$$\mathbf{F} = \begin{bmatrix} 0.4342 \\ 0.3460 \\ 0 \\ 2.8751 \end{bmatrix}$$

$$\mathbf{W} = \begin{bmatrix} 1.8000 \\ 0.1314 \\ 0 \\ 0 \end{bmatrix}$$

$$|-\hat{\mathbf{f}}_\mathbf{j} + \dot{\mathbf{s}}_{\mathbf{rj}}| = \begin{bmatrix} 36.8686 \\ 17.999 \\ 16.0337 \\ 0.5855 \end{bmatrix}$$

Finally, the following values are determined:

$$k_1 = 17.6782 \qquad k_2 = 5.0449 \qquad k_3 = 5.7012 \qquad k_4 = 4.2231 \tag{4.42}$$

4.5 Simulations

Numerical simulations show the correctness of the rotor swashplate actuation mechanism modeling and the effectiveness of the controller design. The prescribed paths for the leader are the same as above. In these simulations, the numerical values of the nominal dynamic parameters are related to the Ikarus ECO helicopter in [16]:

$$\begin{aligned} \hat{m} = 1.36 \text{ kg} \qquad & \hat{I}_{xx} = 0.137 \text{ kgm}^2 \\ \hat{I}_{yy} = 0.221 \text{ kgm}^2 \qquad & \hat{I}_{zz} = 0.0323 \text{ kgm}^2 \\ \hat{l}_r = 0.1 \text{ m} \qquad \hat{l}_t = 0.635 \text{ m} \qquad & d = 1.0 \text{ m} \end{aligned} \tag{4.43}$$

The wind disturbance described in Eq. (4.40) is applied to the simulations. λ_i's, which are selected to be 1, along with uncertainty in the nominal dynamic parameters and the wind parameters Eq. (4.43) are used to calculate the bounds of the parameter uncertainty in Eq. (3.84).

4.5.1 Taking Off

The first simulation set is to simulate the motion of the follower when the leader helicopter is taking off. The initial positions for the leader and follower are $(0, 0, 0)$ m and $(0, 15, 0)$ m, respectively. The leader has no motion in either x-axis or y-axis direction. It only has an upward speed of -1 m/s (the positive direction is defined downwards) in the z direction. The follower receives a command to follow the leader in the way that the lateral distance is $l_{12}^d = 10$ m, the view angle is $\alpha_{12}^d = \pi/2$ rad, the vertical distance is $z_{12}^d = -1$ m, and a yaw angle is $\psi_2^d = 0$ rad. The results of the simulation in Figures. 4.4(a), 4.4(b), 4.5(a) and 4.5(b) show the motion of the follower; Fig. 4.6(a) shows the control parameters l_{12}, α_{12}, z_{12} and ψ_2. Fig. 4.6(b) shows $\theta_o, \delta_\phi, \delta_\theta$, and θ_ψ. It is shown that θ_o has some fluctuations at the beginning and then reaches 1.35 degree; δ_ϕ undertakes some fluctuation at beginning but reaches 0 m after 10 seconds; δ_θ is about -0.01 m; and θ_ψ is around 5.4 degree. From the 3D drawing of the two helicopters' trajectories (Figure. 4.7), it is noticed that the follower does follow the leader's taking off perfectly. Furthermore, the controller displays good time response while the control inputs are not too large and physically achievable. Figure. 4.8 compares the results with and without wind disturbance. Trajectories in both case are almost identical. This means that the controller performances well in the presence of the wind disturbance.

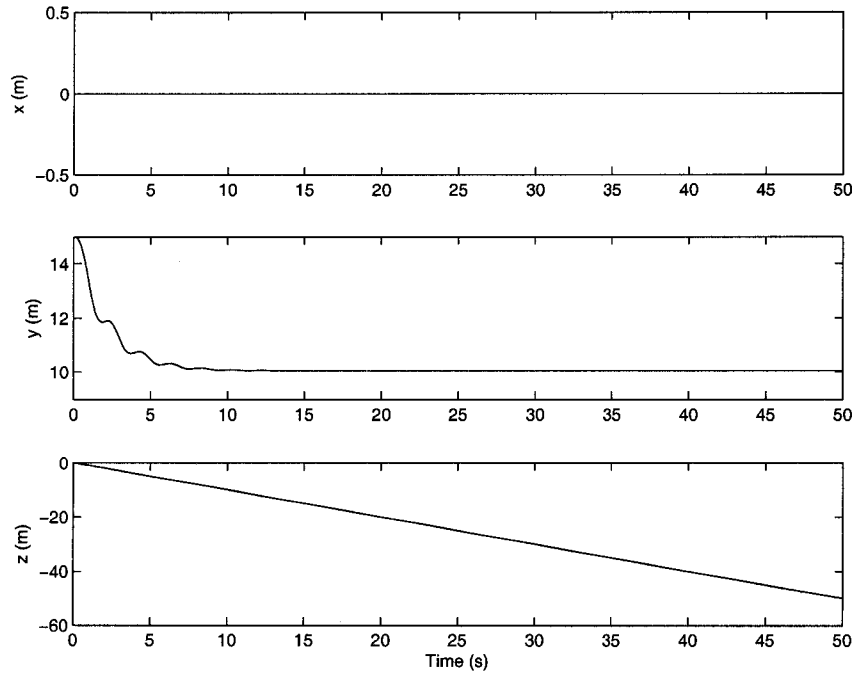

(a)

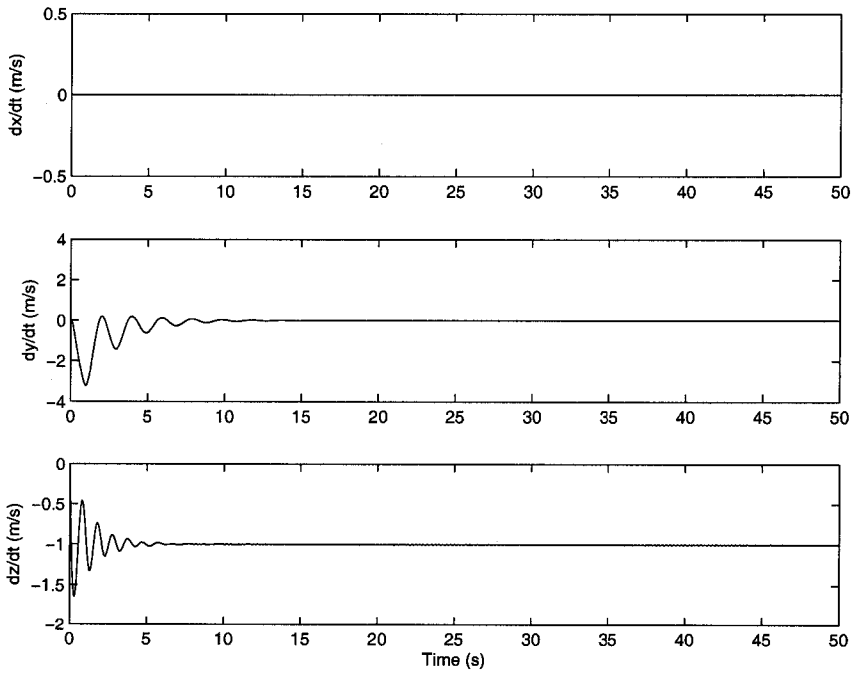

(b)

Figure 4.4: The states of the follower when the leader is taking off. (a) Position, and (b) Velocities

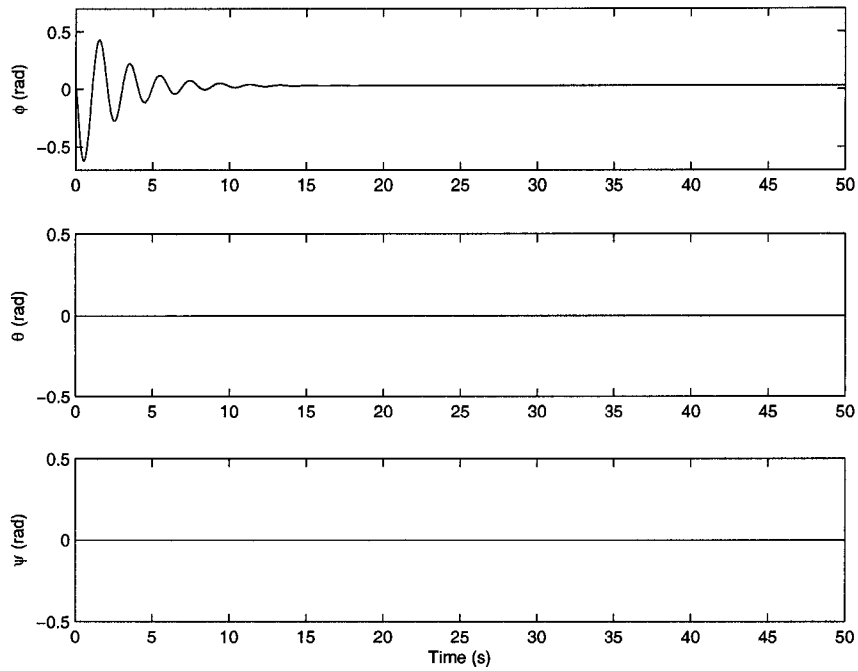

(a)

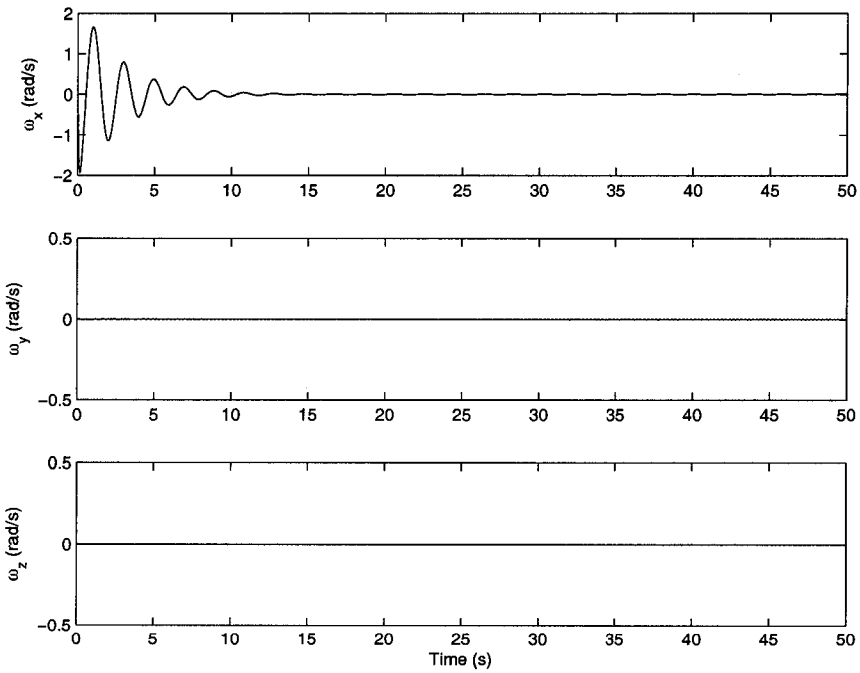

(b)

Figure 4.5: The states of the follower when the leader is taking off. (a) Euler angles, and (b) Angular velocities

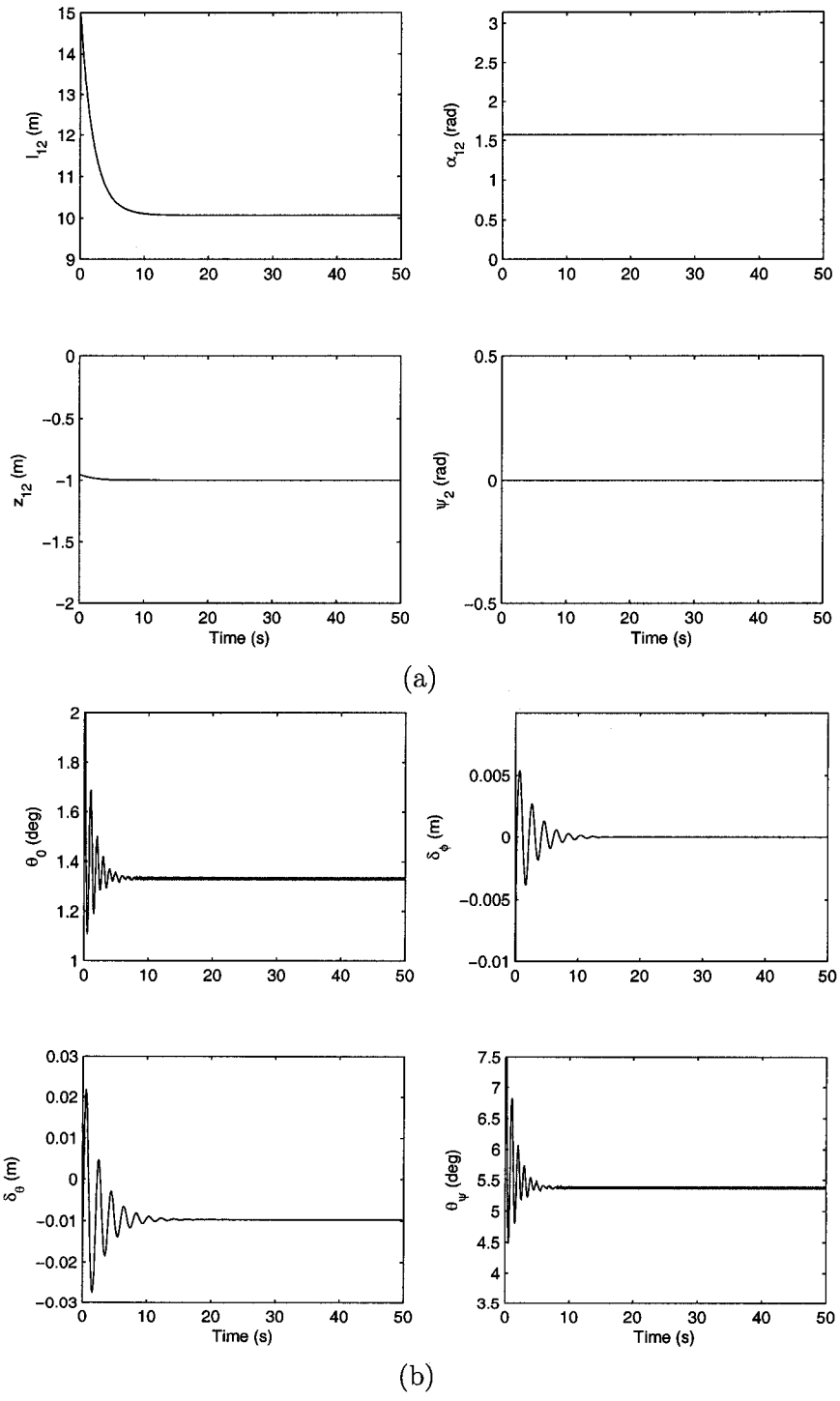

Figure 4.6: (a) Formation parameters, (b) Control displacement when the leader is taking off

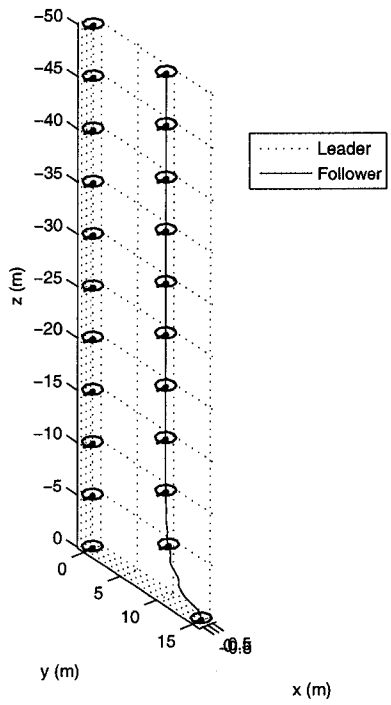

Figure 4.7: Trajectories of both helicopters when the leader is taking off with the wind disturbance and the controller in Chapter 4

4.5.2 Sinusoidal Wave Movement

This part is to simulate the motion of the follower when the leader is moving on a sinusoidal path in the $x-y$ plane. For the leader helicopter, the initial position is $(0,0,0)$ m. The leader has a constant velocity in the x-axis direction, while its velocity in the y-axis direction is $1 \times \sin(t+\pi/2)$ m/s. The leader has no motion in the z-axis direction. The follower starts at $(0,15,0)$ m and receives a command to follow the leader in the way that the lateral distance is $l_{12}^d = 10$ m, the view angle is $\alpha_{12}^d = \pi/2$ rad, a vertical distance is $z_{12}^d = -1$ m, and a yaw angle is $\psi_2^d = 0$ rad. The results of the simulation in Figs. 4.9(a), 4.9(b), 4.10(a) and 4.10(b) show the motion of the follower; Figure 4.11(a) shows the control parameters l_{12}, α_{12}, z_{12} and ψ_2. Figure 4.11(b) shows $\theta_o, \delta_\phi, \delta_\theta$, and θ_ψ. It is shown that θ_o, δ_ϕ, and δ_θ present sinusoidal shapes; and θ_ψ is 5.05 degree. Figure. 4.12 shows the trajectories of both helicopters. From the 3D drawing of the two helicopters' trajectories, it is noticed that the follower does follow the leader's trajectory perfectly. Furthermore, the controller displays good time response.

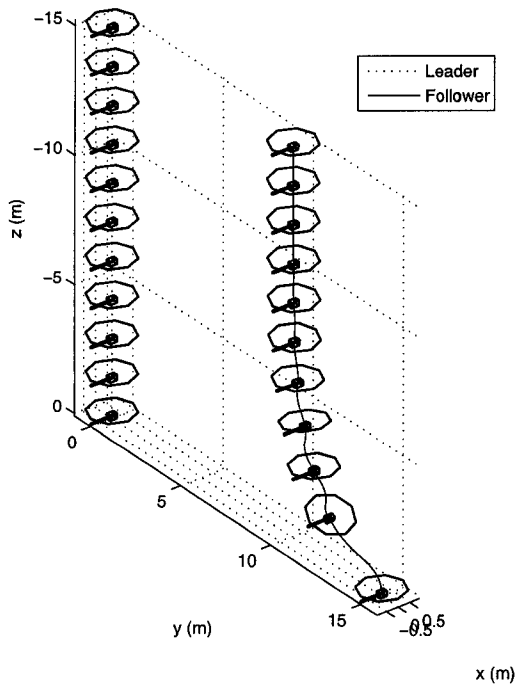

(a)

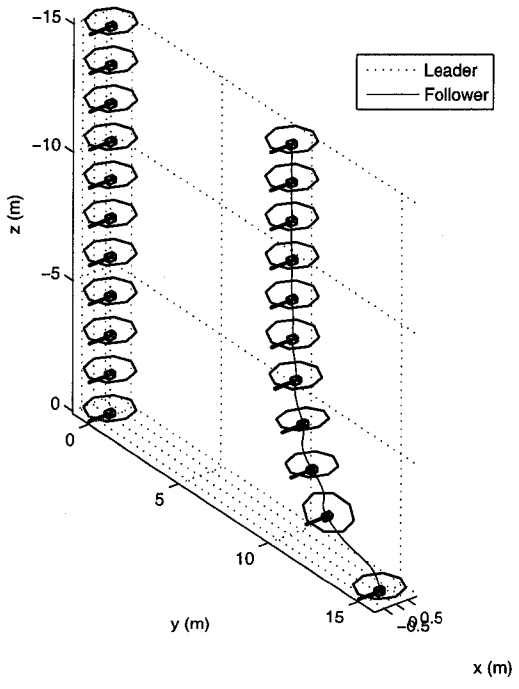

(b)

Figure 4.8: Trajectories of both helicopters when the leader is taking off (first 15 sec), (a) without the wind disturbance and the controller in Chapter 3, and (b) with the wind disturbance and the controller in Chapter 4

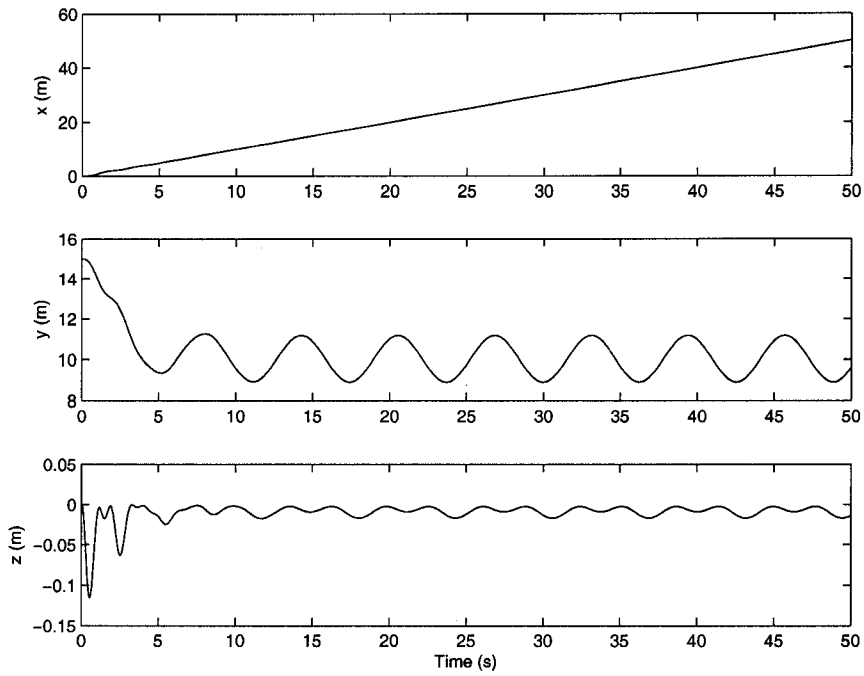

(a)

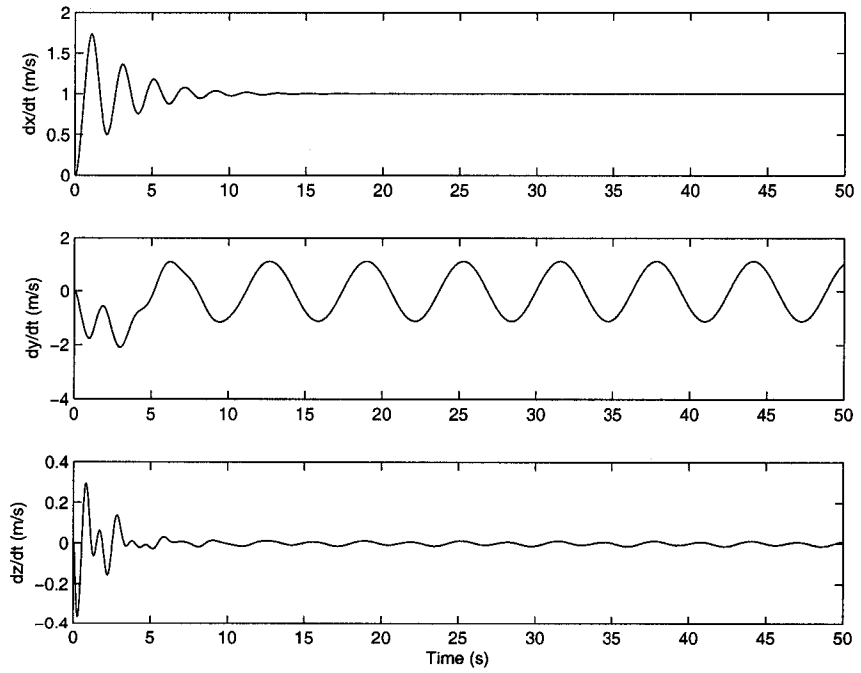

(b)

Figure 4.9: The states of the follower when the leader is moving on a sinusoidal movement path. (a) Position, and (b) Velocities

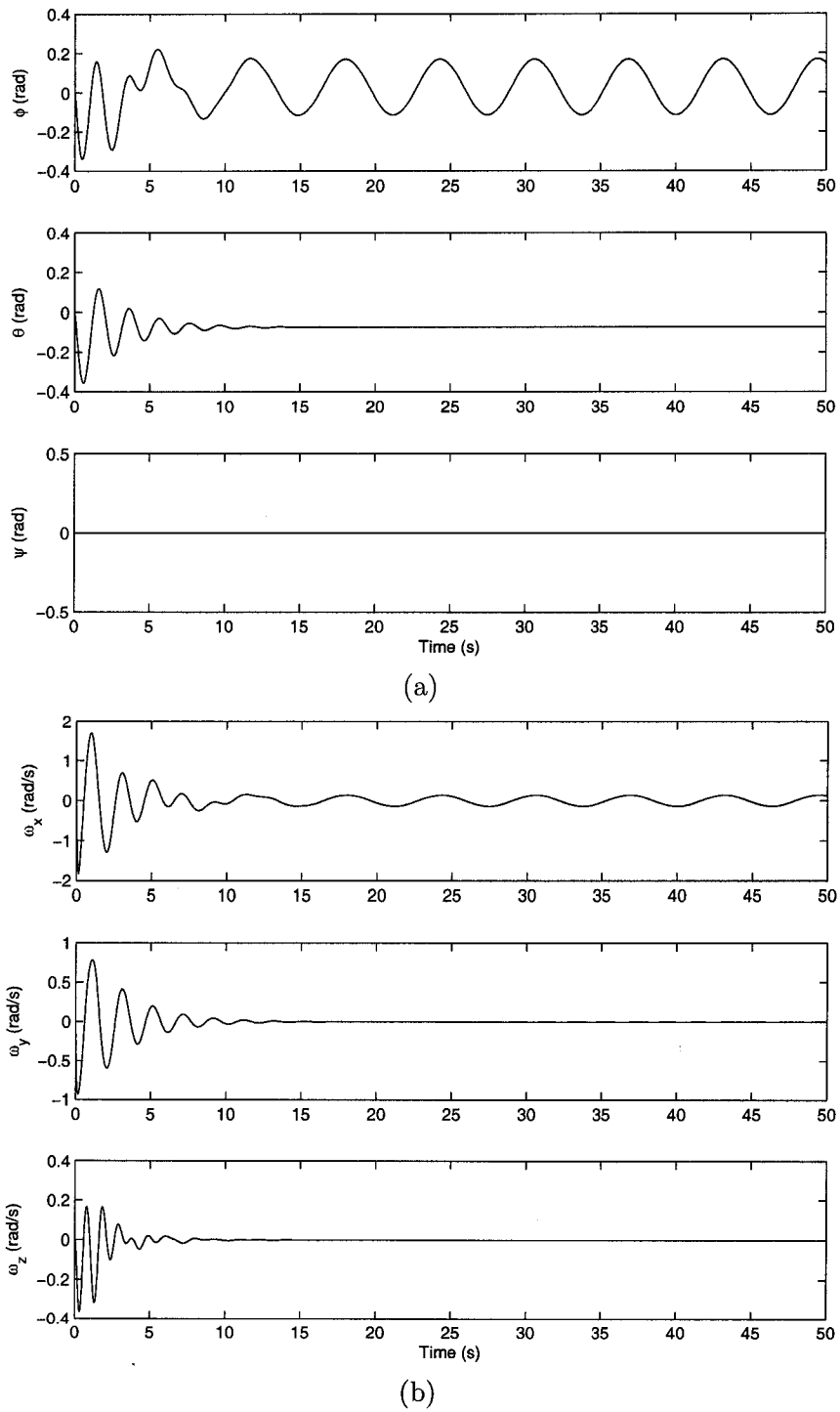

Figure 4.10: The states of the follower when the leader is moving on a sinusoidal movement path. (a) Euler angles, and (b) Angular velocities

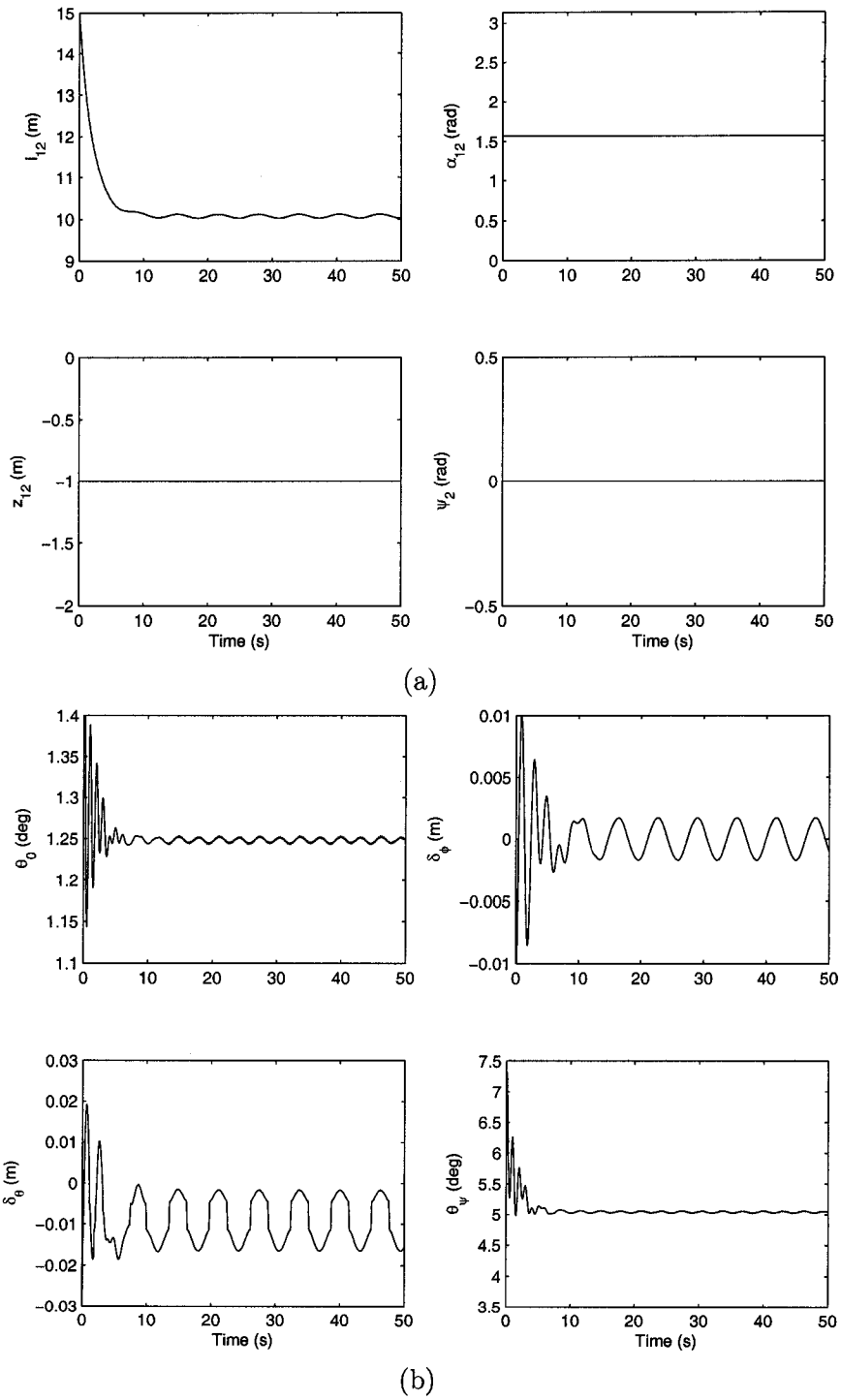

Figure 4.11: (a) Formation parameters, (b) Control displacement when the leader is moving on a sinusoidal path

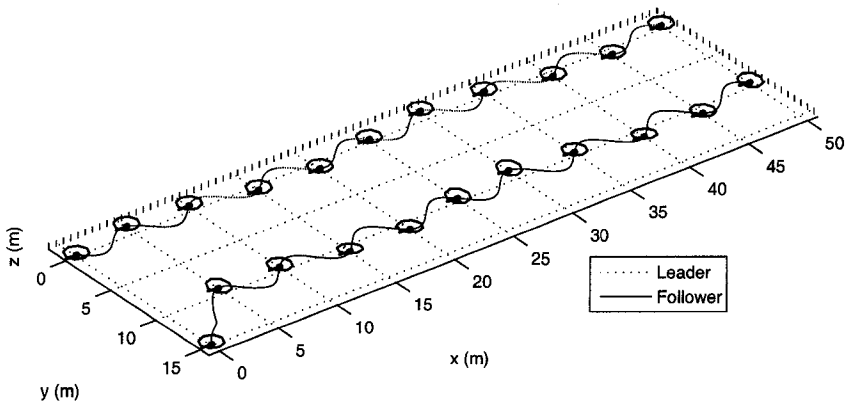

Figure 4.12: Trajectories of both helicopters when the leader is moving on a sinusoidal path

4.5.3 Circular Movement

This simulation set is to simulate the motion of the follower when the leader is moving on a circular path in the $x-y$ plane. In this case, the initial position of the leader is $(10, 0, -4)$ m. The leader moves in a counterclockwise circle with radius of 10 m in the $x-y$ plane at the height of 4 m and the linear velocity is 1 m/s. Both helicopters' yaw angles start at $\pi/2$ and the yaw angle rate of leader is 0.1 rad/s, which means it does not have to face the same direction as defined in the initial condition while moving on a circle. The initial position of the follower is $(8, 0, 0)$ m. The follower receives a command to follow the leader in the way that the lateral distance is $l_{12}^d = 10$ m, the view angle is $\alpha_{12}^d = pi/2$ rad, a vertical distance is $z_{12}^d = -1$ m, and the yaw angle rate is 0.1 rad/s. The results of the simulation in Figures. 4.14(a), 4.14(b), 4.13(a) and 4.13(b) show the motion of the follower; Figure. 4.15(a) shows the control parameters l_{12}, α_{12}, z_{12} and ψ_2. Figure. 4.15(b) shows $\theta_o, \delta_\phi, \delta_\theta$, and θ_ψ. It is shown that θ_o starts at 1.28 degree and then goes to 1.24 degree; δ_ϕ undertakes some fluctuation at the beginning but reaches 0 m after 15 seconds; δ_θ takes a sinusoidal wave shape; and θ_ψ is around 5 degree. Figure. 4.16 shows the trajectories of both helicopters. From the 3D drawing of the two helicopters' trajectories, it is noticed that the follower does follow the leader's trajectory perfectly. Furthermore, the controller displays good response.

For all simulations in this chapter, the results are close to the ones in Chapter 3. Note that the wind disturbance is present in Chapter 4's simulations but not in the Chapter 3's simulations. Therefore, if the controller had not designed properly, the results would have been different. Similarity of the results shows that the new controller rejects disturbance very well.

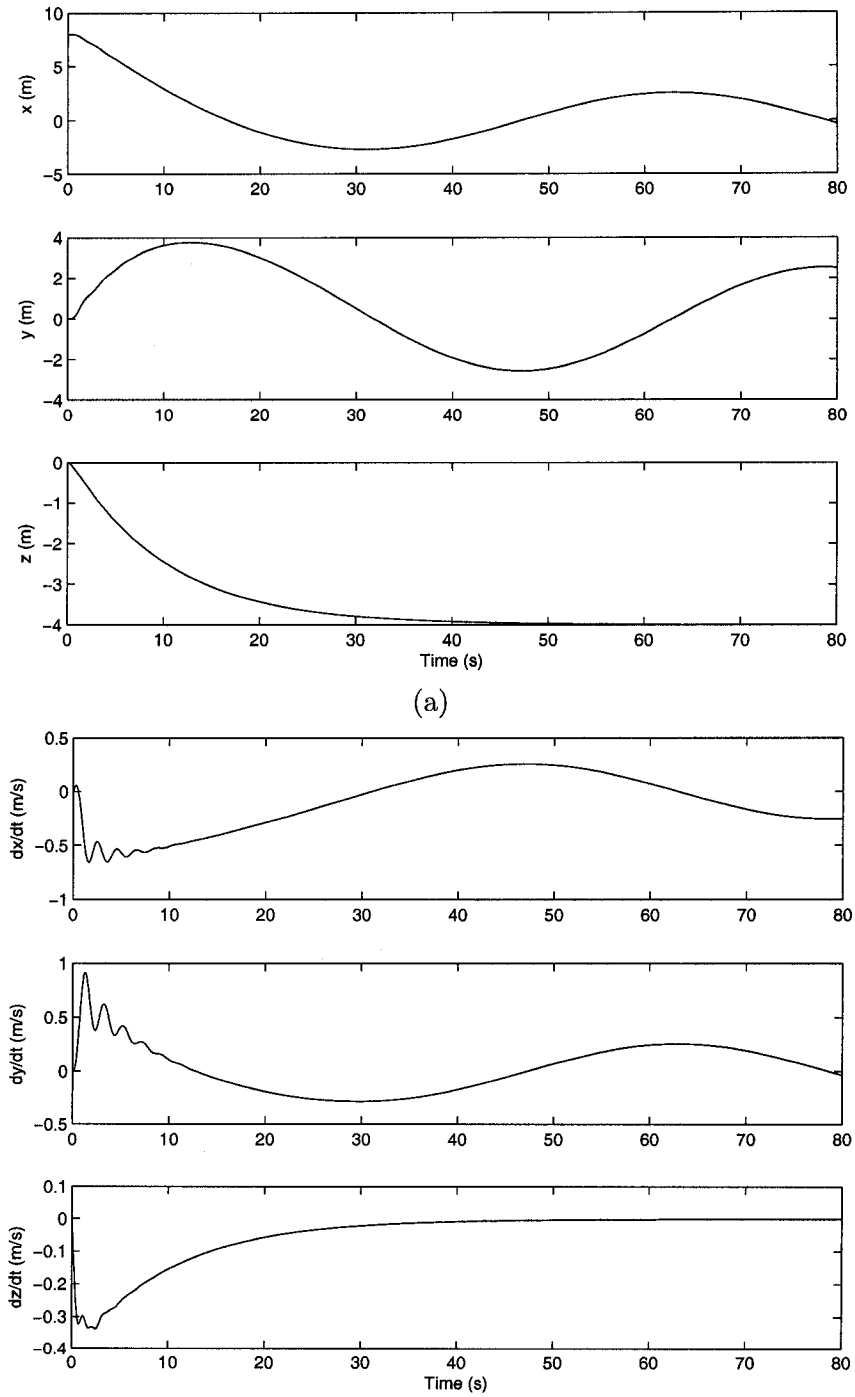

Figure 4.13: The states of the follower when the leader is moving on a circular path. (a) Position, and (b) Velocities

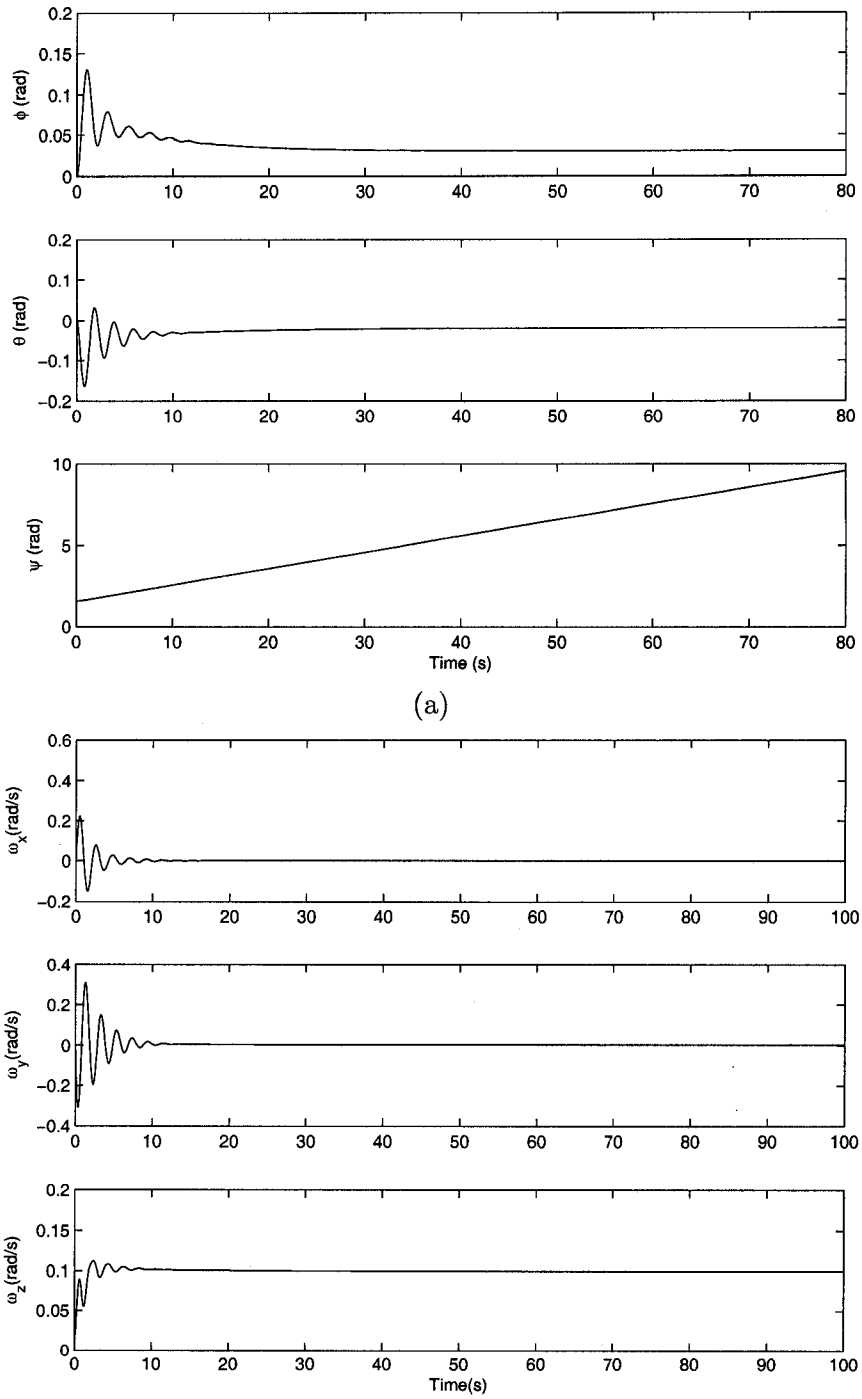

Figure 4.14: The states of the follower when the leader is moving on a circular path. (a) Euler angles, and (b) Angular velocities

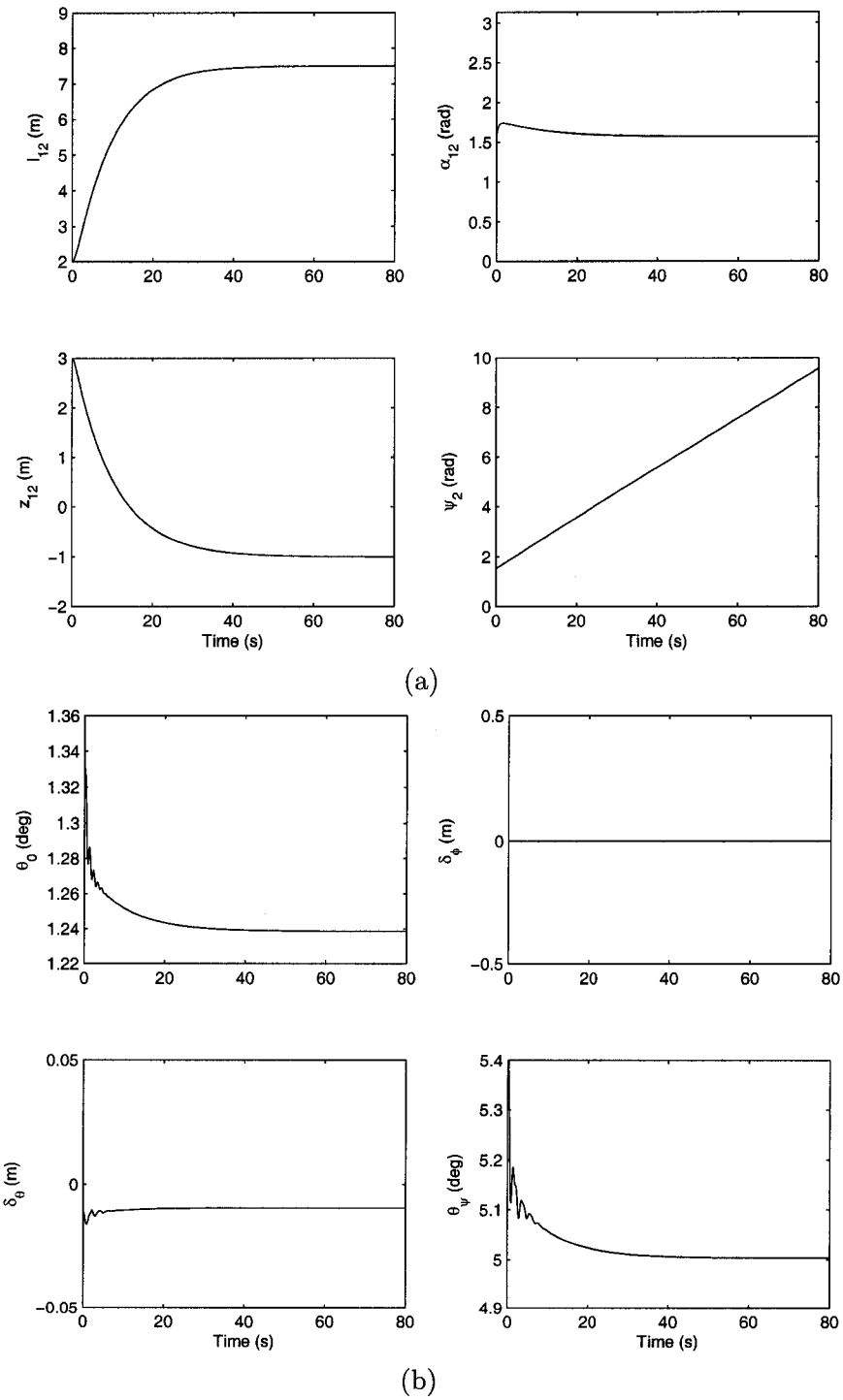

Figure 4.15: (a) Formation parameters, (b) Control displacement when the leader is moving on a circular path

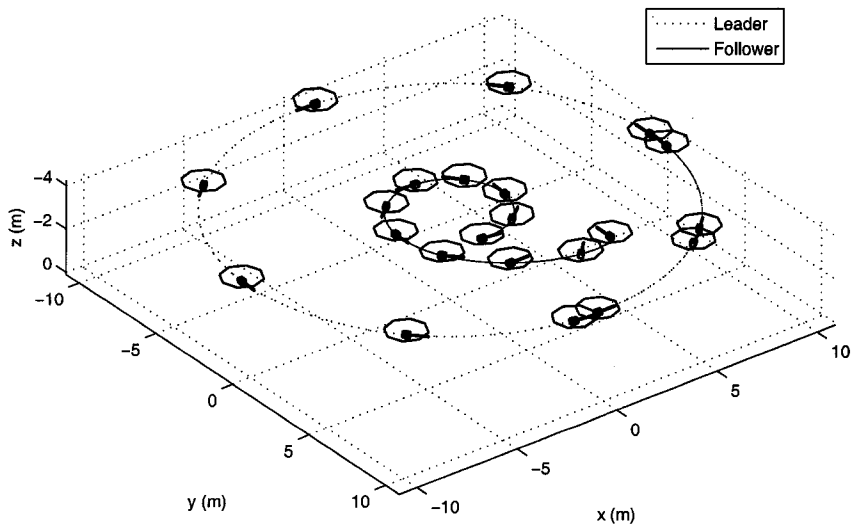

Figure 4.16: Trajectories of both helicopters when the leader is on a circular path

CHAPTER 5

HARDWARE IMPLEMENTATION

In the previous chapters, two sliding mode controllers, one with $[T\ M_\phi\ M_\theta\ T_T]^T$ as outputs and the other with $[\theta_0\ \delta_\phi\ \delta_\theta\ \theta_\psi]^T$ as output, are developed. In this chapter, the xPC Target is employed as a prototyping environment that connects the Simulink to the physical systems. A target PC, as the controller, downloads and executes the control code in real time in the experimental set. For this project, the hardware to be controlled is the servo motors of the helicopter.

xPC Target has many advantages including: High capabilities for fast prototyping and hardware-in-the-loop simulation of control systems; automatically generating code and uploading the code to a second PC that runs the xPC Target real-time kernel. It also supports more than 250 standard I/O boards and offers host-target communications via TCP/IP protocol. The graphical user interface (GUI) and MATLAB command-line interface configure the computer to communicate with the xPC Target computer as the controller.

For the servo motors, the length of the pulse command applied to the motor is proportional to the position that the output shaft needs to move to. The control wire built in the motor is to communicate the angle to which the servo should turn. The angle is decided by the duration of a pulse that is applied to the control wire, which is called Pulse Width Modulation (PWM). In every 0.02 seconds, the length of the pulse determines how far the motor turns. A function that converts an input servo angle into a corresponding number of clock ticks to hold the PWM signal high and low is found by Michael Dawson, one of the summer students in the laboratory, by test and trial method:

$$p = (0.01 \times 10^{-3})u + 1.5 \times 10^{-3} \tag{5.1}$$
$$H = f \times p$$
$$L = f \times (T - p)$$

where $f = 80$ MHz is the reference frequency, $T = 0.02$ second is the period, p is the pulse duration in seconds, u is the input angle in deg, H is the number of clock ticks to hold

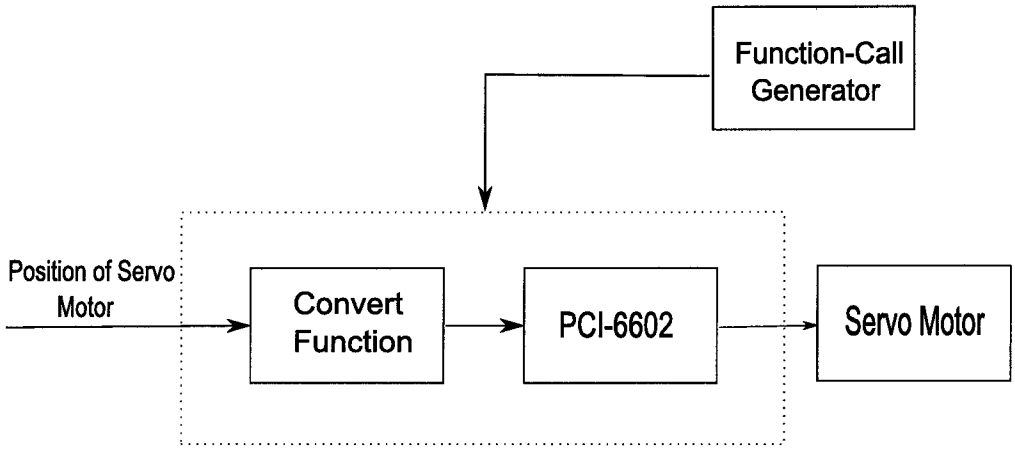

Figure 5.1: A flow diagram of hardware implementation

voltage high (Hz), and L is the number of clock ticks to hold voltage low (Hz).

The National Instruments PCI-6602 is used to perform pulse generation. The Function-Call Generator is employed to implement the iterator operation in the Simulink. On each 0.02 second, the Function-Call Generator execute the PCI-6602 (Pulse Generator).

A flow diagram of the hardware implementation is given in Fig. 5.1. Specifically, Fig. 5.2 shows a program for the servo motors control procedure. The inputs of the program have to be converted to the corresponding positions of the servo motors first, followed by the above mentioned hardware implementation.

- The collective pitch movement is a result of both the roll input and the pitch inputs, as shown in Fig. 5.3. Here, a known displacement of the swashplate due to the collective pitch movement is assumed.

- The roll servo inputs to the swashplate leads to the roll movement, as shown in Fig. 5.4. Two roll servos have the same position change, but in opposite directions. A known angle change of the swashplate due to the roll movement is assumed.

- A pitch servo input to the swashplate results the pitch movement, as shown in Fig. 5.5. This also leads to the change for the two roll servo motors (the same position and the same direction). A known angle change of the swashplate due to the pitch movement is assumed.

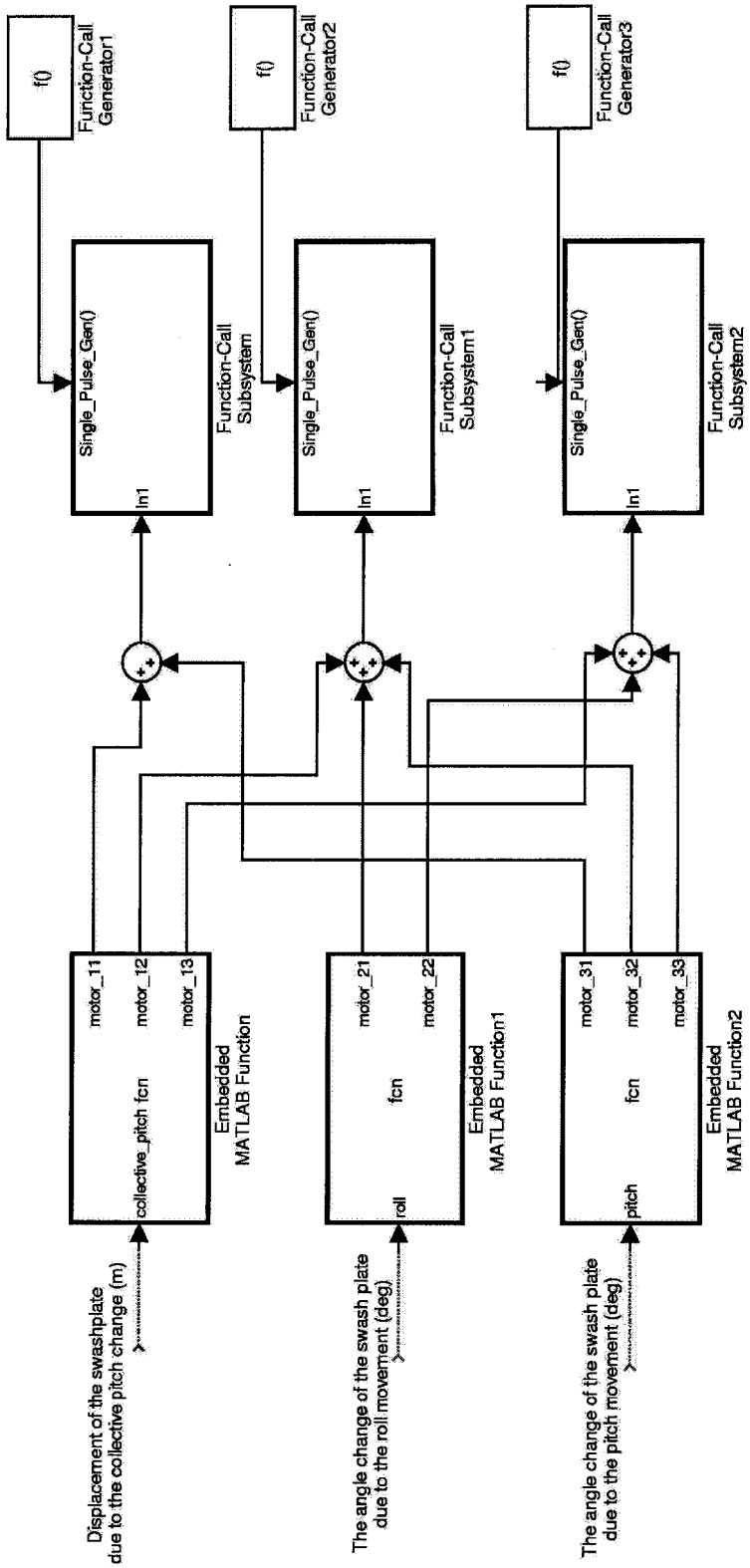

Figure 5.2: Servo motors Control

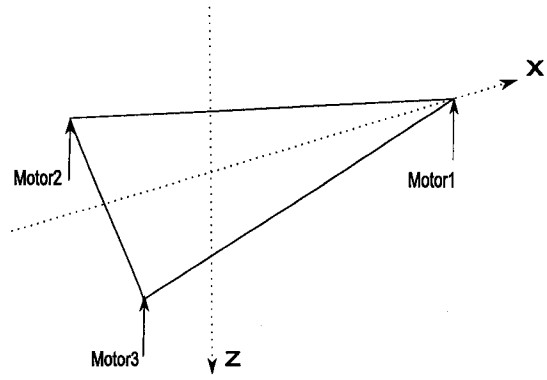

Figure 5.3: The collective command. All motors move equally.

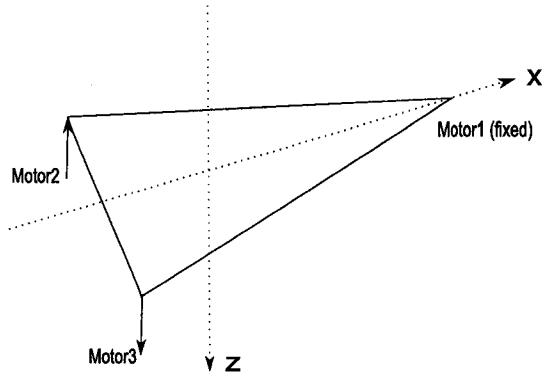

Figure 5.4: The roll command. Motor 2 and 3 move opposite to each other; Motor 1 is fixed.

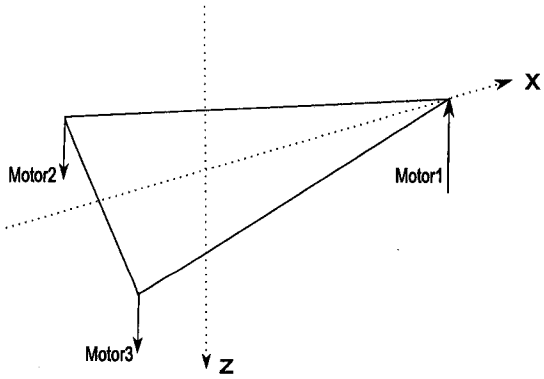

Figure 5.5: The pitch command. Motor 2 and 3 move the same direction; Motor 1 moves opposite to Motor 2 and 3 and the displacement of Motor 1 is twice of the other two motors.

CHAPTER 6

CONCLUSIONS AND FUTURE WORK

6.1 Conclusions

In this work, a control strategy for forming arbitrary formations of multiple autonomous helicopters was presented. The sliding mode controllers developed in the work only used the state information of the neighboring helicopters.

First, a 6-DOF dynamic model of the helicopter without the rotors' actuation part was considered. In this case, the designed controller had two forces and two moments as the actuation means. However, it is difficult to control the actuation forces and moments directly in real systems. Based on this, the modeling of the main rotor's actuation mechanism was developed. In this case, the pitch angles of the main blades and tail blades, and the displacements of the swashplate were directly controlled. Then, these parameters were converted to the servo motors angles. The control of the actual helicopter servos was also presented.

In both cases, the control parameters, i.e., the relative distances and orientation of the helicopters, were stabilized. The robustness of the control law were demonstrated in the presence of the existence of parameter uncertainty in the dynamic model and wind disturbances. The effectiveness of the controllers was shown through simulation results.

6.2 Future Work

The current results show that this autonomous formation control strategy is promising, however, further work has to be done in order to present a complete formation approach. Therefore, possible future research works can be summarized as below:

- In this work, the physical parameters used in the mathematical simulations are based on the Ikarus ECO electric helicopter. System Identification is needed for the Maxi-Joker 2 helicopter. Considering the high nonlinearity of the mathematical model, a single-input-single-output method is recommended by restricting the motion of helicopter to isolated single degree of freedom.

- The onboard computer box design with onboard processors, sensors and GPS navigation system must be completed. Programs supporting communications among the helicopters need to be integrated in the processors in order to safely fly in the unknown environment. Sensors and GPS systems must be calibrated to the states of the helicopters.

- Testbed must be designed for testing and calibrating all the sensors integrated on the helicopters. Sensors need to give the accurate information about the states of the helicopters that are fedback to the controller. In order to do the above, a test bed has to be designed such that it can collect the states of an attached helicopter, such as positions, orientations, and velocities. A real time data collecting system has to be set up that collects data both from the test bed and the helicopter. The hardware selection and software interface have also to be considered. The data from the testbed and the helicopter's sensors then has to be compared with each other to make sure that the sensors are calibrated correctly.

- The proposed control scheme is only one of the distributed formations controllers required for the general 3D formation. An additional $l - l$ controller should be developed to control the distance of a follower helicopter with two leader helicopters. Combining $l - \alpha$ and $l - l$ schemes, the complete robust formation controller design for autonomous helicopter is achieved.

BIBLIOGRAPHY

[1] An bal Ollero and Lu s Merino. Control and perception techniques for aerial robotics. *Annual Reviews in Control*, 28:167–78, 2004.

[2] A.J. Calise and R.T. Rysdyk. Nonlinear adaptive flight control using neural networks. *Control Systems Magazine, IEEE*, 18:14 – 25, Dec. 1998.

[3] D.W. Casbeer, R.W. Beard, T.W. McLain, Sai-Ming Li, and R.K. Mehra. Forest fire monitoring with multiple small UAVs. *American Control Conference, 2005. Proceedings of the 2005*, 5:3530 – 3535, June 2005.

[4] W. Dunbar and R. Murray. Model predictive control of coordinated multi-vehicle formations. *Decision and Control, 2002, Proceedings of the 41st IEEE Conference on*, 2002.

[5] D. Galzi and Y. Shtessel. UAV formations control using high order sliding modes. *Proceedings of the 2006 American Control Conference*, 2006.

[6] F. Giulietti, L. Pollini, and M. Innocenti. Autonomous formation flight. *Control Systems Magazine, IEEE*, 20:34 – 44, Dec. 2000.

[7] Fabrizio Giulietti, Mario Innocenti, Marcello Napolitano, and Lorenzo Pollini. Dynamic and control issues of formation flight. *Aerospace Science and Technology*, 9:65–71, 2005.

[8] Y. Gu, B. Seanor, G. Campa, M.R. Napolitano, L. Rowe, S. Gururajan, and S. Wan. Design and flight testing evaluation of formation control laws. *Control Systems Technology, IEEE Transactions on*, 14(6):1105 – 1112, Nov. 2006.

[9] Henry Hexmoor, Swetha Eluru, and Hadi Sabaa. Plan sharing: Showcasing coordinated UAV formation flight. *Informatica*, 20:183–192, June 2006.

[10] Richard NI. Howard and Isaac Kaminer. Survey of unmanned air vehicles. *Proeesdlnpr of the American Control Confsnsnce*, 1995.

[11] J. S. Jang and C. Tomlin. Design and implementation of a low cost, hierarchical and modular avionics architecture for the dragonfly UAVs. *Proceedings of the AIAA*

Guidance, Navigation, and Control Conference, Monterey, AIAA, pages 2002–4465, August 2002.

[12] Eric N. Johnson, Anthony J. Calise, Ramachandra Sattigeri, Yoko Watanabe, and Venkatesh Madyastha. Approaches to vision-based formation control. *Proceedings of the IEEE Conference on Decision and Control*, 2:1643–1648, Dec. 2004.

[13] W. Johnson. *Helicopter Theory.* Dover, New York, 1980.

[14] Aaron D. Kahn and Richard J. Foch. Attitude command attitude hold and stability augmentation systems for a small-scale helicopter UAV. *AIAA/IEEE Digital Avionics Systems Conference - Proceedings*, 2:p 8.A.4/1–8.A.4/10, 2003.

[15] N.P. Kakirde, A. Davari, and J. Wang. Trajectory tracking of unmanned aerial vehicle using servomechanism strategy. *Proceedings of the 37th Southeastern Symposium on System Theory (SSST05)*, pages 163–166, Mar 2005.

[16] S.K. Kim and D.M. Tilbury. Mathematical modeling and experimental identification of an unmanned helicopter robot with flybar dynamics. *Journal of Robotic Systems*, 21(3):95–116, March 2004.

[17] T. J. Koo and S. Sastry. Output tracking control design of a helicopter model based on approximate linearization. *Proceedings of the 37th IEEE Conference on Decision and Control*, 1998.

[18] Y. Li, B. Li, Z. Sun, and Y.D. Song. Fuzzy technique based close formation flight control. *32nd Annual Conference of IEEE*, page 5 pp, November 2005.

[19] Najib Metni and Tarek Hamel. Visual tracking control of aerial robotic systems with adaptive depth estimation. *International Journal of Control, Automation, and Systems*, 5:51–60, Feb 2007.

[20] Minicopter. *Maxi-Joker Manual.* 2005.

[21] Abdellah Mokhtari, N.K. M'Sirdi, K. Meghriche, and A. Belaidi. Feedback linearization and linear observer for a quadrotor unmanned aerial vehicle. *Advanced Robotics*, 20:71–79, 2006.

[22] Lu Sardinha Monteiro, Terry Moore, and Chris Hill. What is the accuracy of DGPS. *The Journal of Navigation*, 58:207–225, 2005.

[23] Wei Ren. On constrained nonlinear tracking control of a small fixed-wing UAV. *Journal of Intelligent and Robotic Systems*, 48(4):525–537, April 2007.

[24] Allison Ryan, Marco Zennaro, Adam Howell, Raja Sengupta, and J. Karl Hedrick. An overview of emerging results in cooperative UAV control. *Proceedings of the IEEE Conference on Decision and Control*, pages 602 – 607, 2004.

[25] Reza Olfati Saber and Richard M. Murray. Flocking with obstacle avoidance: Cooperation with limited communication in mobile networks. *Proceedings of the IEEE Conference on Decision and Control*, 2:2022–2028, Dec. 2003.

[26] C. J. Schumacher and R. Kumar. Adaptive control of UAVs in close-coupled formation flight. *Proceedings of American Control Conference*, 2:849–53, 2000.

[27] Sahjendra N. Singh, Meir Pachter, Phil Chandler, Siva Banda, Steve Rasmussen, and Corey Schumacher. Input-output invertibility and sliding mode control for close formation fying of multiple UAVs. *International Journal of Robust and Nonlinear Control*, 10:779–797, 2000.

[28] Sahjendra N. Singh1, Phil Chandler, Corey Schumacher, Siva Banda, and Meir Pachter. Nonlinear adaptive close formation control of unmanned aerial vehicles. *Dynamics and Control*, 10(2):179–194, April 2000.

[29] Jean-Jacques Slotine and Weiping Li. *Applied Nonlinear Control.* Prentice Hall, 1991.

[30] John William Ransom Taylor and Kenneth Munson. *Jane's pocket book of remotely piloted vehicles : robot aircraft today.* New York : Collier Books, 1977.

[31] Haitao Wang and Jinyuan Gao. Control system design for UAV trajectory tracking. *Proceedings of SPIE, Sixth International Symposium on Instrumentation and Control Technology: Sensors, Automatic Measurement, Control, and Computer Simulation*, 6358, 2006.

[32] Xiaohua Wang, Vivek Yadav, and S.N. Balakrishnan. Cooperative UAV formation flying with stochastic obstacle avoidance. *Collection of Technical Papers - AIAA Guidance, Navigation, and Control Conference*, 1(AIAA 2005-5832):135–157, Aug 2005.

[33] Feng Xie, Ximing Zhang, Rafael Fierro, and Mark Motter. Autopilot-based nonlinear UAV formation controller with extremum-seeking. *Proceedings of the 44th IEEE Conference on Decision and Control, and the European Control Conference*, 2005:4933–4938, 2005.

[34] S. Zelinski, T.J. Koo, and S. Sastry. Hybrid system design for formations of autonomous vehicles. *Decision and Control, 2003. Proceedings. 42nd IEEE Conference on*, 1:1–6, Dec. 2003.

Appendix A

MATLAB and Simulink Programs

A.1 Controller Design: Forces and moments as Control Inputs

This part of program is to implement the controller designed in Chapter 4, when the rotor's actuation mechanism of the helicopter is not considered. Starting from the whole Simulink block diagram, it then gives all the components in the following sequence: Follower, Leader, Controller Parameters formation, Desired Parameters, and Controller.

Compared with the taking-off movement, it only involves the change of the initial conditions and the desired parameters to get the sinusoidal and circulation movements. Here, only give the example of the taking-off motion.

A.2 Controller Design: Rotor's Actuation Commands as Control Inputs

This part of the program is to implement the controller designed in Chapter 5, when the rotor's actuation mechanism of the helicopter considered. It gives the whole Simulink block diagram and the leader part.

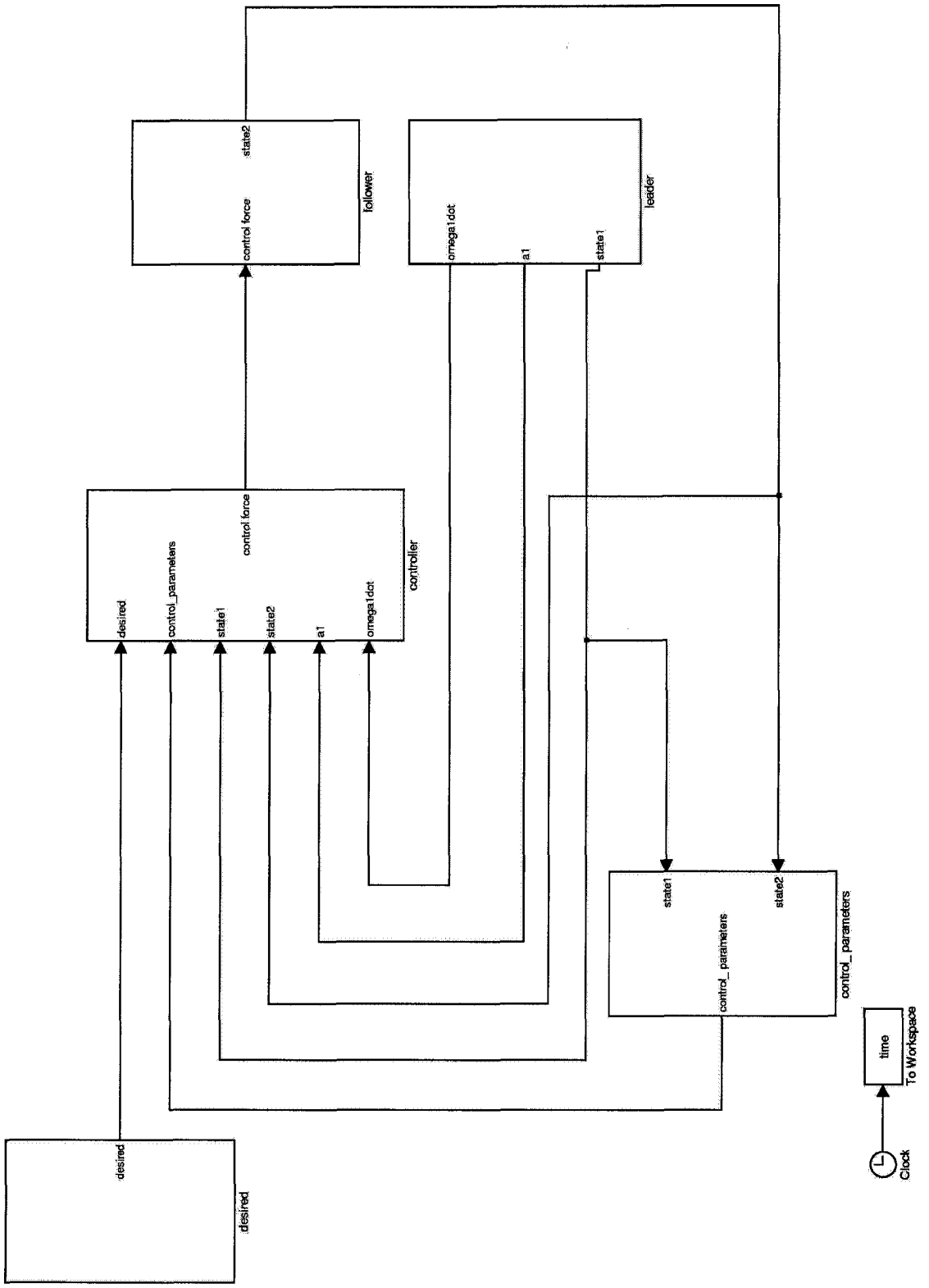

Figure A.1: The Simulink diagram for the whole program

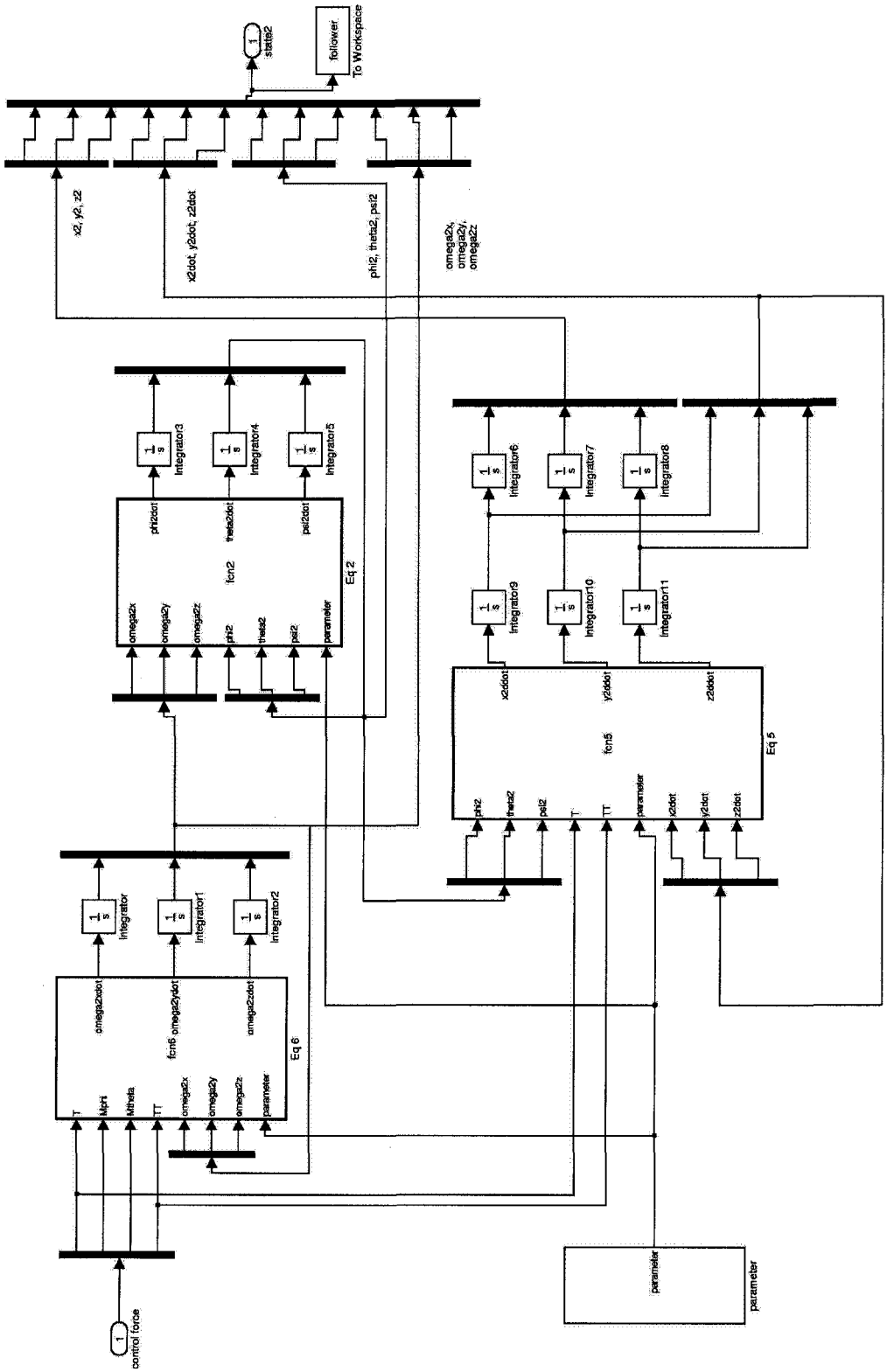

Figure A.2: The Simulink diagram for the follower part

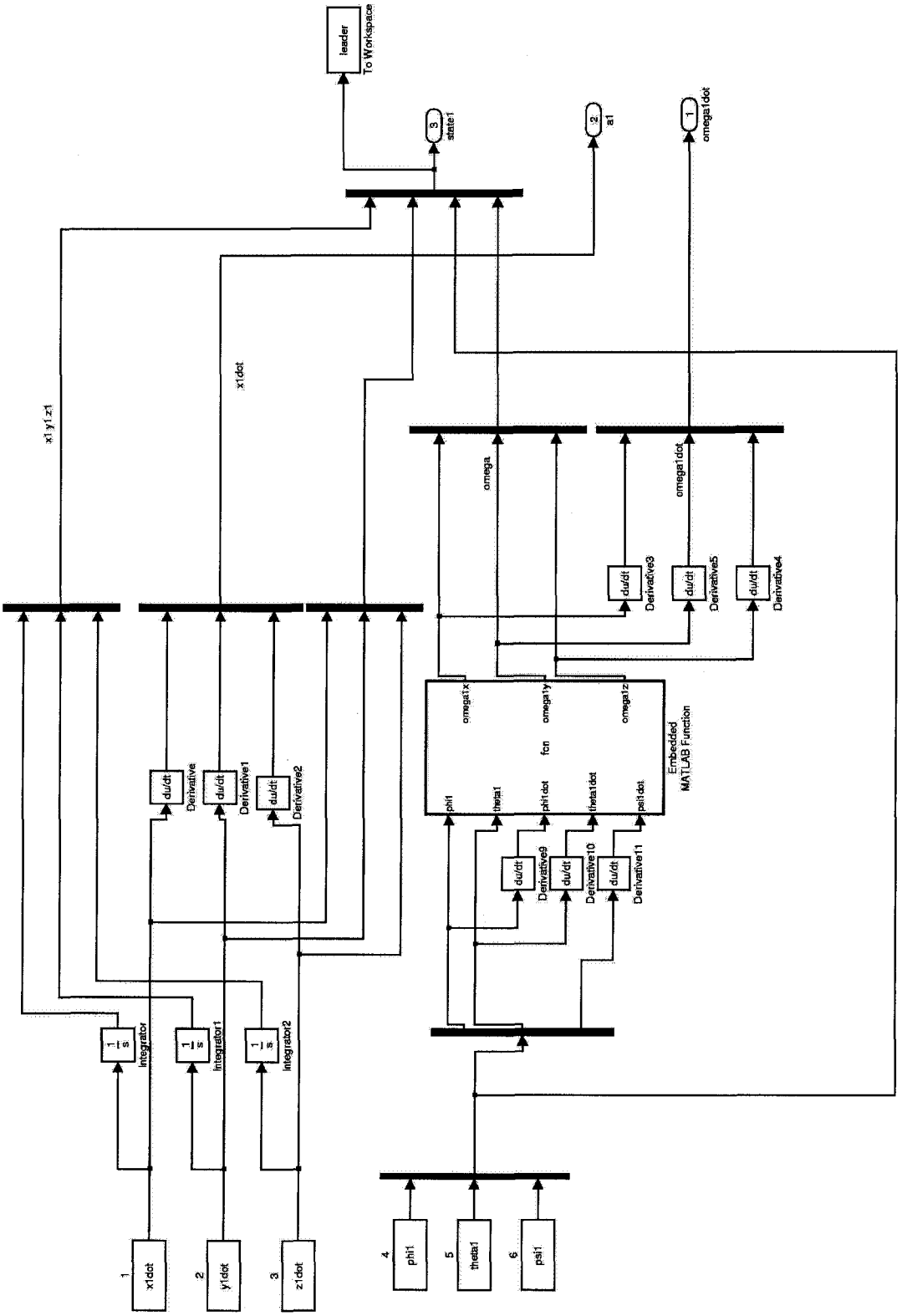

Figure A.3: The Simulink diagram for the leader part

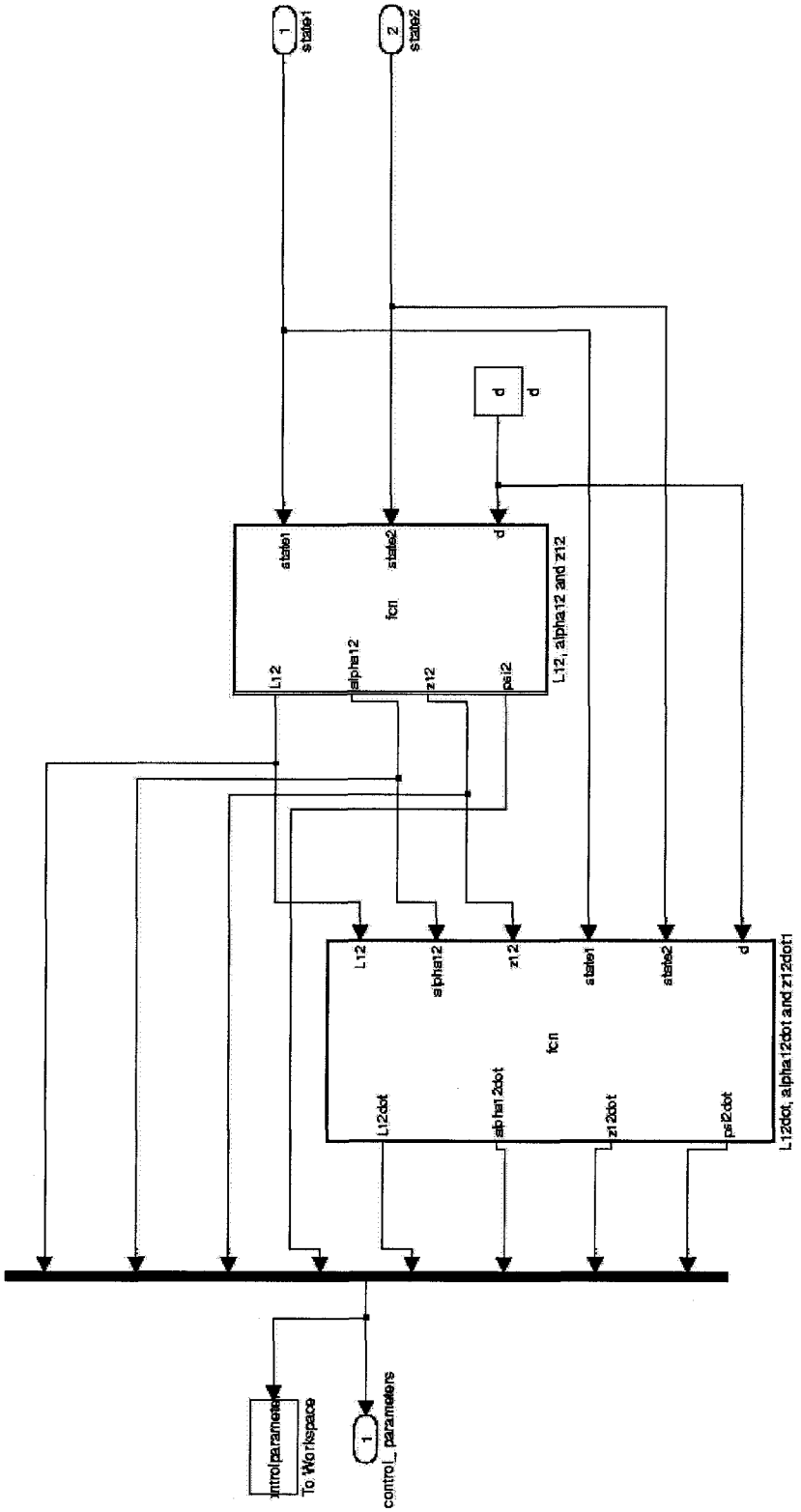

Figure A.4: The Simulink diagram for the parameter formation

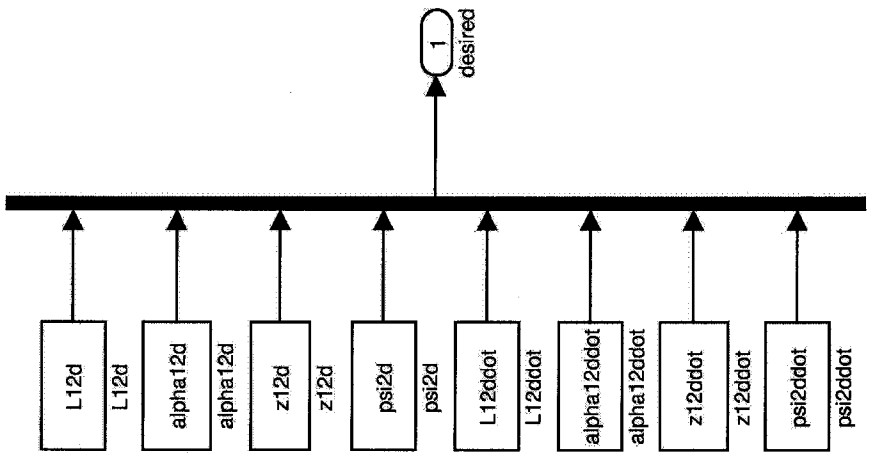

Figure A.5: The Simulink diagram for the desired parameters

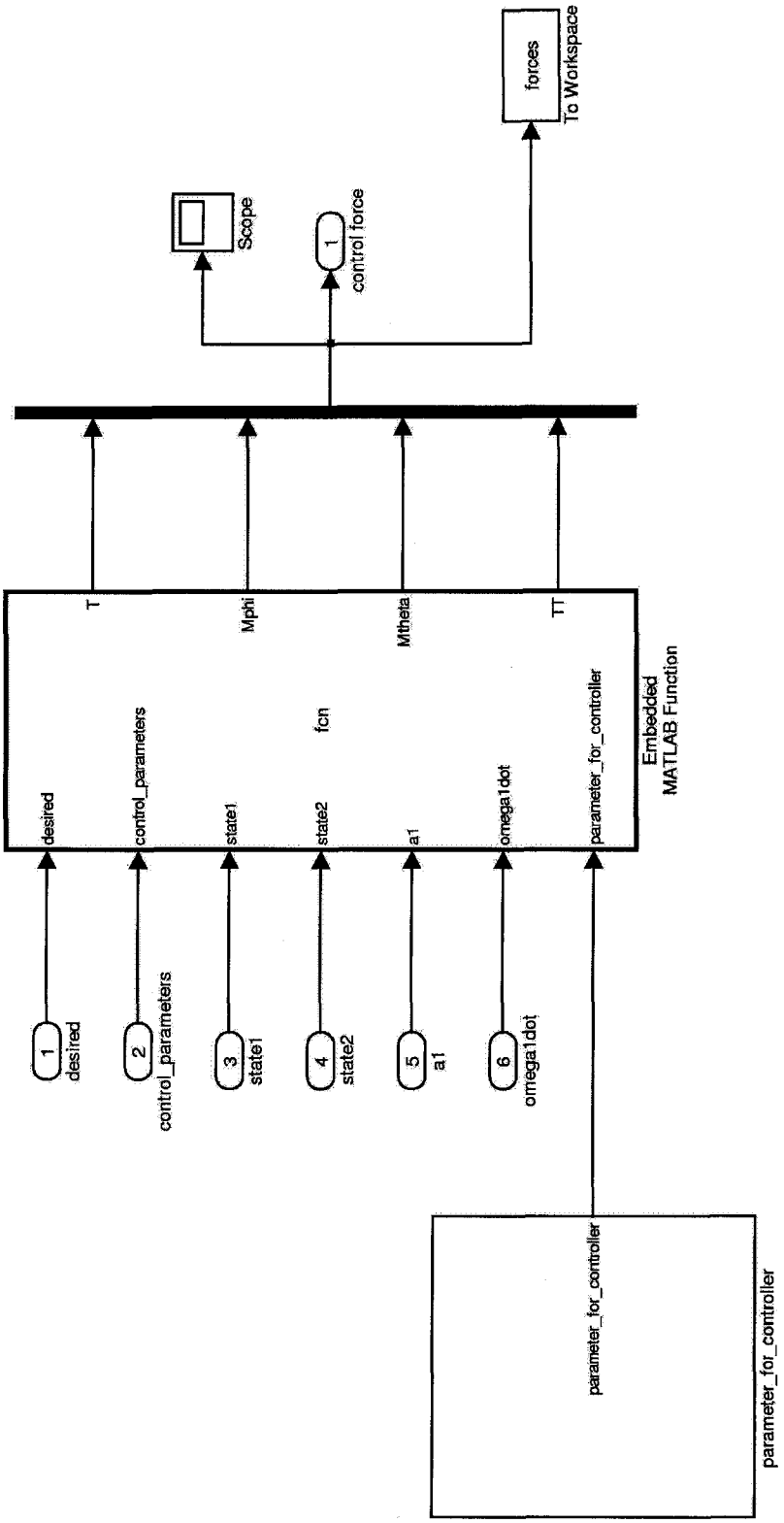

Figure A.6: The Simulink diagram for the controller

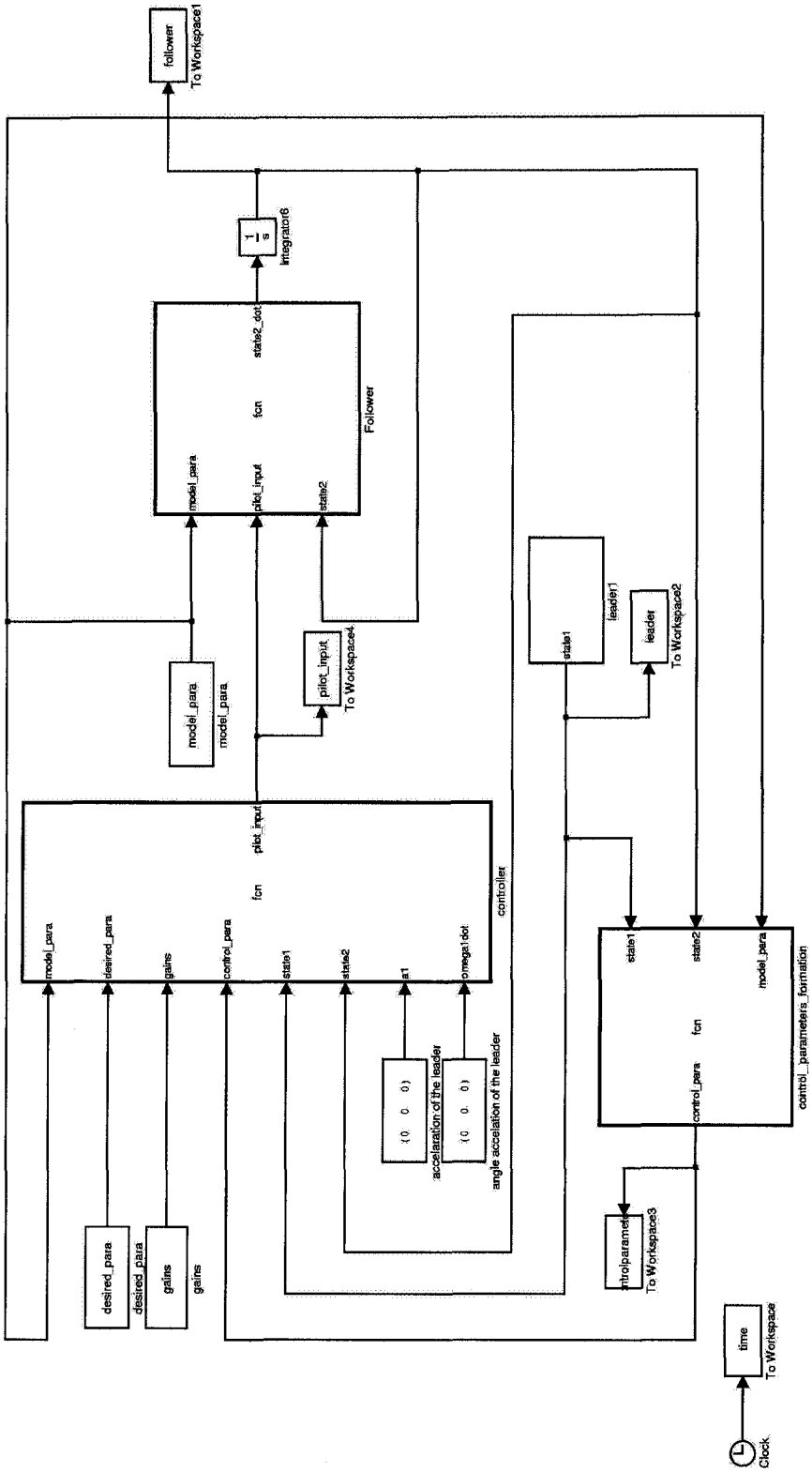

Figure A.7: The Simulink diagram for the whole program (2)

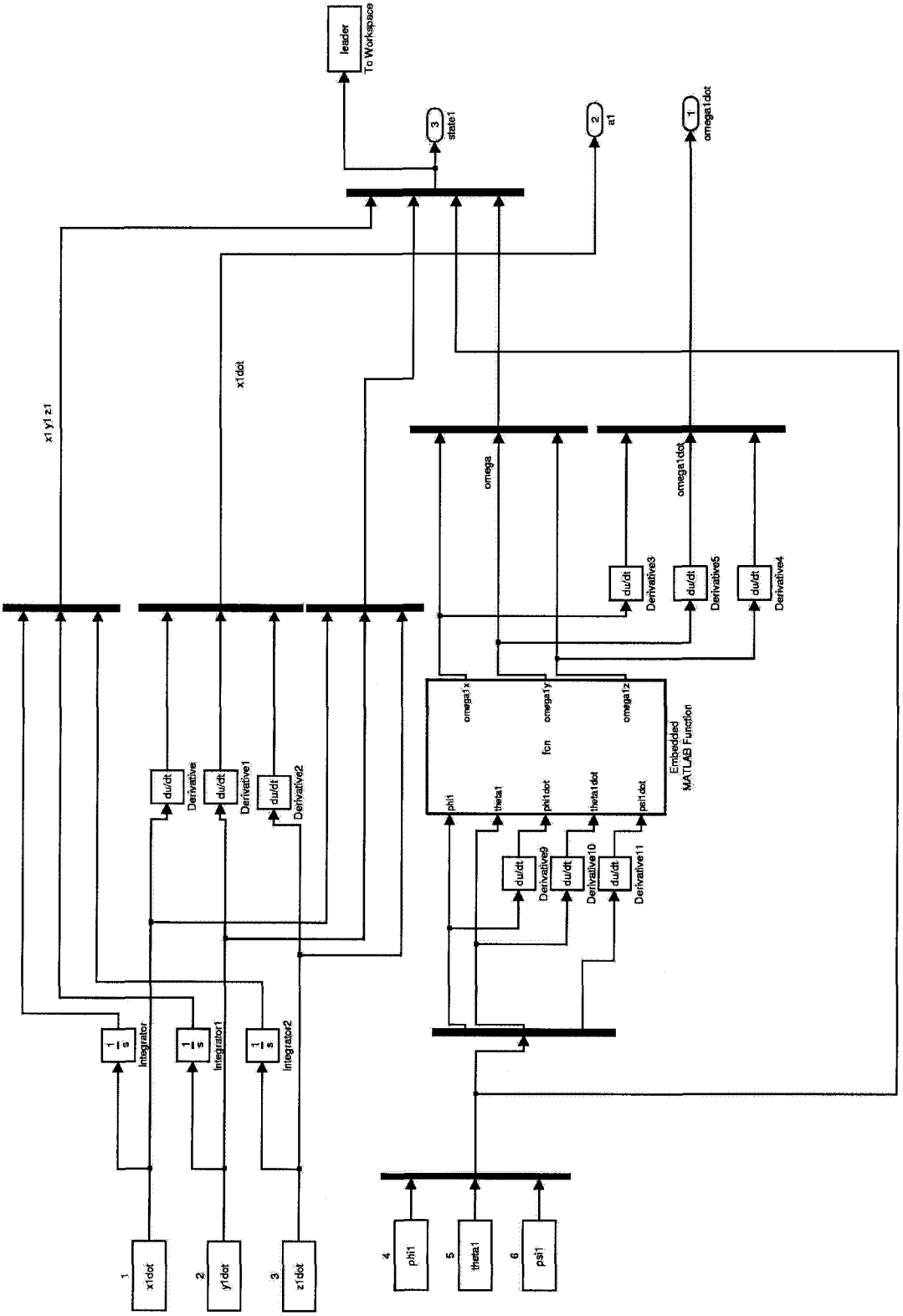

Figure A.8: The Simulink diagram for the leader part (2)